PRODUCTION OF VALUABLE CHEMICALS FROM PLASTIC WASTES CONTAINING POLYETHYLENE AND POLYPROPYLENE

A THESIS SUBMITTED TO
THE GRADUATE SCHOOL OF NATURAL AND APPLIED SCIENCES
OF
MIDDLE EAST TECHNICAL UNIVERSITY

BY

ABDUL REHMAN RAJABALI HABIB

IN PARTIAL FULFILLMENT OF THE REQUIREMENTS
FOR
THE DEGREE OF MASTER OF SCIENCE
IN
CHEMICAL ENGINEERING

AUGUST 2019

Approval of the thesis:

PRODUCTION OF VALUABLE CHEMICALS FROM PLASTIC WASTES CONTAINING POLYETHYLENE AND POLYPROPYLENE

submitted by **ABDUL REHMAN RAJABALI HABIB** in partial fulfillment of the requirements for the degree of **Master of Science in Chemical Engineering Department, Middle East Technical University** by,

Prof. Dr. Halil Kalıpçılar
Dean, Graduate School of **Natural and Applied Sciences** _____

Prof. Dr. Pınar Çalık
Head of Department, **Chemical Engineering** _____

Prof. Dr. Naime Aslı Sezgi
Supervisor, **Chemical Engineering, METU** _____

Prof. Dr. Timur Doğu
Co-Supervisor, **Chemical Engineering, METU** _____

Examining Committee Members:

Prof. Dr. Nuray Oktar
Chemical Engineering, Gazi University _____

Prof. Dr. Naime Aslı Sezgi
Chemical Engineering, METU _____

Assoc. Prof. Dr. Dilek Varışlı
Chemical Engineering, Gazi University _____

Assist. Prof. Dr. Bahar İpek Torun
Chemical Engineering, METU _____

Assist. Prof. Dr. Emre Büküşoğlu
Chemical Engineering, METU _____

Date: 28.08.2019

I hereby declare that all information in this document has been obtained and presented in accordance with academic rules and ethical conduct. I also declare that, as required by these rules and conduct, I have fully cited and referenced all material and results that are not original to this work.

Name, Surname: Abdul Rehman Rajabali Habib

Signature:

ABSTRACT

PRODUCTION OF VALUABLE CHEMICALS FROM PLASTIC WASTES CONTAINING POLYETHYLENE AND POLYPROPYLENE

Habib, Abdul Rehman Rajabali
Master of Science, Chemical Engineering
Supervisor: Prof. Dr. Naime Aslı Sezgi
Co-Supervisor: Prof. Dr. Timur Doğu

August 2019, 138 pages

Global plastic consumption has significantly increased recently creating a serious environmental threat due to the non-biodegradability of plastics. Disposal methods like landfilling and incineration result in soil pollution and emission of toxic gases, respectively. Thus the catalytic thermal degradation of plastic offers a safer and economical alternative.

In this study, aluminium and/or tungstophosphoric acid (TPA) loaded silica aerogel was used in the pyrolysis of polyethylene and polypropylene. The silica aerogel was synthesized using sol-gel technique and wet impregnation was used to incorporate the metals into the silica aerogel framework using different Al and W/Si molar ratios. Aluminum isopropoxide and tungstophosphoric acid hydrate were used as metal sources. The pyrolysis reactions were performed in the temperature range of 400-450°C with a heating rate of 5°C/min, nitrogen atmosphere at a flow rate of 60 cc/min and a catalyst to polymer weight ratio of 1/2.

All synthesized materials exhibited Type IV isotherms with pore sizes in the mesoporous material range. DRIFTS analysis revealed the existence of Lewis and Brønsted acid sites in the synthesized materials. SEM images revealed the mesoporous structure of silica aerogel. Both aluminum and TPA impregnated silica aerogel

catalysts reduced the degradation reactions' activation energy and the degradation temperature.

Gas products of catalytic pyrolysis revealed that aluminium loaded silica aerogel had high methane and acetylene selectivity while TPA loaded silica aerogel had high propylene and isobutane selectivity for both polyethylene and polypropylene degradation reactions.

Liquid products of catalytic pyrolysis revealed an increase in the amounts of gasoline C5-C12 hydrocarbon range. The SA-7Al-3W and SA-3Al-7W catalysts resulted in the best results for the catalytic pyrolysis of PE and PP, respectively.

Keywords: Pyrolysis, silica aerogel, polypropylene, polyethylene, catalysts

ÖZ

POLİETİLEN VE POLİPROPİLEN İÇEREN PLASTİK ATIKLARDAN DEĞERLİ KİMYASALLARIN ÜRETİMİ

Habib, Abdul Rehman Rajabali
Yüksek Lisans, Kimya Mühendisliği
Tez Danışmanı: Prof. Dr. Naime Aslı Sezgi
Ortak Tez Danışmanı: Prof. Dr. Timur Doğu

Ağustos 2019, 138 sayfa

Son zamanlarda plastiklerin doğada biyolojik olarak parçalanamadıklarından dolayı ciddi bir çevresel tehdit oluşturarak küresel plastik tüketimi önemli ölçüde artmaktadır. Toprağa gömme ve yakma gibi bertaraf yöntemleri, sırasıyla toprak kirliliği ve toksik gaz emisyonu ile sonuçlanmaktadır. Bu yüzden plastiğin katalitik ısıl bozunması daha güvenli ve ekonomik bir alternatif sunmaktadır.

Bu çalışmada, polietilen ve polipropilenin pirolizinde alüminyum ve/veya tungstofosforik asit (TPA) yüklü silika aerojeli kullanılmıştır. Silika aerojel sol-gel tekniği kullanılarak sentezlenmiş ve farklı Al ve W/Si molar oranlarında metalleri silika aerojelin yapısına ıslak emdirme yöntemi kullanılarak yüklenmiştir. Metal kaynağı olarak alüminyum izopropoksit ve tungstofosforik asit hidrat kullanılmıştır. Piroliz reaksiyonları 400-450°C sıcaklık aralığında 5°C/dak ısıtma hızında azot atmosferinde 60 cc/dak akış hızında ve katalizör polimer kütlece 1/2 oranında gerçekleştirilmiştir.

Sentezlenen tüm malzemeler gözenekli malzeme gözenek boyut aralığına sahip Tip IV izotermleri göstermiştir. DRIFTS analizi, Lewis ve Brønsted asit bölgelerinin sentezlenen malzemelerdeki varlığını ortaya koymuştur. SEM görüntüleri silika aerojelin mezogözenekli yapısını ortaya koymuştur. Hem alüminyum hem de TPA

emdirilmiş silika aerojel katalizörlerinin bozunma reaksiyonun aktivasyon enerjisini ve bozunma sıcaklığını düşürdüğü gözlenmiştir.

Katalitik pirolizin gaz ürünleri, alüminyum yüklü silika aerojelinin yüksek metan ve asetilen seçiciliğine sahip olduğunu, TPA yüklü silika aerojelinin, hem polietilen hem de polipropilen bozunma reaksiyonları için yüksek propilen ve izobütan seçiciliğine sahip olduğunu ortaya koymuştur.

Katalik pirolizin sıvı ürünleri C5-C12 hidrokarbon aralığında, benzin miktarında artış olduğunu göstermiştir. SA-7Al-3W ve SA-3Al-7W katalizörleri PE ve PP'nin katalik pirolizi için en iyi sonuçları vermiştir.

Anahtar Kelimeler: Piroliz, silika aerojel, polipropilen, polietilen, katalizör

For my Parents.

ACKNOWLEDGEMENTS

Firstly, I would like to express my sincerest thanks to my supervisor Prof. Dr. Naime Aslı Sezgi for her patient guidance, encouragement and advice that she provided me with throughout my time as her student. I have been extremely lucky to have a supervisor who cared so much about my work, and who always responded to all my questions and queries so promptly. I would like to thank my co-supervisor Prof. Dr. Timur Doğu for his guidance and support throughout this study.

I would like to thank my Kinetic lab partners especially Arzu Arslan Bozdağ, Merve Sarıyer, İlker Şener, Seda Sivri and Ulviye Ersoy for their friendship and help in carrying out various parts of my experimental work. Furthermore, I would like to thank Sohrab Nikazar, Pınar Değirmencioğlu, Sevil Göktürk, Salih Ermiş and Saeed Khan for their friendship and support throughout my study.

I would like to thank Ms. Mihrican Açıkgöz for her assistance during my TGA analysis and Mr. İsa Çağlar for his help fixing my broken reactors. I would also like to thank the staff of the METU Chemical Engineering Department.

I would like to thank BAP for financing this study through the project YLT-304-2018-3720.

I would also like to thank my aunt, Nazmin Manjothi, who was a pillar of support and strength throughout my studies. I would also like to thank my younger brother Ijaz Habib for his motivational attitude and moral support.

Finally, I would like to thank my parents Rozmin and Rajabali Habib for encouraging and advising me in all of my pursuits and inspiring me to follow my dreams. They taught me the value of hard work and taught me the value of patience.

TABLE OF CONTENTS

LIST OF TABLES

TABLES

LIST OF FIGURES

FIGURES

LIST OF ABBREVIATIONS

BJH: Barrett, Joyner, and Halenda

EDS: Energy Dispersive Spectroscopy

FID: Flame Ionization Detector

FTIR: Fourier Transform Infrared

GC: Gas Chromatograph

HDPE: High Density Polyethylene

IUPAC: International Union of Pure and Applied Chemistry

LDPE: Low Density Polyethylene

MCM-41: Mobil Composition of Matter No. 41

PE: Polyethylene

PP: Polypropylene

SEM: Scanning Electron Microscopy

TCD: Thermal Conductivity Detector

TEOS: Tetraethyl Orthosilicate

TGA: Thermal Gravimetric Analyzer

TMCS: Trimethylchlorosilane

TMOS: Tetramethyl Orthosilicate

TPA: Tungstophosphoric Acid

TPD: Temperature-Programmed Desorption

XRD: X-ray Diffractometer

ZSM – 15: Zeolite Socony Mobil–15

NOMENCLATURE

A: Pre-exponential factor

$A_{average:}$ Average area of GC peaks (mVolt*sec or Volt*sec)

A_i: GC peak area of component i (mVolt*sec or Volt*sec)

EA: Activation Energy (kJ/mol)

M: Molarity (mol/l)

m_i: Mass of substance i (g)

MW_i: Molecular weight of substance i (g/mol)

n_i: Number of moles of substance i (moles)

n: Reaction order

P: Polymer

q: Heating rate (°C/min)

R: Gas constant (J/mol.K)

S_i: Selectivity of component i

T: Temperature (°C)

y_i: Mole fraction of component i.

z_i: Volume fraction of component i.

α: Fraction of polymer decomposed

β: Gas chromatograph calibration factor

ρ_i: Density of component i, (g/ml)

CHAPTER 1

INTRODUCTION

Currently, plastic materials are some of the most widely used consumer products in the world. This may be attributed to their low prices, high production capacity and simple processing techniques. Such promising properties have made plastics become greatly important in industrial applications. Plastics can be used for household packaging, agricultural, automotive and building constructions, as they are lightweight, highly chemically stable and long lasting. Presently, the global plastic production is around 300 million tons/year with the European union alone accounting for around 57 million tons/year (Ratnasari et al , 2017). However, there is a major drawback in the use of plastic materials: they are non-biodegradable. This simply means that they do not decompose biologically in nature. This creates an accumulation of plastic wastes as the decomposition cannot match the annual production rates. Plastic accumulation is therefore a major cause for environmental pollution. This can be seen in daily life when one walks near dumpsites and sees that the major portion of current waste are plastic materials.

The disposal of plastic-based waste is ever increasingly becoming a global issue due to the high production rate and high demand. The generation and types of plastic wastes vary greatly from country to country mainly due to a difference in income levels. This then makes it hard for a proper disposal system that can cater for the large variety of plastic waste. As a result, high income countries can easily dispose of their plastic waste while low income countries struggle with the effects of such large amounts of non-biodegradable plastic waste. Furthermore, the direct recycling of plastics is limited by the recycling cycles depending on the type of plastic material used. This means that many people simply dispose of plastics after using them a few

times. This then necessitates the development of proper disposal methods to cater for the ever increasing waste (Singh et al., 2017)

Throughout the years many techniques have been used to recycle plastic wastes. These techniques have not been very economical or environmentally friendly. One of these methods is landfilling which is a short-term solution. Since plastic waste is bulkier than organic waste it tends to occupy large amounts of spaces in landfills and due to the limited nature of land availability coupled with rises in cost of buying or hiring land, this method is costly and moreover it has negative impacts on the environment as it leads to soil and water pollution. Another method is incineration which involves the burning of the plastic wastes. Since plastic wastes are made up of chemical additives, this process leads to the emission of poisonous gases which end up having detrimental effects on living organisms. For example, the chlorine in polyvinyl chloride (PVC) is harmful when ingested or inhaled by biological organisms. Furthermore, extra equipment like gas scrubbers need to be installed to clean the gas before being emitted making this process expensive. It is due to these reasons that safe and effective plastic recycling methods need to be researched and developed (Miandad et al., 2016).

Pyrolysis is a method that can be used in the recycling of plastics and is a relatively low-cost operation that yields in a wide range of products. Pyrolysis can be defined as the chemical decomposition of polymeric compounds subjected to heating in an inert atmospheric condition. Since the process involves chemical changes, there is bond breaking process which is endothermic thus heat needs to be supplied to the system so that the reaction can occur leading to the production of olefins and aromatic organic. These materials can then be further processed and used as raw materials in other chemical processes and fuels like gasoline. Since heat must be supplied to a pyrolysis reaction it is a very energy intensive process. The reaction should be carried out at high temperatures around 450-600°C for polymer decomposition to occur. The products obtained usually have a wide molecular weight distribution. To overcome the aforementioned challenges, catalysts are widely used in pyrolysis. These catalysts

efficiently lower the reaction temperature and residence times of the reaction thus significantly saving energy and time. Moreover, using catalyst results in products that are of high quality, stable and have a narrow molecular weight distribution thus increasing their market values (Almeida et al., 2015).

Silica aerogels are an example of mesoporous materials that have pore diameters in the range of 2-50 nm. They possess high surface area values of around 800 m^2/g, low density (approximately 0.003 g/cm^3), high porosity of around 95% (Rao et al., 2005). In recent years, researchers have been looking into the use of different precursors and modifying the synthesis parameters with an emphasis on using ambient pressure drying for commercial production (Dorcheh et al., 2008). The use of ambient pressure drying of silica aerogel over supercritical drying is promising as it is not only an economical way of synthesis but also less dangerous. In supercritical drying there is heating and evacuation of extremely flammable solvents like alcohols which is a risk as the process is carried out at high temperatures and pressures (Rao et al., 2005). The most common method of silica aerogel production is by the sol-gel technique with silicon alkoxides precursors like tetramethylorthosilicate (TMOS) and tetraethylorthosilicate (TEOS). TEOS is polymerized in two steps: hydrolysis and condensation where hydrogen chloride (HCl) is a hydrolysis catalyst, and ammonia (NH_3) is the condensation catalyst (Tamon et al., 1998). The silica aerogel obtained from this process results in hydrophilic aerogels, however, research has been undertaken into converting silica aerogel into a hydrophobic material using trimethylchlorosilane (TMCS). The hydrophobicity results in a silica aerogel structure that is stable against humidity (Rao et al., 2005). Furthermore the addition of TMCS results in a silica aerogel structure that is not only light but also does not develop cracks (Shi et al., 2006). The TMCS is used to modify the surface of the aerogel by replacing the polar -OH group by a non-polar -CH_3 groups (Mahadik et al., 2011).

Using mesoporous materials in their pure siliceous form as catalysts possess some problems due to the low acidity of these materials when compared to microporous materials which generally include zeolites. Zeolites contain strong Brønsted acid sites

making them very suitable catalysts. Hence it is necessary to improve the acidity of mesoporous materials and this is achieved by incorporating metal ions like Al^{+3}, Fe^{+3}, Pd^{+3}, V^{+5} (Obali et al., 2011). The addition of aluminium ions into a mesoporous material like silica aerogel, SBA-15 leads to the formation of Brønsted acid sites and the sources for the Al^{+3} can be sodium aluminate, aluminium iso-propoxide, aluminium hydroxide, aluminium sulphate and aluminium nitrate (Obali et al., 2011). The structural properties of the material determine the performance and functionality of the solid catalysts. The dependence on the structure depends on both the size and shape of the polymeric materials as the bulky and large nature of polymers is important when choosing a suitable catalyst. In other words, the catalyst should be able to allow the bulky polymer molecules to access the active sites in the catalysts which is a major disadvantage when using microporous materials. Therefore, even though zeolites have stronger acid sites as compared to siliceous mesoporous materials, they have a major drawback when used in degradation of polymeric materials. Since zeolites are microporous materials, their pore diameters range around 1.0 nm. These small pores hinder the access of the much bulkier polymeric materials to the acid sites inside the channels. Furthermore, the problem of coking also occurs hence the catalyst can be deactivated (Obali et al., 2012).

In this study, the mesoporous silica aerogel materials were synthesized using hydrothermal synthesis and impregnation method was used to introduce the acid sites to the silica aerogel. The synthesized materials were then tested using the thermogravimetric analysis and then degradation experiments were conducted in the pyrolysis reaction set up. The gaseous and liquid products obtained from the pyrolysis reaction were analyzed using gas chromatography.

CHAPTER 2

POLYMERS

2.1. Introduction

A polymer is a large molecule that consists of numerous smaller molecules and can be linear, branched, or interconnected. Monomers are the small molecules that are used as the basic building blocks for the larger molecules i.e. a polymer consists of many interconnected monomers (Kasapoğlu, 2013). The monomer of polyethylene is ethylene while propylene is the monomer for polypropylene. Polymer properties vary as some are either rigid while others are brittle or elastic. Polymers differ from metals and ceramics as their physical properties can vary significantly with temperature and pressure.

2.2. Historical Development

The word polymer is an amalgamation of two Greek words: “poly” meaning “many” and “meros” meaning “part”. Therefore, polymers can simply be described as a macromolecule that contains a structural unit that is in a repeating order and connected to each other using covalent bonds. Henry Braccanot is known to carry out the first known research into cellulose compounds in 1811. Later in the 19^{th} century, rubber was vulcanized to improve its strength. A century later, Belgian chemist Leo Baekeland became the first person to synthesize Bakelite, the first completely synthetic polymer. Until the 1920s the molecular structure of the polymers wasn’t fully understood even though there were significant improvements in the synthesis and characterization of polymers during this period. During the 1920s, Wallace Carother was working on the synthesis of polymers from their individual monomer units. In the year 1963, Italian chemist Giulio Natta and German chemist Karl Ziegler worked together to develop the Ziegler-Natta catalyst and were awarded the Nobel

Prize in Chemistry for this discovery. Almost 10 years later, Paul Flory was awarded the Nobel Prize for his contribution to polymer science through his research into "kinetics of step-growth polymerization", "addition polymerization chain transfer", "excluded volume", the "Flory-Huggins solution theory" and the "Flory convention" (Aydemir, 2010).

2.3. Properties of Polymers

The physical properties of polymers are affected by certain parameters that can be categorized as follows: chain length, arrangement of monomers, tacticity, crystallinity and chain conformation. Polymers can also be classified using their mechanical properties like tensile strength and elasticity.

2.3.1. Chain Length

The physical properties of a polymer are greatly affected by the chain length. An increase in chain length results in higher boiling point temperature, increased glass transition temperature, high viscosity and increased resistance to flow in the melt state. The mechanical properties of the material like tensile strength, impact resistance and toughness are also increased with increasing chain length. This is due to the increase in entanglements in the polymer chains due to increase in Van der Waals forces resulting in a more stable, immobilized and resistant individual chain that is held strongly in its position (Aydemir, 2010).

2.3.2. Monomer Arrangements

This is a concept defined for copolymers. Copolymers are a type polymer classification where the structure has two or more distinct types of monomer present. Copolymers can further be classified into 5 groups depending on the arrangement of these repeating monomers which are: alternating copolymers, periodic copolymers, statistical copolymers, block copolymers and graft copolymers (Aydemir, 2010).

- Alternating copolymers consist of regularly arranged monomers that appear in an alternating pattern in the form of $[AB\ldots]_n$

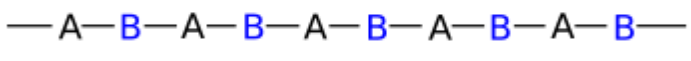

- Block copolymers consist of two or more homopolymer sub units that are connected to each other by covalent bonds. When the number of the same distinct sub units are two or three, they are referred to as di-block and triblock copolymers, respectively.

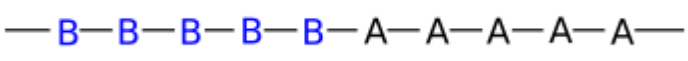

- Graft copolymers consist of side chains with different monomer units than the main chain.

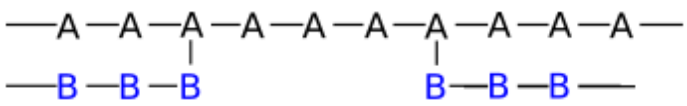

2.3.3. Tacticity

This is the spatial arrangement of chiral centers within structural units in a macromolecule. Tacticity can be subdivided into three categories: atactic polymers which are generally amorphous, have the substituent groups arranged in a random manner. Syndiotactic polymers have the substituents arranged in an alternating manner. Isotactic polymers have the substituents all on the same side of the main chain. Both isotactic and syndiotactic polymers have higher strength than atactic polymers (Aydemir, 2010).

2.3.4. Crystallinity

One of the most important characteristics of a polymer is its degree of crystallinity which determines the polymers' mechanical properties like impact stress, elastic modulus and yield stress. Crystallinity is temperature dependent (Kong et al., 2002).

In synthetic polymers, crystallinity can be described in terms of the three-dimensional ordering in an atomic scale. It is possible for a polymer to contain both crystalline and

amorphous phases. The degree of crystallinity also affects the physical appearance of polymers as zero crystallinity appears transparent while increase in crystallinity makes the polymer more opaque (Aydemir, 2010).

2.3.5. Chain Conformation

Conformation is the type of shape a polymeric chain can have. For example, a polyethylene chain can appear as a linear zig-zag. An important feature of real chains is their oscillation and movement due to thermal vibrations of the molecular structure. These thermal vibrations increase in both frequency and amplitude with an increase in temperature, the most important rotation being about the single bond while the double bond is rigid. As a result of extra rotational motion, the number of chain conformations increases rapidly with increasing temperature (Peacock, 2000).

2.3.6. Mechanical Properties

Some of the mechanical properties of polymers are tensile strength and elasticity. These properties affect the behavior of a polymer and greatly influence its final application.

2.3.6.1. Tensile Strength

This is the amount of stress required to break a polymer sample. In tensile strength test the polymer material being studied is stretched until it reaches its deformation point (Balani et al., 2015). Tensile strength is an important criterion for a polymer used in applications requiring physical strength of the material and can be improved by increasing the chain length and crosslinking in the polymer structure (Aydemir, 2010).

2.3.6.2. Elasticity

Elasticity is the ratio of the change of stress to strain and is defined using Young's Modulus which is temperature dependent. As is the case with tensile strength, elasticity is extremely important for polymers that are used in applications requiring physical strength. (Aydemir, 2010).

Polymers that possess a high Young's modulus are rigid in nature while ductile polymers also have similar elastic modulus but have higher fracture toughness. Elastomers with lower Young's modulus values are generally rubbery in nature (Balani et al., 2015).

2.4. Commonly Used Polymers

This section lists the most widely produced and used polymers which include polyethylene (PE), polypropylene (PP).

2.4.1. Polyethylene (PE)

A polyethylene molecule in its simplest form is made up of a long backbone of covalently linked carbon atoms each attached to a pair of hydrogen atoms. The chain ends consist of methyl groups as shown in Figure 2.1 (Peacock, 2000). Polyethylene is naturally white in color and has a melting point between 120-140°C.

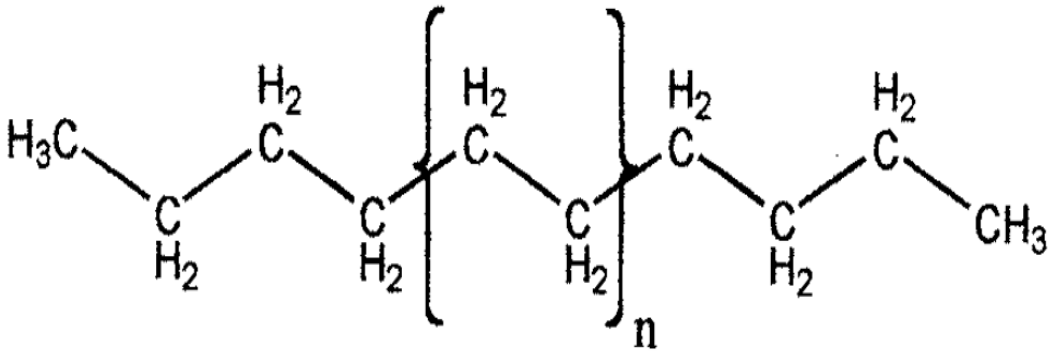

Figure 2.1 Structure of Polyethylene (Peacock, 2000).

The global production of polyethylene (PE) accounts for approximately 40% of the total demand for thermoplastic materials and roughly a third of the overall plastic demand. This large proportion can be attributed to the simple and inexpensive structure of PE. Furthermore, its chemical resistance, low density when compared to

other polymers and less environmental impact have made PE a widely used material in fields ranging from medical applications to packaging and infrastructure materials like pipes (Jeremic, 2010).

PE is generally divided into three categories according to the density of the polymer. These are: low-density polyethylene (LDPE), high-density polyethylene (HDPE); and linear low-density polyethylene (LLDPE).

PE density directly correlates to its crystallinity which depends on the branching present in the polymer chain and the nature of monomers which are usually short chain polar alkyl compounds or α-olefins. LDPE and LLDPE are soft solids and appear transparent in bulk. Films that are made using low density polyethylene are also transparent. High density materials are more rigid and appear as opaque. HDPE films are firm. Amorphous PE has a density of 880 kg/m^3 while fully crystalline PE has a density of 1000 kg/m^3 (Jeremic, 2010).

Some of the applications of PE are (Jeremic, 2010):

- LDPE - Rigid containers, plastic film applications (plastic bags, film wraps).
- LLDPE - Bubble wrap, multilayer and composite films, cable coverings, toys, buckets, containers.
- HDPE - Milk jugs, detergent bottles, margarine tubs, garbage containers, water pipes.

Polyethylene is a very good polymeric material for pyrolysis. It needs temperatures higher than 500°C due to its branched structure. It converts into wax instead of liquid oil when it undergoes thermal pyrolysis. When PE undergoes catalytic pyrolysis, wax is formed on the external sites of the catalyst while further cracking of the wax into gaseous and liquid products occur in the internal site of the catalyst (Miandad et al., 2016).

2.4.2. Polypropylene (PP)

Since its discovery in 1954 and industrial production beginning in 1957, polypropylene has quickly gained popularity due to its low density when compared to other commodity plastics. Furthermore, PP has exceptional chemical resistance and can be processed using conventional methods like extrusion and injection molding (Maddah, 2016).

Polypropylene is prepared catalytically using propylene as a monomer through additional polymerization and has a translucent appearance. Its resistance to high temperature makes it suitable for use in manufacture of trays, bottles, funnels and instrument jars that require frequent sterilization for use in hospitals (Maddah, 2016). Polypropylene is an example of a vinyl polymer where each carbon atom is attached to a methyl group as shown in Figure 2.2.

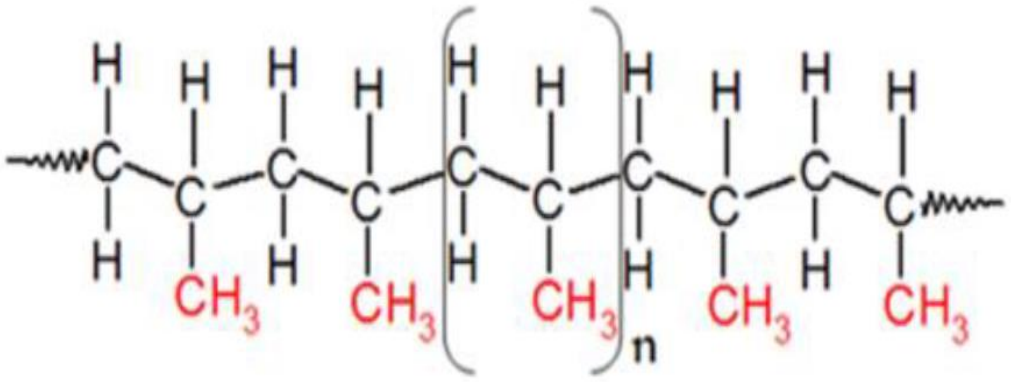

Figure 2.2 Polypropylene Structure (Maddah, 2016).

In terms of configurations, PP can be classified into three types: *isotactic*, the methyl groups are located one side of the polymer main chain as shown in Figure 2.2, *syndiotactic*, the methyl groups alternate on both sides of the main chain and *atactic*, where the methyl groups are irregularly arranged on either side of the main chain. Isotactic PP has a melting point of 171°C, while syndiotactic PP has a melting point of 130°C (Maddah, 2016).

Polypropylene is suitable for pyrolysis reactions. Non-catalytic pyrolysis of PP requires high temperature but in its catalytic pyrolysis reactions, the catalyst lowers the temperature and results in high aromatic compounds in the liquid product (Miandad et al., 2016).

CHAPTER 3

POROUS MATERIALS

3.1. Introduction

As the name suggests, porous materials contain a large number of pores. Porous materials consist of a solid phase forming the basic porous frame. The empty voids within the frame are formed when the liquid used in the synthesis is removed during drying (Liu et al., 2014).

The IUPAC classification categorizes porous materials into three groups: microporous (< 2nm), mesoporous (2-50 nm) and macroporous (>50 nm). These classifications are summarized in Figure 3.1 (Aydemir, 2010).

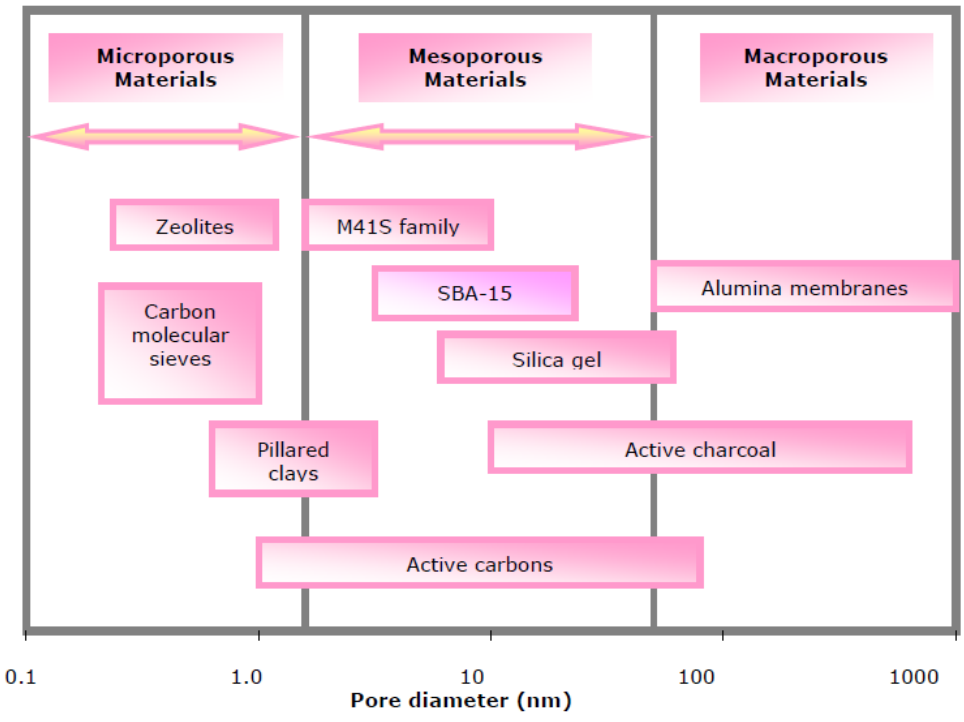

Figure 3.1 Classification of porous materials according to pore diameter (Aydemir, 2010).

3.2. Microporous Materials

Microporous materials have pore diameters less than 2 nm. The most common types of microporous include zeolites, some metal phosphates like titanium, zirconium etc., amorphous silica, inorganic gels and carbon molecular sieves (Aydemir, 2010).

Zeolites have shown exceptional properties as catalysts for the catalytic pyrolysis of polymer materials. These properties include strong acidic sites that promote carbon-carbon bond scission (Obali et al., 2012). However due to the bulky nature of polymers and the aforementioned small pore size of microporous zeolites, there is a challenge in performing pyrolysis as the degradation reactions are controlled by the pore size of the catalyst used. The small pore sizes of micropores restrict the access of the polymer molecules into the inner channels of the catalyst (Obali et al., 2009). Furthermore, there is a drawback in using microporous materials like zeolites in pyrolysis reactions due to formation of coke which results in catalyst deactivation (Obali et al., 2012).

Another drawback of using zeolite as catalyst is that it requires longer residence times hence increasing production cost (Almustapha et al., 2013).

3.3. Mesoporous Materials

Mesoporous materials have pore diameters in the range of 2-50 nm. The interest in these materials has increased in the last few years mainly due to the following factors. Firstly, they provide an increased diversity in the composition and structure of the materials. Secondly it increases the ability to process materials on a macroscale and finally, the application fields of mesoporous materials are wider as they can be used in traditional areas like catalysis and sorption but also in newer areas like optics and electronics (Schüth et al., 2002).

Mesoporous materials are more suitable for polymer pyrolysis reactions due to their larger pore sizes compared to micropores. This allows polymer molecules access to acid sites promoting cracking. However, due to the relative low acidity of mesoporous

materials, metal ions like aluminium, tungsten, iron etc. can be incorporated into the structure of mesoporous to overcome the low acidity (Obali et al., 2012). Some of the materials classified in this category include silica aerogel, SBA-15, MCM-41 (Aydemir, 2010).

3.3.1. Heteropoly Acids

Commonly used heteropoly acids include tungstophosphoric acid (TPA) and silicotungstic acid (STA). Heteropoly acids are solid acid catalysts with high Brønsted acid sites capacity and are extensively used in acid catalyzed reactions. They are environmentally friendly and economical (Aydemir, 2010). Heteropoly acids occur with two molecular structures: Keggin and Dawson. Keggin is the major structure with a formula of $[H_{8-n}XM_{12}O_{40}]$, where X is a central atom e.g. phosphorus (P), silicon (Si) that is surrounded by a metal-oxygen octohedra, M e.g. tungsten (W), Molybdenum (Mo). TPA has three protons while STA has four protons. The Dawson structure is a combination of two Keggin molecules (Degirmenci et al., 2010). Figure 3.2 shows the general structure of TPA – a Keggin structure molecule.

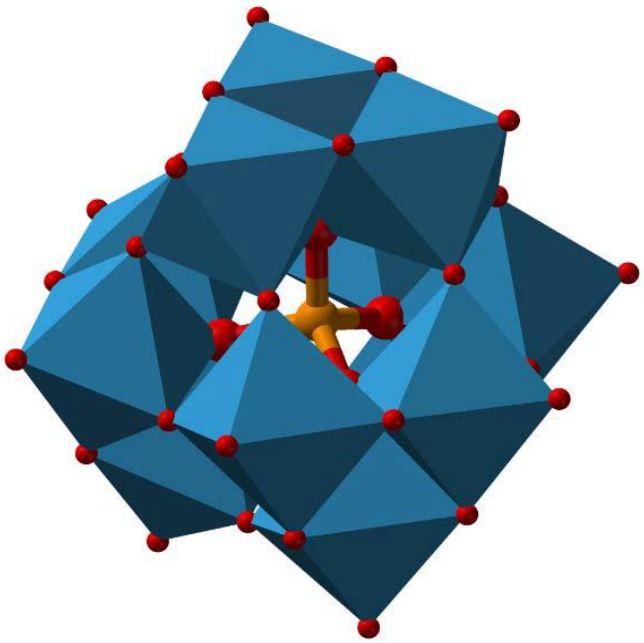

Figure 3.2 General structure of the TPA molecule (Aydemir, 2010)

Due to their acid strength, stability and availability, heteropoly acids with Keggin structure are most commonly used in catalysis applications. However, despite having high acid capacity which is desirable in polymer cracking reactions, heteropoly acids have major drawbacks to being used as catalysts in their pure form due to their low thermal stability and low surface area (Aydemir, 2010). When incorporated into the structure of mesoporous support materials, heteropoly acids overcome their low surface area and low thermal stability drawbacks. Hence, they can be used as catalysts in polymer pyrolysis at high temperatures.

For this study the heteropoly acid used was TPA, this was due to its high acidity and in order to compare with previous studies carried out on the pyrolysis of polymeric materials. Furthermore, aluminium was also used due to its high thermal stability and to study the effect of using both metals in the same catalyst.

3.3.2. Silica Aerogels

Over the past few years silica aerogel has attracted a lot of research interest due to its extraordinary properties that enable it to be applied in a wide range of technological areas from electronic applications to use in catalytic processes. A lot of research has been done into silica aerogel synthesis and characterization showing that it has high surface area, high porosity, low density and excellent heat insulation capability. In this section the synthesis, properties and characterization of silica aerogels will be discussed.

3.3.2.1. Introduction to Silica Aerogels

Aerogel is a term generally used to refer to materials that are derived from organic, inorganic or hybrid molecular precursors and these aerogels are normally prepared using a sol-gel process and a suitable drying process that conserves the three-dimensional and extremely porous network (Maleki, 2016). Silica aerogels have a unique structure that is 90% air and 10% solid silica that is formed into a highly cross-linked network structure (Shi et al., 2006).

Recently research into hydrophobic silica aerogel has proven to be fascinating in its applications in areas like absorption of organic liquids and adsorption of toxic substances. Hydrophobicity can be achieved through surface modification using silylating reagents which replace the surface polar -OH group with a non-polar -CH_3 group (Mahadik et al., 2011).

The properties displayed by silica aerogels are greatly influenced by the synthesis conditions like synthesis temperature, pH, time taken for precipitation, addition of surfactants, methods of washing and drying (Rida et al., 2014). Silica aerogel has some extremely desirable properties which include:

- Low density: 0.003-0.5g/cm^3 (Maleki, 2016),
- High surface area: 500-1200 m^2/g (Maleki, 2016; Gurav et al., 2010)
- High porosity: 80-99.8% (Maleki, 2016; Gurav et al., 2010),
- Low thermal conductivity (~0.01W/m.K) (Gurav et al., 2010),
- Low dielectric constant (~1.0 - 2.0) (Gurav et al., 2010),
- Low refractive index (~1.05) (Gurav et al., 2010),
- Tailor made surface chemistry (Maleki, 2016),
- Ability of being able to be processed into a variety of morphologies and sizes (Maleki, 2016).

These properties can be useful in a vast range of applications like catalysis, adsorption, thermal insulation and drug delivery systems (Shi et al., 2006).

3.3.2.2. History of Silica Aerogels

Steven Kistler is credited with the synthesis of the first silica aerogel in the 1930s. His technique involved replacing the liquid phase with a gas phase resulting in a slight shrinkage in the gel. He used a wide range of materials like alumina, ferric oxide, tin oxide, tungsten oxide, cellulose, gelatin, rubber and egg albumen to prepare his aerogels. Since Kistler's method was tedious and time-consuming, there was no development in aerogel technology until 1968 when researchers led by a French

Professor S. J. Teichner who revisited the synthesis of aerogels. Professor Teichner was able to simplify Kistler's procedure by using a solvent to conduct the sol-gel transition and using supercritical conditions to remove the solvent. This then led to further research into silica aerogel application in a variety of fields like thermal insulation, electronic devices, catalysis and cosmic dust collection (Gurav et al., 2010). Even though Kistler used a wide range of starting molecules for his aerogel synthesis, successive research primarily focused on silica (SiO_2) type of aerogels (Maleki, 2016). Figure 3.3 shows the generalized structure of an oxide aerogel that contains both mesoporous and microporous parts.

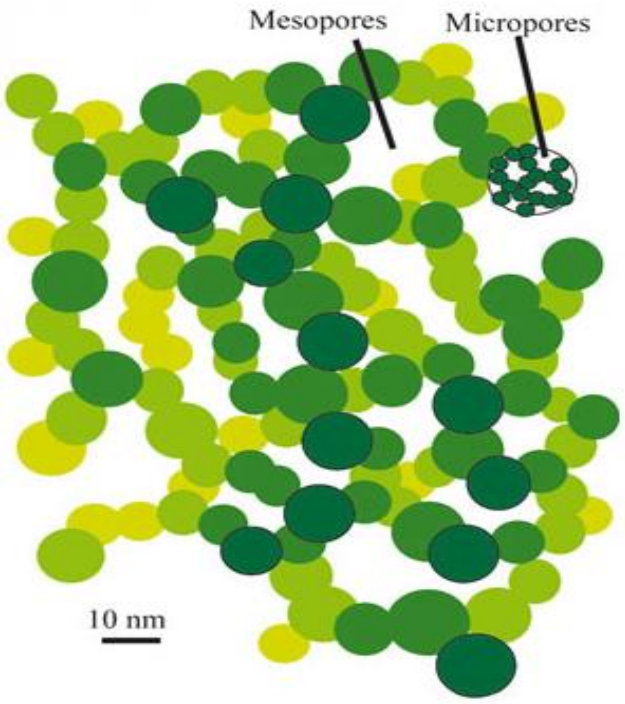

Figure 3.3 The general structure of an oxide aerogel (Aegerter et al., 2011).

3.3.2.3. Synthesis of Silica Aerogel

There is a common synthesis procedure amongst all types of aerogels. The preparation procedure of aerogels entails three crucial steps: sol-gel process, aging and finally drying. These three steps are outlined in Figure 3.4 (Maleki, 2016).

The microstructure and surface groups of aerogels which are determined by the sol-gel process greatly influence the application of the resultant aerogel. Thus, it is extremely important to choose a suitable synthesis procedure in order to meet the requirements of the target application (Maleki, 2016).

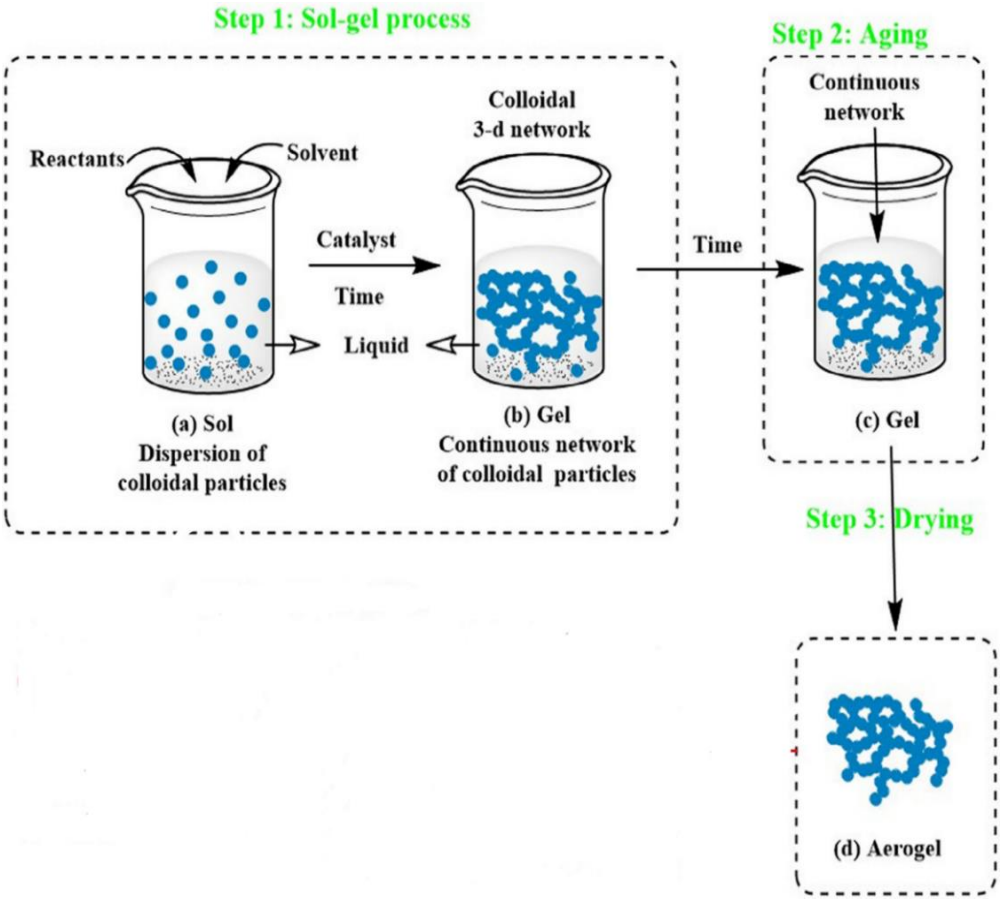

Figure 3.4 A generalized aerogel preparation route using sol-gel technique (Maleki, 2016).

3.3.2.4. Sol-gel Process

Almost all the aerogels known are prepared using a wet chemical synthesis method known as sol-gel reaction. The parameters that differentiate the final aerogels are starting precursors, operating conditions and provision requirements (Maleki, 2016).

3.3.2.5. Sol-Gel Reactions

A majority of aerogels are prepared using the sol gel reaction which is a wet chemical synthesis approach using a variety of starting precursors and reaction conditions. Generally, silica aerogel is synthesized using two types of silica precursors, i.e. organosilanes for example tetraethylorthosilicate, tetramethylorthosilicate, methyltrimethoxysilane, polyethoxydisiloxanes or inorganic silicates like water glass (Li et al., 2016).

Sol can be defined as a very dispersed solution of colloidal primary particles resulting hydrolysis and polycondensation reactions, and are prepared using a mixture of precursors, solvents, water and catalysts. These colloidal particles can be connected to form a three-dimensional interconnected network through the addition of a chemical cross-linker. This can also be achieved by changing the physical conditions of the reaction like pH and temperature. It should be mentioned that the formation of the three-dimensional porous network is the most important and determinant part of the aerogel synthesis.

The naming of the aerogels depends on the solvent that fills the pores of the wet gels. If it is an **alcohol,** it is named alcogel while acetogels use acetone. Hydrogels are gels that are prepared using natural polymers (Maleki, 2016). Generally, if an alkoxide is used in the aerogel synthesis, the reaction can proceed by using a single-stage acid or base catalysis or a two-step reaction starting with an acid followed by a base catalyst. In the hydrolysis reaction, the alkoxide (-OR) is replaced with the hydroxyl (-OH) group. The subsequent polycondensation reaction involves the formation of siloxane bonds from silanol groups and alcohol and water as by-products. Both the condensation and hydrolysis reactions initiate simultaneously and continues throughout the entire sol-gel reaction (Maleki, 2016).

The versatility of the sol-gel reaction can allow modifications to the gel nanostructure through adjustments to the reaction parameters. Parameters like the precursor and solvent concentration, type of solvent, temperature, pH and ratio of water to silica

precursors can significantly help in tailoring the final material properties to suit the end use of the aerogel. Furthermore, the sol-gel reactions can allow for incorporation of molecular compounds that add special features to the gel network. For examples, the addition of hydrophobic groups like methyl (-CH_3) into the gel network helps improve the stability of the aerogel against moisture. Moreover, the integration of the polymeric network increases the aerogel's mechanical strength (Maleki, 2016).

Figure 3.5 shows the sol-gel reaction mechanism for the preparation of a silica (SiO_2) network.

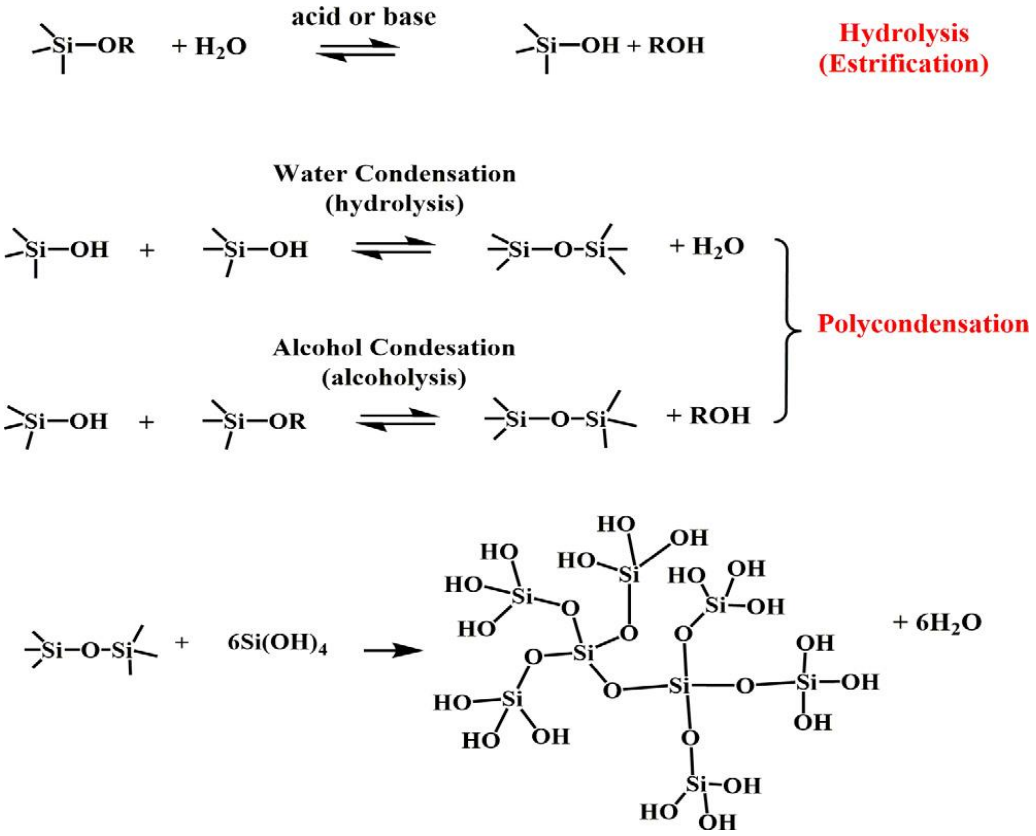

Figure 3.5 Summary of the sol-gel mechanism (Maleki, 2016).

Generally, pure silica aerogel has Si-OH groups which are hydrophilic hence can easily become wet when exposed to moisture and water. Due to the fragile nature of the aerogel network, this moisture can lead to deterioration due to bonding between

the polar -OH groups in the aerogel and the atmospheric moisture content. For this reason, it is necessary to modify the aerogel surface to make it hydrophobic (Wang et al., 2008).

3.3.2.6. Aging

This is a crucial step in the synthesis of aerogels as the formation of the gel does not guarantee that the chemical reactions have finished. This may be attributed to the probability of the gel network to continue growing in the gelation solvent since the solvent inside the pores contains the reactive species like -OH or other unreacted monomers that can condense into the network. The aging process can last hours or days and is carried out in the initial sol or a suitable solvent by controlling the conditions (Maleki, 2016).

One of the main purposes of this step is to improve the mechanical strength of the aerogel's network. This is because of a phenomenon known as ''Ostwald ripening" or ''coarsening". The Ostwald ripening occurs when the molecules in the solution dissolve from the less energetically favored places and accumulates on the more energetically favored network sites hence strengthening and coarsening the network as a result (Maleki, 2016).

Parameters like pH, time and temperature are the most influential factors that affect the aging procedure. Furthermore, most of the properties of the gels like pore size, porosity, and surface area change during aging. Aging is as an easy and reliable procedure to strengthen the network of the aerogel (Maleki, 2016).

3.3.2.7. Drying

Special drying methods need to be applied to ensure that the solid network structure is maintained when the pore liquid is replaced with air (Gurav et al., 2010). It is very important that the drying of the silica aerogel is carried out in a way that does not result in any failure of the original porous structure. Supercritical drying using alcohol or carbon dioxide and ambient pressure drying are some of the drying techniques used

(Maleki, 2016). These methods result in a monolithic sample and are briefly discussed below:

i) ***Supercritical drying*** – This is the most proper and efficient method of drying wet gels by using supercritical conditions to remove the pore liquid. During this process the wet gel is placed in a closed pressure vessel so that its temperature and pressure can overpass the critical point of the solvent in the pore of the wet gel. Capillary stresses do not occur in this technique hence there are no cracks formed in the resultant solid gel structure. The conditions for supercritical drying vary depending on the solvent being used. The most common solvent used in this technique is carbon dioxide as it offers more safe and convenient conditions compared to when alcohol is used (Maleki, 2016). This method has some drawbacks in that it is energy intensive and dangerous making real practice and commercialization difficult (Shi et al., 2006).

ii) ***Ambient pressure drying*** – This is a promising, easy and safe technique for drying the wet gels and furthermore it offers a reasonably costing technique (Shi et al., 2006). The ambient temperature and pressure conditions are more suitable for both small scale and industrial production. One drawback for this method is that the surface of the pores of the gels need to be modified using non-polar groups to prevent further compressions by capillary stresses. Furthermore, the solvent in the pores must be exchanged with a solvent of less surface tension to avoid capillary stresses on the pore walls. The repulsion caused by the non-polar groups create a spring back effect in the gel whereby the dried gel recovers its original dimensions (Maleki, 2016).

3.3.2.8. Surface Modification

As previously mentioned, the hydrophilic nature of silica aerogel has some drawbacks. It is therefore necessary to undertake some surface modification reactions to remedy this and turn the silica aerogel surface hydrophobic. The new hydrophobic silica

aerogel can then be used in numerous applications like absorption of organic liquids and oils, biotechnological applications and adsorption of toxic materials (Mahadik et al., 2011).

The main reason for surface modification is that the surface silanol groups (Si-OH) undergo condensation reactions which results in irreversible shrinkage in the gel during the drying process. Therefore, an appropriate surface modifying agent is required to make the aerogel hydrophobic. These agents include trimethylchlorosilane (TMCS), methyltrimethoxysilane (MTMS) and hexamethyldisilazane (HMDZ) (Gurav et al., 2010).

Surface modifying agents work by replacing the surface polar -OH groups with a non-polar -CH_3 group (Mahadik et al., 2011). This step is very important especially when using the ambient pressure drying method as the hydrophobic nature of the aerogel is more stable against atmospheric humidity hence reduces chances of gel shrinkage (Rao et al., 2005). This reaction can be summarized in Figure 3.6 when TMCS is used as the modifying agent as is the case for this study.

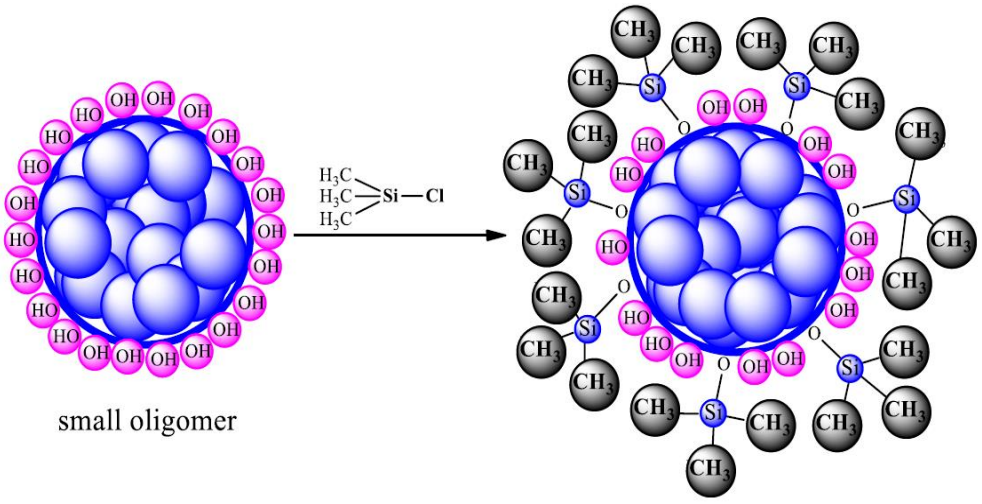

Figure 3.6 Effect of TMCS as a surface modifier on silica aerogel (Li et al., 2015).

3.4. Applications of Silica Aerogels

1) Silica Aerogel as a catalyst. Since silica aerogel has a high surface area, it can be used as a chemical absorber in cleaning up spills. This high surface area also makes it suitable to be used as a catalyst or catalyst support. It can be used in heterogenous catalysis where the reactants can be either gas or liquid. The high surface area per unit mass and high porosity of silica aerogel make it very suitable for catalysis (Gurav et al., 2010).
2) Thermal insulating (transparent) aerogels. Silica aerogels can be used for transparent thermal superinsulation in buildings (double windows). This results in energy savings in both domestic and plant heating systems in the northern hemisphere and thus has better environmental compatibility due to the release of fewer pollutants like greenhouse gas (CO_2), and also NOx and SOx effluents (Pajonk, 2003).
3) Cosmic dust collection by silica aerogels. The collection of comet dust is a major area of interest for planetary scientists. Transparent silica aerogels are used to capture comet dust that travels at very high velocity while still intact. The low density, transparency, high surface area, stability to ultra violet radiation and low thermal conductivity make silica aerogels suitable for this endeavor (Pajonk, 2003). For example, NASA used silica aerogel to collect the dust from a comet during its Stardust mission (S.A et al., 2016).
4) Environmental clean-up. Silica aerogels can be used in air cleaning. This is done through the adsorption of CO_2 from atmospheric air, industrial and municipal. It can also be used in the adsorptive removal of volatile organic contaminants. Finally, it can also be used in the water treatment process to adsorb oil and other hazardous organic compounds and heavy metal ions. The aforementioned contaminants are major pollutants currently that cause serious environmental problems like global warming and hazards for human health (Maleki, 2016).
5) Used in shock wave studies at high pressures (Rao et al., 2005).

6) Silica aerogels are also used in high energy physics to manufacture Cerenkov radiation detectors (Rao et al., 2005).

CHAPTER 4

PYROLYSIS OF POLYMERS

4.1. Introduction

Plastics are some of the most commonly used household materials due to their versatility and relatively low cost leading to a large global annual production hence a significant amount of plastic waste is left behind. This ever-increasing accumulation of plastic wastes results in environmental pollution problem hence the disposal of plastic waste becomes an important issue due to the non-biodegradability of the plastics. To overcome this problem, several disposal methods for plastic waste have been developed throughout the years.

4.2. Classical Disposal Methods for Plastic Waste

These methods have been used in the disposal of plastic waste materials for many years. However due to their simple nature they are not very effective in properly and efficiently disposing off plastic wastes. These methods include incineration, landfilling and mechanical recycling.

Incineration is a waste treatment process involving the combustion of organic materials that are present in the waste. Through this process the plastic waste is converted into ash and flue gas. The incineration of plastic waste is not a desirable disposal method due to the emission of greenhouse gases and ash formation. This process leads to the problem of smoke formation and has become a source of breathing problem for living organisms. This process is not very efficient as it transfers one problem (plastic waste) into another problem (air pollution). There is also the problem of locating the incinerating factories. These plants should be located as far away from

human settlements as possible and this makes this process expensive due to the treatment of the effluent gasses and construction of these plants.

Another method used in the disposal of plastic wastes is called landfilling which is the oldest form of waste treatment. In this method, the plastic wastes are buried into the ground to decompose. Since some plastics are non-biodegradable, landfilling becomes a problem due to the accumulation of these plastics in the ground. Furthermore, the degradation of some polymeric materials can lead to the formation of harmful chemicals that can contaminate the surrounding soil and may also poison the underground water supply. For example, polyvinyl chloride (PVC) upon degradation can lead to the formation of hydrochloric acid (HCl) which is poisonous to organisms that ingest it. Due to the bulky nature of plastic wastes, a large tract of land is needed for landfilling. This leads to an increase in landfilling costs as land is in limited supply and competes with other economic and social activities like farming, housing and industrial constructions

4.3. General Information about Pyrolysis

Pyrolysis is a tertiary recycling method where polymers are converted into liquid oil, char and gaseous products at high temperatures using thermal decomposition (Miandad et al., 2016).

The pyrolysis reaction can be performed at different range of temperature, reaction times and pressures. Additionally, reactive gases, liquids and catalysts may be used in the pyrolysis processes. The pyrolysis of plastic materials can be carried out at temperature ranging from low (<400^{o}C) to high (>600^{o}C) temperatures. Pressure conditions for the pyrolysis reaction can be atmospheric, however when thermally unstable products are formed, sub atmospheric i.e. vacuum conditions can be applied (Aydemir, 2010).

Thermal degradation leads to products that are generally gaseous, liquid and char. The amount of these products depends on type of polymer degraded, mixture ratio of the feed and reaction conditions. The gaseous and liquid products contain a mixture of several organic compounds (Aydemir, 2010).

Since the pyrolysis reaction leads to degradation of the polymeric material this means that bond breaking occurs. For this reason, a large amount of heat needs to be supplied to the system hence pyrolysis reaction is an endothermic one. However, an alternative method of partial oxidation can be carried out, but the products are diluted by oxidation (Aydemir, 2010).

Some of the limitations of pyrolysis include high energy consumption as the process requires high temperatures. The liquid obtained also contains impurities and residues which requires further cleaning. The further cleaning increases production cost (Miandad et al., 2016).

4.4. Non-Catalytic Pyrolysis

As the name suggests, no catalysts are used in this type of pyrolysis and heat is applied to yield any breaking of the polymeric bonds. The pyrolysis of the plastic waste generally involves the thermal decomposition of large macromolecules into smaller molecular chains in the absence of air/oxygen (Almeida et al., 2015).

The type of the plastic used plays an important role in this process. Condensation polymers like PET and nylon can be turned into their respective monomer units using various depolymerization techniques. For vinyl polymers like PE and PP, it is difficult to degrade them to their monomer units due to the random splitting of the carbon bonds in the polymer chain. Non-catalytic pyrolysis results in a wide product variety and require very high operating temperature ranging from 500ºC to 900ºC. This means that this process is extremely energy intensive and has low product selectivity. Further processing is also needed to improve the quality of the products (Singh et al., 2017).

The thermal degradation of the large polymeric materials in the plastics results in a wide range of hydrocarbon products. These products range from non-condensable gas fractions, liquid fractions consisting of paraffins, olefins and aromatics and solid residue. These products range from hydrogen to coke (Almeida et al., 2015). Furthermore, the yield and concentration of these products are influenced by both the temperature and the time taken for the pyrolysis reaction. Almeida et al., (2015) further describes the pyrolysis process that proceeds according to radical chain reactions that have hydrogen transfer steps along with the gradual breaking of main chains. This mechanism involves the following stages: initiation, propagation and/or free radical transfer that is followed by the β chain scission and formation. When compared the thermal cracking of high-density polyethylene (HDPE) is more difficult than that of low-density polyethylene (LDPE) while PP is the easier than both HDPE and LDPE. This may be attributed to the high tertiary carbon content in PP.

The initiation step involves the homolytic breaking of the carbon-carbon bond. This may occur through random chain scission. PP and PE both undergo random chain scission. The second step is the hydrogen transfer reaction that form stable radicals. The final step is called the termination reactions which occur by disproportionation which can produce different olefins and alkanes. Moreover, branched products can be formed from the interactions between two secondary radicals or between a primary and secondary radical (Almeida et al., 2015).

The liquid oils produced through the non-catalytic pyrolysis contain large carbon chain compounds and have a low quality due to low octane number. Moreover, there is a large amount of sulphur, nitrogen, chlorine and phosphorus impurities (Miandad et al., 2016).

4.5. Catalytic Pyrolysis

Catalytic pyrolysis is a type of pyrolysis that uses catalysts hence it offers many advantages as compared to the non-catalytic pyrolysis. As mentioned in the previous section, the non-catalytic pyrolysis requires very high temperatures hence highly energy intensive and products have low quality. Furthermore, the products have a wide molecular weight distribution. By introducing a catalyst into the system, these drawbacks can be overcome.

The catalysts reduce the reaction activation energy hence the decomposition temperature is reduced to an efficient level as compared to the non-catalytic decomposition. In current global environment the energy efficiency of catalytic pyrolysis is very attractive to reduce operation costs in related industries and better environmental footprint. Furthermore, the reaction rate is higher in catalytic pyrolysis which means faster reaction time. There is also an improvement in the quality and distribution of products due to the presence of catalysts. This makes catalytic degradation a promising recycling method for polymer wastes (Miandad et al., 2016).

Homogeneous and heterogeneous catalytic systems can be used in polymer cracking reactions however heterogeneous catalysts are more widely used as they are easy to separate and recover once the reaction is finished. Zeolites, silica-alumina and mesostructured catalysts like MCM-41 are example of heterogeneous catalysts while Lewis acids like $AlCl_3$ are used as homogenous catalysts.

Zeolites have been widely used in the pyrolysis of PE and PP because they contain acid sites in its microporous structure which favor the hydrogen transfer reactions hence result in high conversions of gas at low temperatures in the range of 350-500^{0}C. This results in much more favorable operation conditions for the reaction (Almeida et al., 2015). The acid sites in these catalysts are mainly Lewis and Brönsted sites. However, since zeolites have smaller pore sizes as compared to the bulky and large polymeric molecules, they are not completely suitable for pyrolysis reactions. Mesoporous materials like MCM-14, SBA-15 and silica aerogel loaded with metal

ions offer good alternatives as they have much larger pore sizes which allow organic molecules to access acid sites.

4.6. Operating Conditions

Polymer pyrolysis significantly depends on the process variables and system's operating conditions. These conditions include temperature, pressure, reaction time, type of reactor and type of the catalyst used.

4.6.1. Temperature

Temperature is the most important parameter of any degradation reaction as it determines the rate and stability of the products. The quality and quantity of pyrolysis products are greatly affected by temperature as it alters the yield of gaseous and liquid products (Miandad et al., 2016).

Generally, high temperature (>600°C) and low pressure (i.e. vacuum) favor the production of low molecular weight gaseous products. On the other hand, low temperature (<400°C) and higher pressure favor the production of high molecular weight liquid products, larger number of secondary products and coke formation is seen. At a temperature of around 300°C, most plastic materials start to degrade but the presence of additives within commercial polymers may affect the pyrolysis temperature (Aydemir, 2010).

4.6.2. Reaction Time

The reaction time greatly depends on the temperature. The residence time of the reactants influences the type of products formed. (Aydemir, 2010).

4.7. Catalyst

Catalysts can be defined as special compounds or materials which are specifically chosen, designed and synthesized in order to influence the reaction mechanism being studied. Catalyst help fasten the reaction rate which helps efficiently reduce the

decomposition temperature as a result of the decrease in the activation energy of the reaction hence it is a good way to reduce cost by proper energy utilization (Miandad et al., 2016).

In addition to this, catalyst is used in pyrolysis reactions to improve the quality of the products. Three main points need to be considered when selecting a suitable catalyst to be used in a specific reaction i.e. selectivity, activity and stability (Aydemir, 2010).

4.8. Modes of Polymer Decomposition

The decomposition of polymers is a very complex process where numerous reactions occur simultaneously, and it is hard to define these reactions one by one. Furthermore, factors like molecular structure of the polymer, presence of complex chain systems within the polymer or presence of catalysts, initiators, etc. can influence the nature of these reactions.

The following is the list of modes of polymer decomposition (Aydemir, 2010).

- Unzipping: This involves decomposition of the polymeric molecule into its monomer units. An example is the unzipping of PMMA resulting in methyl methacrylate which is used in acrylic varnishes.
- Random fragmentation: In this type of decomposition, products of varying lengths from the main chain are formed. Polyethylene (PE) and polypropylene (PP) undergo random fragmentation. PE is fragmented into PE waxes that contain a high number of α-olefins while PP leads to more branched product mixture.
- Unzipping and random fragmentation: This is a combination of unzipping and random fragmentation modes. Polystyrene (PS) and polyisobutylene (PIB) decompose through these two steps. Through this method, PS is converted into styrene monomers.
- Elimination of simple stable molecules from adjacent atoms: This decomposition results in unsaturated charring residues. Upon decomposition polyvinyl chloride

(PVC) forms HCl, polyvinyl acetate (PVAc) forms acetic acid and polyvinyl alcohol (PVOH) forms water.

- Elimination of side chains: This decomposition applies to most thermosets and cross-linked polymers. The elimination of side chains results in cross-linking and a porous charred residue is formed. This residue also includes non-volatile additives.

CHAPTER 5

LITERATURE SURVEY

The accumulation of plastic wastes is a major cause of pollution around the world. There have been numerous techniques used to recycle or dispose of these wastes. In recent years, the use of catalysts has become more important in the recycling of plastic wastes. Catalysts help lower the activation energy for the thermal degradation of plastic wastes making the reaction conditions more manageable by lowering the reaction conditions. Furthermore, obtaining narrow molecular weight distribution of products is also an added advantage. However, more research is needed to find more suitable catalysts that offer better results for the pyrolysis of polymeric materials.

Shi et al., (2006) researched into a novel procedure that involves the ambient drying of silica aerogel synthesized using ethanol/hexane/trimethylchlorosilane (TMCS) solution for the surface modification of the silica wet gel. The TMCS is used to make the hydrophilic silica aerogel hydrophobic by modifying Si-OH group in the material into Si-CH_3. It was found that the use of ethanol/hexane/ TMCS solution resulted in the synthesis of light and crack-free silica aerogels that had a density of around 0.128-0.136 g/cm^3 and a porosity of around 94%. The synthesized silica aerogel was examined using SEM analysis. SEM results showed the spongy structure while the BET analysis revealed that the surface areas of the synthesized materials were around 559-618 m^2/g. The adsorption/desorption isotherms exhibited Type IV behavior which is indicative of a mesoporous structure which goes hand in hand with the SEM results. Further analysis by FTIR revealed peaks at 3435 and 1630 cm^{-1} showing physically adsorbed water, 1091 and 463 cm^{-1} are peaks that appear in all silica products and the peaks observed at 2963, 1256 and 846 cm^{-1} are due to the surface modification by TMCS indicating that the silica aerogel is hydrophobic.

In a study (Obali et al., 2011) it was observed that the performance of aluminium loaded mesoporous SBA-15 material depended on the source of aluminium used in the catalyst synthesis and the ratio of Al/Si in the catalytic degradation of polypropylene (PP). Like silica aerogel, SBA-15 is also a silica based mesoporous material. Aluminium sulphate and aluminium iso-propoxide with different Al/Si ratios were used as the sources of aluminium. The TGA analysis revealed that the activation energy for PP degradation significantly reduced from 172 kJ/mol (without catalyst) to a range of around 51-89 kJ/mol. It was also noted from the TGA results that the catalysts synthesized using aluminium sulphate as the aluminium source was more effective. From the BET analysis it was found that both the pure and aluminium loaded materials exhibited an adsorption isotherm that is Type IV which is characteristic of mesoporous materials. Further analysis was conducted using DRIFTS. This analysis of the pyridine adsorbed materials revealed the presence of both Lewis and Brønsted acid sites. Furthermore, it was concluded that the use of aluminium sulphate as an aluminium source led to the Brønsted acid sites being stronger than the Lewis acid sites.

A similar study was conducted by Aydemir et al. (2011) using TPA impregnated SBA-15 in the degradation of polyethylene. Well-ordered TPA loaded SBA-15 were synthesized using W/Si ratios of 0.10, 0.25 and 0.40 with surface areas of 323, 298 and 287 m^2/g, respectively. These catalysts exhibited Type IV isotherms with a H1 hysteresis. These catalysts were mesoporous as the pore diameter was around 6.5nm. It was proven by DRIFTS that loading TPA into SBA-15 resulted in creation of Lewis and Brønsted acid sites. TGA analysis of these synthesized materials showed that activation energy decreased with an increase in TPA loading. The non-catalytic degradation of PE had an activation energy of 136 kJ/mol while in the presence of 10%, 25% and 40% TPA loaded SBA-15 catalysts, the activation energies of PE degradation reaction was found to be 74, 60 and 62 kJ/mol, respectively.

A study related to the performance of acidic MCM-like aluminosilicate catalysts used in the pyrolysis of polypropylene (PP) was conducted by Obali et al., (2009).

Hydrothermal synthesis route was used to synthesize mesoporous aluminosilicate catalysts with different Al/Si ratios using different sources of aluminium like aluminium iso-propoxide and aluminium nitrate. The BET analysis of these synthesized materials showed that the surface areas were in the range of 520-1001 m^2/g and the adsorption isotherms were of Type IV which is expected for mesoporous materials. Further Nuclear Magnetic Resonance (NMR) analysis showed that the aluminium formed a tetrahedral framework in the catalyst's structure when aluminium nitrate was used as the aluminium source. TGA was used to obtain the activation energies of PP degradation reaction in the presence of the synthesized materials. Degradation of pure PP had an activation energy of 172 kJ/mole. When aluminium nitrite was used as the aluminium source in the catalysts, its activation energy was found to be in the range of 24-28 kJ/mole (Al/Si ratio: 0.02-0.16). On the other hand, aluminium iso-propoxide resulted in an activation range of 20-90 kJ/mole. The difference can be attributed to less incorporation of aluminium into the MCM-41 structure during the synthesis. The lower solubility of aluminium iso-propoxide compared to aluminium nitrite is also a factor for the different activation energy values

A polyethylene degradation reaction over mesoporous support loaded with alumina and TPA was conducted in a semi batch reactor at 390, 410, 430 and 460°C for 15 minutes using different metal loading percentages (Aydemir et al., 2013). When the reaction was carried out without any catalyst i.e. the non-catalytic pyrolysis, it was found that the selectivity of C_3 and C_4 hydrocarbons was high. However, when a catalyst was introduced it was observed that ethylene and C_4 hydrocarbon selectivities were significantly increased. In the non-catalytic pyrolysis, it was reported that hydrocarbons greater than C_{18} were observed. The use of catalysts leads to a decrease in the carbon number of the hydrocarbons in the liquid which was in the range of C_5-C_{14}. The liquid products had a low carbon number distribution in the catalytic degradation as compared to the non-catalytic degradation. For aluminium loaded catalysts it was noted that heavier hydrocarbons in the range of C_{13}-C_{18} decreased as both temperature and amount of aluminium loaded increased. By increasing the TPA

loading, the number of lighter hydrocarbons in the range of C_5-C_{12} increased. This was attributed to the decrease in the surface area of the catalyst with TPA loading. It was also reported that acid sites formed by metal loading played an important role in the PE pyrolysis. The impregnation of aluminium into the pure MCM-41 led to the formation of Brønsted acid sites. This increase in acidity led to a decrease in PE degradation temperature and furthermore it also decomposed heavier hydrocarbons into lighter ones as the initiation step in the degradation of PE occurs over Brønsted acid sites.

Ratnasari et al., (2017) conducted a study that involved a two-stage pyrolysis-catalysis of high-density polyethylene (HDPE). Nitrogen gas was used as a carrier gas and provided an inert atmosphere. Furthermore, nitrogen gas carried away the product gases through the reactor. The first stage involved the non-catalytic pyrolysis of the HDPE to produce gaseous products which were then carried by the nitrogen gas into the second stage. In other words, the first stage was to induce pre-cracking of the larger polymeric molecules to form smaller molecules which would then flow into the second stage. The second stage was the catalytic degradation of the gases produced in the first stage. This stage involved the use of a solid acid catalyst to produce gasoline in the range of C_8-C_{12}. In the second stage, a mesoporous catalyst (MCM-41) was layered on top of a microporous catalyst (ZSM-5) to maximize the conversion of the waste plastics into gasoline. In several runs the MCM-41 and ZSM-5 were used separately in the second stage. The use of only ZSM-5 catalyst resulted in a higher carbon number of gaseous products while pure MCM-41 yielded a high amount of oil products. The most desirable results were obtained when the catalysts were layered in an MCM-41: ZSM-5 ratio of 1:1 which resulted in the formation of 83.15wt% of oil products. The main gaseous products were ethene, propene, butene and butadiene whereas the liquid products mainly consisted of 95.85wt% aromatic compounds. 97.72wt% of the aromatic compounds obtained were found to be in the gasoline range of C_8-C_{12}.

Ahmad et al., (2015) studied the effect of temperature on the overall yield of polypropylene (PP) cracking and product (gas and oil) formation. For PP, it was observed that with an increase in temperature from 250 to 300°C, the overall yield increased from 86.32% to 98.66%. This was attributed to the ease in degradability of PP and a high proportion of tertiary carbons in PP which promote thermal cleavage of C-C bonds. The liquid yield increased to a maximum value then decreased as temperature increased. From 250 to 300°C, liquid yield increased from 57.27 to 69.82%. A further rise in temperature from 350 to 400°C resulted in a decrease in liquid yield from 67.74 to 63.23%. The gaseous product yield was found to be in the range of 29–31% for the temperature range of 250 to 400°C. Solid residue changed inversely with an increase in temperature up to 300°C and then increased linearly after 300°C.

5.1. Motivation for this study

It was noted throughout the literature survey carried out for this study that there were virtually no articles that studied the use of metal loaded silica aerogel in the catalytic pyrolysis of polyethylene and polypropylene. Furthermore, there are no articles that studied the use of aluminium and/or TPA loaded individually or simultaneously into silica aerogel support in the catalytic pyrolysis of polymers like polyethylene and polypropylene. This highlighted the importance of this study as it offers a new and unique procedure in the recycling of polymeric materials like polyethylene and polypropylene.

The goals of this study are summarized as follows:

- To synthesize and characterize silica aerogel and silica aerogel impregnated with aluminium and tungstophosphoric acid.
- To determine the kinetic parameters of the degradation of both polyethylene and polypropylene using thermogravimetric analyzer (TGA).

- To test the activities of the synthesized catalyst and to get more information about the product distribution in polyethylene and polypropylene degradation reactions.
- To investigate the effect of aluminium and TPA loading amounts on the gas and liquid product distributions for the pyrolysis reactions of polyethylene and polypropylene.

CHAPTER 6

EXPERIMENTAL METHODS

The experimental study was divided into three main parts. In the first step, the catalysts have been synthesized and characterization of the catalysts has been carried out using several techniques such as BET, XRD, SEM, FTIR. Secondly, the activation energies of PE and PP degradation reactions over the synthesized catalysts were determined using the thermogravimetric analyzer. Finally, the pyrolysis experiments of PE and PP were performed to test the performance of these catalysts and get information about the product distribution of the liquid and gaseous products obtained. For the catalytic pyrolysis of PE, two experiments at different times with a reaction time of 15 minutes were carried out per catalyst at the same experimental conditions while for the catalytic pyrolysis of PP, three experiments at different times with a reaction time of 30 minutes were carried out at the same experimental conditions. Repeatability experiments were performed for both degradation reactions.

6.1. Synthesis and Characterization of Catalysts

In this part of the study the catalyst synthesis method and the several characterization techniques carried out are discussed briefly. The catalysts were synthesized to be used in the degradation of both PE and PP. Aluminium and tungstophosphoric acid (TPA) were loaded into the silica aerogel individually or together into the same silica aerogel support. The synthesized materials were characterized using several techniques: X-ray diffraction (XRD), energy dispersive spectroscopy (EDS), nitrogen physisorption, scanning electron microscopy (SEM), and Fourier transform infrared spectroscopy (FTIR).

6.2. Synthesis of Silica Aerogel Material

Silica aerogel was synthesized using sol-gel technique which was carried out in two steps. The first step involved an acid catalyzed step called hydrolysis reaction followed by a base catalyzed reaction step referred to as condensation reaction. Tetraethylorthosilicate (TEOS) was used as the silica precursor while trimethyl chlorosilane (TMCS) was used for surface modification.

6.2.1. Synthesis Procedure for Silica Aerogel Material

Before the synthesis was carried out, the first step involved the preparation of the following chemicals, 100 mL 1M ammonia (NH_3, 25% v/v, Merck), 100 mL 1M hydrochloric acid (HCl, 37% v/v, Merck) and 100 mL ammonium fluoride (NH_4F, Merck). Ammonia acts as a basic catalyst while HCl is the acidic catalyst. NH_4F is the gelling agent.

The first step of the synthesis involved the addition of 1.73 g distilled water, 5.64 g ethanol (Sigma Aldrich), 10.01 g TEOS (Merck) and 62 µL HCl in order. This is the hydrolysis reaction step and this mixture was stirred in an airtight beaker at room temperature for 2 h. Then 3.85 g distilled water, 9.92 g ethanol, 650 µL NH_3 and 800 µL NH_4F were added but mixture was gently stirred during addition of NH_4F which was done drop wise. This constituted the condensation step. The gel was formed in this step. This gel was then cut into smaller pieces and ethanol was added to fully cover the gel. The contents were then left to rest at room temperature for 8h. After this, the ethanol was removed and 30 mL of hexane (Sigma Aldrich) was added. The gel was then put into a water bath at 45°C for 2 h. Following this, hexane was removed, another 30 mL hexane was added followed by TMCS. At this point HCl fumes were observed hence this step was carried out in a fume hood. The hexane-water mixture was then separated from the gel and the hexane part was carefully re-added to the gel and the contents were re-placed into the water bath at 45°C for 5 h. The hexane was removed again and another fresh 30 mL hexane was added to the gel and placed into water bath at 45°C for another 5 h. Finally, the hexane was removed and the beaker

containing the gel was placed into an oven at 125°C for 2 h after drying the gel was crushed, weighed and stored in a dry container. The summary of silica aerogel synthesis is shown in Figure 6.1.

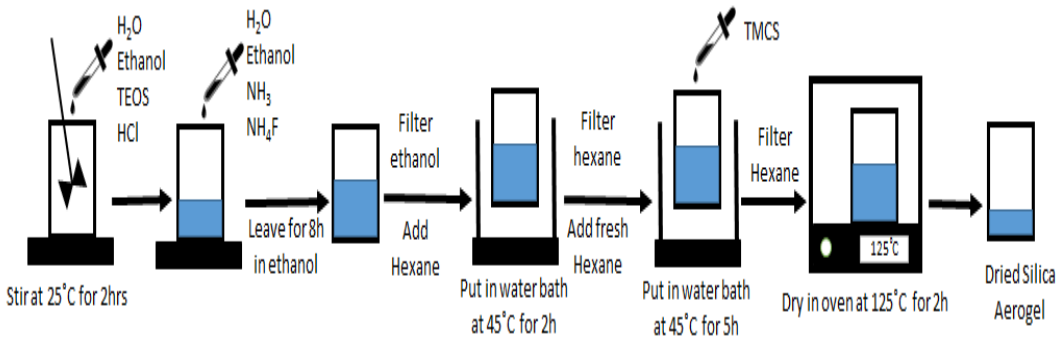

Figure 6.1 The summary of silica aerogel synthesis.

6.2.2. Incorporation of Aluminum into Synthesized Silica Aerogel Material Using Impregnation Method

Aluminium iso-propoxide (Merck) was used as the aluminium source and was loaded into the silica aerogel structure using the impregnation method. Firstly, 1 g of silica aerogel support was dispersed in ethanol and stirred at room temperature for 2 h. According to the desired Al/Si molar ratio, determined amount of aluminium iso-propoxide was dissolved in ethanol and stirred at room temperature for 2 h. The calculation for amount of aluminium loaded is given in Appendix A.

Then, as the silica source was being stirred, aluminium source was added drop wise to the solution and the obtained mixture was kept stirred for 24 h. Finally, the mixture of ethanol, aerogel and metal source was kept in the oven at 125°C for 5 h to obtain aluminium loaded silica aerogel catalyst. Figure 6.2 represents the procedure for synthesis of aluminium loaded silica aerogel catalysts.

The aluminium loaded silica aerogel catalyst was then calcined in a quartz tubular reactor which was heated in a tubular furnace under dry air at a flow rate of 80 mL/min. The furnace temperature was set at 450°C with a heating rate of 1°C/min for 6 h.

6.2.3. Incorporation of Tungstophosphoric Acid into Synthesized Silica Aerogel Material Using Impregnation Method

As in aluminium loading, TPA was also loaded into silica aerogel using impregnation method. Phosphotungstic acid hydrate (Acros Organics, code: 208311000) was used as the TPA source. Firstly, 1 g of silica aerogel support was dispersed in ethanol and kept stirred at room temperature for 2h. According to the desired W/Si molar ratio, determined amount of TPA was dissolved in ethanol and stirred at room temperature for 2h. The calculation for amount of TPA loaded is given in Appendix A.

Then, as the silica aerogel solution was being stirred, TPA previously dissolved in ethanol was added drop wise to the solution and the mixture was kept stirred for 24h at room temperature. Finally, the mixture of ethanol, silica aerogel and TPA was kept in oven at 125^{o}C for 5h to obtain TPA loaded silica aerogel catalyst. Figure 6.2 is a summary of the TPA loading procedure into silica aerogel.

The TPA loaded silica aerogel catalyst was then calcined in a quartz tubular reactor which was heated in a tubular furnace under dry air at a flow rate of 80 mL/min. The furnace temperature was set at 350°C with a heating rate of 1°C/min for 6 h.

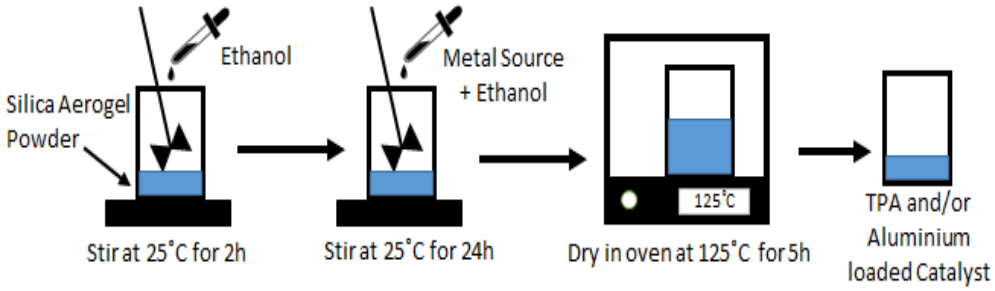

Figure 6.2 Steps in the synthesis of metal loaded silica aerogel support.

6.2.4. Catalyst Nomenclature

The metal loaded catalysts are named depending on their loading percent. The loading percent in terms of moles. The general naming method is SA-XR where SA stands for the support material which is silica aerogel and X is the numeric value of metal mole percent in the support and R is the metal ion. For example, SA-7Al is silica aerogel loaded with 7 mole percent of aluminium. For double metal loaded catalyst, SA-XR-YS is used where the additional Y and S represent mole percent of second metal ion and the metal ion, respectively. For example, SA-7Al-3W is silica aerogel loaded with 7 mole percent aluminium and 3 mole percent TPA.

6.3. Characterization Techniques for the Synthesized Materials

The physical, chemical and structural properties of the synthesized materials were determined using several techniques: X-Ray Diffraction, Energy Dispersive Spectrometry, Nitrogen physisorption, Temperature-Programmed Desorption, Scanning Electron Microscopy and Fourier Transform Infrared Spectroscopy.

6.3.1. X-Ray Diffraction (XRD)

This method was used to obtain information about the structural regularity of the synthesized materials. This analysis was carried out at METU Central Laboratory using a Rigaku Ultima-IV X-ray Diffractometer. The wide angle XRD patterns were obtained in the Bragg angle values in the range of 10-90° with a step size of 1°C/min. During the operation, the voltage and current were 20 kV and 40 mA, respectively.

6.3.2. Nitrogen Physisorption

The nitrogen adsorption technique was used to determine the physical properties like surface area, pore diameter, pore volume and pore size distribution of the synthesized materials. Multipoint BET surface area measurement, adsorption/desorption isotherms and the materials' average pore size were measured using the Micrometrics

Tristar II 3020 equipment. The samples were degassed at 200°C for 3 h prior to the analysis.

6.3.3. Ammonia Temperature-Programmed Desorption (TPD)

Ammonia-TPD analysis was conducted in the Kinetic Lab of the Chemical Engineering Department at METU using the Micromeritics TPx System. This technique was used to determine the acid capacity of the synthesized catalyst. The catalyst was subjected to argon gas with a flow rate of 50 mL/min at 200°C for 1 h. The sample was then cooled to room temperature and the flow of 5% ammonia in helium gas was started at a rate of 50 mL/min for 1 h. After this argon flow over the catalyst was carried out at 50 mL/min for 15 min at room temperature to purge ammonia. The catalysts were heated from room temperature to 125°C with a heating rate of 30°C/min. The helium flow rate was 30 mL/min. Subsequently the heating rate was lowered to 10°C/min and the sample was heated from 125°C to 600°C under helium flow of 30 mL/min.

6.3.4. Diffuse Reflectance Fourier Transform Infrared Spectroscopy (DRIFTS)

DRIFT spectra of the synthesized materials were obtained using Perkin Elmer-Spectrum One FTIR spectrometer in the wavelength range of 400-4000 cm^{-1}. In order to observe the nature of the acid sites located on the synthesized materials, DRIFTS analysis was carried out using pyridine free and pyridine adsorbed samples.

Before the analysis was done, two samples from each synthesized material were measured. These samples were then put into an oven at 110°C for 12 h. After this period the non-pyridine samples were ready for analysis in the machine. 0.1 g of the sample was mixed with 1 mL of pyridine and put into an oven at 40°C for 2 h to allow pyridine to evaporate. Finally, for the information on the acid sites of the synthesized materials, the spectra of pyridine free sample were subtracted from the spectra of pyridine adsorbed sample.

6.3.5. Inductively Coupled Plasma Mass Spectroscopy (ICP-MS)

ICP was done to obtain information about the type of metal present in a sample and weight percent of the metal. This analysis was done in the METU Central Lab using the Perkin Elmer DRC II. The samples were dissolved in HNO_3, HCl and HF before the start of the analysis.

6.3.6. Scanning Electron Microscopy (SEM)

Morphology of the catalysts was analyzed at the METU Central Lab using a QUANTA 400F field scanning electron microscope. The samples were prepared in two steps. These steps involved adhesion of material on a carbon tape and coating with gold and palladium (Au/Pd). A trace amount of the synthesized material was spread homogeneously on the surface of the carbon tape to get as thin coating as possible. Secondly, the materials were coated with Au and Pd for the analysis.

6.3.7. Energy Dispersive Spectroscopy (EDS)

The energy dispersive spectroscopy was used to determine the elements within the synthesized materials. EDS detects X-rays emitted from the sample during bombardment by an electron beam to characterize the elemental composition of the analyzed volume. EDS was carried out using JSM 6400 Electron Microscope equipped with NORAN system 6X-Ray Microanalysis System & Semafore Digitizer. All the samples were coated with Au and Pd for the analysis.

6.4. Thermogravimetric Analysis (TGA)

For this test the polymers, PE (Aldrich Co.) of M_n 1,700, density 0.92 g/mL and a melting point range of 90-110°C and PP (Aldrich Co.) of M_n 67,000, density 0.9 g/mL and a melting point range of 160-165°C were used.

Thermogravimetric analysis experiments were performed under nitrogen atmosphere having a flow rate of 60 cc/min, in the temperature range of 30-550°C with a constant heating rate of 5°C/min. Testing samples were prepared with a catalyst to polymer

weight ratio of 1/2. The Shimadzu DTG-60H equipment located in the METU Chemical Engineering Department was used to carry out TGA analysis.

The used catalyst obtained at the end of the pyrolysis experiment was analyzed using thermogravimetric analyzer. The analysis was carried out under air at 60 cc/min with a heating rate of 5°C/min and temperature range from room temperature to 900°C. This analysis was carried out to find out the amount of coke formation per catalyst used for both PE and PP degradation.

6.5. Polymer Degradation Reaction System

6.5.1. Pyrolysis system

The experimental setup for the pyrolysis reaction is given in Figure 6.3. A nitrogen tank was present in the pyrolysis system. It was used as the carrier gas. The carrier gas provided good mixing of the catalyst and polymer. The nitrogen tank was connected to a rotameter (Cole-Parmer) which was used to adjust the gas flow rate to the desired value. The gas entered the reactor from the bottom part of the reactor, which was located inside a tubular furnace which was heated using an electric furnace (Protherm PTF 12/105/700). Insulating material was used to cover the furnace to prevent heat loss from the system to the surroundings.

There were two glass reactors used, one for PE and the other for PP pyrolysis experiments. The reactor for PE pyrolysis was 113 cm in length and 1.1 cm in diameter. The spiral part was 39 cm long and the porous part (sample holder) was 43.5 cm from the top of the reactor. For PP pyrolysis, the reactor was 116 cm long and 1.1 cm in diameter. The spiral part was 62 cm long while the porous part (sample holder) was 24 cm from the top of the reactor.

The reactor was mainly composed of three parts. Firstly, the bottom part of the reactor consisted of a spiral part that increased the contact time of the flowing gas for efficient heating. This spiral portion contained tiny glass particles that increased the contact

time. Above the spiral part, there was a special porous glass where the mixture of the polymer and catalysts were placed. The porous glass provided good dispersion of gas in the reactor and to prevent any backflow of the polymer melt. A thermocouple was inserted into the reactor to measure the reaction temperature. The third and the upper part of the reactor was cylindrical in shape and connected to the condenser by a steel pipe that was covered with a heating tape and insulation material.

The reactor outlet stream was to be heated up to the reaction temperature in a pipe covered with a heating tape to prevent early condensation of the products before reaching the condenser. A thermocouple in this location was connected to a temperature controller in order to control the heating tape temperature.

The vapors from the reactor were sent to the spiral condenser where the non-volatile products were collected inside glass vessels surrounded by water cooling jackets. Water at -12°C was circulated through the condenser for this purpose. The non-condensed gaseous products were collected in the gas sampling bulb and with the help of an injector the gas samples were taken from the gas sampling bulb and analyzed in a gas chromatograph. A soap bubble meter that measured the gas flow rate was connected to the outlet stream of the gas sampling bulb. The gas stream was then passed out to the vent.

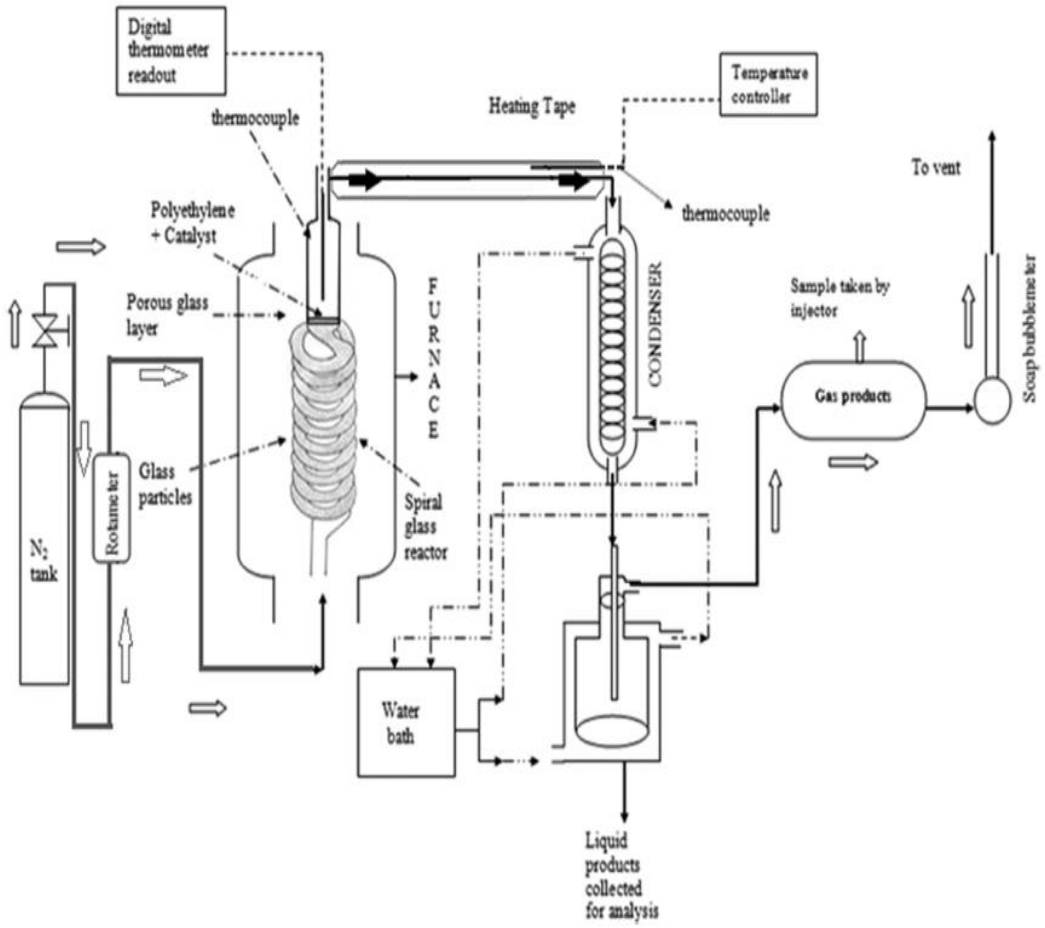

Figure 6.3 The experimental set-up for the degradation of polyethylene and polypropylene (Aydemir, 2010).

6.5.2. Experimental Procedure

At the beginning of the analysis, depending on the nature of the reaction, the polymer-catalyst mixture was fed to the reactor from the upper part. In catalytic pyrolysis a mixture of 1.0 g of polymer and 0.5 g of catalyst was used. The same amount of polymer was used in the non-catalytic pyrolysis experiments. After the polymer or polymer-catalyst mixture was placed into the reactor, the thermocouple was inserted into the reactor, and the system was tightly closed using the fitting at the upper part to

prevent any gas leakage. The system is then checked for any gas leakage. After this step the nitrogen flow rate was adjusted to 60 cc/min.

After this, the furnace was adjusted to the desired reactor temperature with a constant heating rate of 5°C/min. The temperature of the pipe wrapped with a heating tape and connecting the exit stream of the reactor to the inlet stream of the condenser was adjusted to the reactor temperature. The condenser was cooled with the water coming from the water bath, which was adjusted -12°C.

During the experiment, at intervals of 15 min, the flow rate and temperature of the furnace, reactor, and water bath were checked in order to obtain reliable data. Gas samples were collected with the gas sampling bulb during the experiment. Liquid samples and solid residue/catalysts were collected after the system was cooled down to room temperature.

Polymer remaining in the residue was collected by turning the reactor upside down and reheating it in the furnace until the remaining material melted while only catalyst remaining in the solid residue was easily collected by turning the reactor upside down and collecting the residue into a sample holder. The collected liquid products, catalyst and solid residue was weighed and recorded.

Table 6.1 summarizes the experimental conditions and number of experimental runs for the degradation of both polyethylene and polypropylene.

Table 6.1 Experimental conditions for the degradation of PE and PP.

Material	Furnace Temperature (℃)	Reaction Temperature (℃)	Time (min)	Number of experimental runs
Pure PE	460	450	15	2
Pure PE	540	430	15	2
PE + Pure SA PE + 7Al PE + 10Al PE + 7W PE + 10W PE + 7Al-3W PE + 3Al-7W	540	430	15	2
Pure PP	495	425	30	3
Pure PP	475	400	30	3
PP + Pure SA PP + 7Al PP + 10Al PP + 7W PP + 10W PP + 7Al-3W PP + 3Al-7W	475	400	30	3

6.5.3. Product Analysis Procedure

Analysis of the gas and liquid products were performed in a gas chromatograph (GC). Gas samples were taken from the gas sampling bulb using a gas-tight syringe during the reaction and injected to the gas chromatograph to be analyzed. Liquid products

were collected in the liquid collecting bottle and injected to the gas chromatograph using a microliter liquid syringe.

6.5.3.1. Analysis of Gas Products

Gas samples were routinely taken at several time intervals during the reaction. These samples were then analyzed using the GC equipment that had a packed column (Propac Q). The data was analyzed using the Varian Star Chromatography Workstation version 6.2 program. The conditions for the gas analysis are provided in Table 6.2.

Table 6.2 GC conditions for the analysis of gas products obtained from pyrolysis reactions.

Oven Temperature (°C):	80 (Isothermal)
Injection Temperature (°C):	110
Column Pressure (psi):	30
Detector Type and Temperature (°C):	TCD, 120
Carrier Gas:	Helium
Carrie Gas Flow Rate (mL/min):	30
Carrier Gas Pressure (psi):	75
Analysis Time (min):	35

6.5.3.2. Analysis of Liquid Products

The quantitative and qualitative chemical analysis of the liquid products were performed using gas chromatography equipped with HP-5 capillary column (28.5 m x 0.320 mm x 0.25 μm). The analysis conditions are summarized in Table 6.3. Varian Star Chromatography Workstation Version 6.2 program was used for the data analysis.

Table 6.3 GC conditions for the analysis of liquid products obtained from pyrolysis reactions.

Oven Temperature:	40°C (10 min hold) to 150°C at 5°C/min (15 min hold) then to 200°C at 1°C/min (70 min hold)
Injection Temperature (°C):	210
Injection Amount (µL):	0.5
Column Pressure (psi):	5
Detector Type and Temperature (°C):	FID, 225
Carrier Gas (mL/min):	Helium at 1.5
Split Ratio:	100:1
Analysis Time (min):	167

CHAPTER 7

RESULTS AND DISCUSSION

7.1. Introduction

This study deals with the investigation of the catalytic activity of metal loaded mesoporous silica aerogel in the degradation of polypropylene and polyethylene. The metal loaded silica aerogel catalysts were synthesized and characterized as explained in the experimental part. The performance of the synthesized catalysts was then studied in the degradation reactions for polyethylene and polypropylene. Non-catalytic polypropylene and polyethylene degradation reactions were also carried out for comparison purposes. Aluminium and tungsten were used as metal ions in this study.

7.2. Characterization of Catalysts

The physical and structural properties of the synthesized pure and metal loaded silica aerogel (SA) catalysts were determined using XRD, Nitrogen Physisorption, SEM, FTIR, DRIFTS, ICP and TPD Analysis.

7.2.1. Characterization Results of Mesoporous Silica Aerogel

7.2.1.1. XRD Results

Figure 7.1 shows the XRD pattern of pure silica aerogel support. There is a broad band at the 2θ value of 22° which indicates that the synthesized silica aerogel is in amorphous structure (Rida et al., 2014).

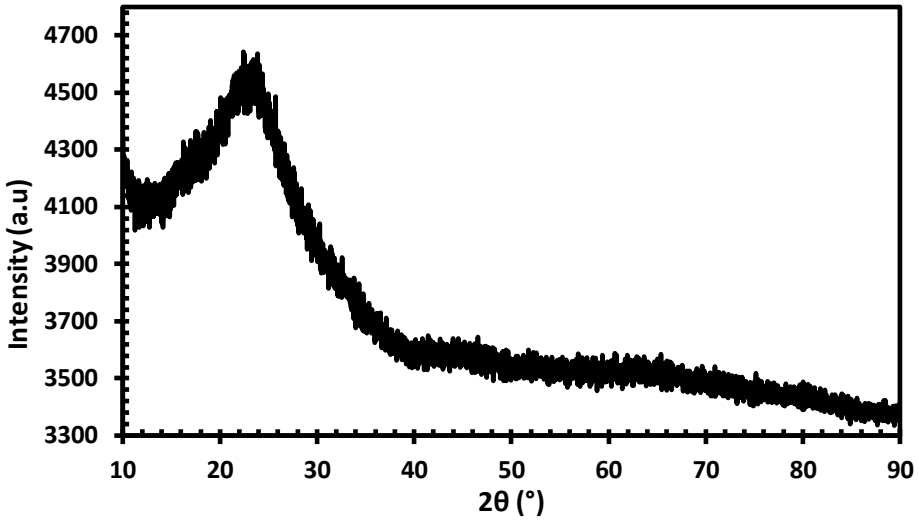

Figure 7.1 XRD pattern for pure silica aerogel.

7.2.1.2. Nitrogen Physisorption Results

Silica aerogel was synthesized four times in different batches. Their surface area, pore size, pore volume and microporosity were determined. The pore sizes are in the range of 10.6 and 11.8 nm. The average pore size was found to be 11.1 nm with a deviation of ±0.5. According to the IUPAC classification system, the synthesized silica aerogels are classified as mesoporous materials as their pore size values are within the range of 2–50 nm (Lowell et al., 2004). Similarly, their average desorption pore volume values were close to each other in the range of 3.21-3.76 cm^3/g. The average pore volume was found to be 3.53 cm^3/g with a deviation of ±0.23. Figure 7.2 shows the nitrogen adsorption/desorption isotherms for each of the synthesized silica aerogels. According to the classification of International Union of Applied Physics and Chemistry (IUPAC), all the silica aerogel support exhibited isotherms of Type IV which is characteristic of mesoporous materials with a H3 type hysteresis loop indicating presence of slit shaped pores (Aegerter et al., 2011 and Sivri et al., 2019).

Figure 7.3 shows the pore size distribution of pure silica aerogel supports using the BJH model. All the samples exhibited mesoporosity as the pore diameter range was

between 6-50 nm. However, all samples did show the existence of macropores in the silica aerogel structure.

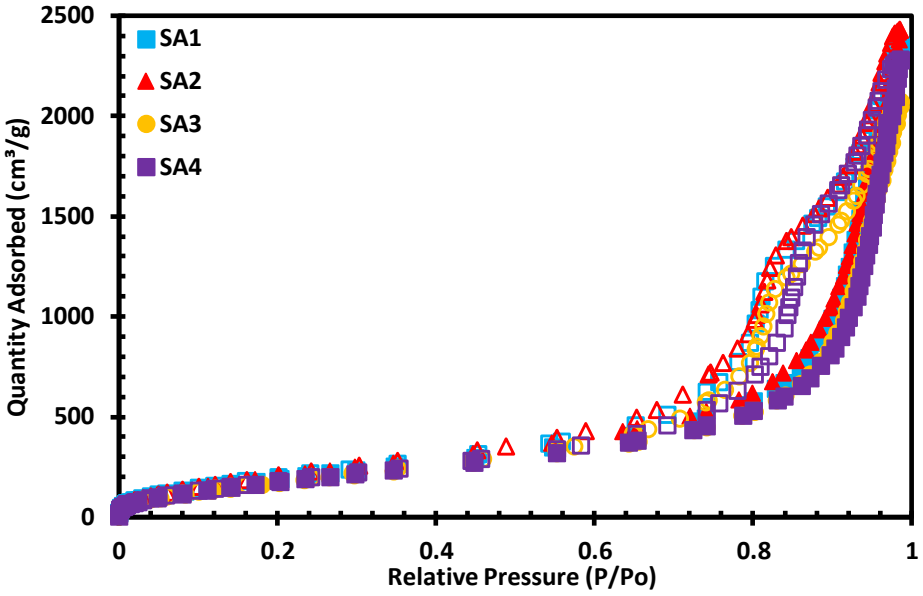

Figure 7.2 Nitrogen adsorption/desorption isotherms of the synthesized silica aerogel supports (filled dots: adsorption branches, empty dots: desorption).

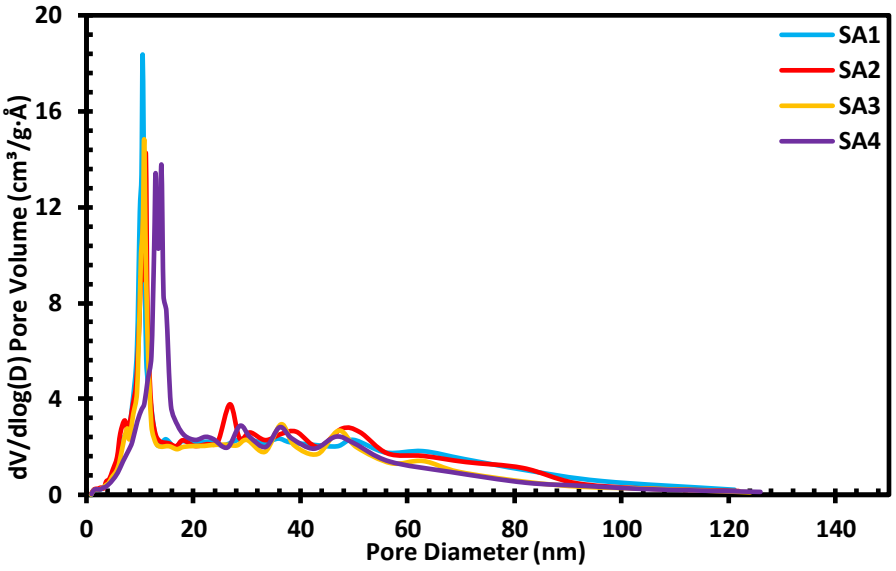

Figure 7.3 Pore size distributions of pure silica aerogel.

The physical properties of the synthesized silica aerogel supports are summarized in Table 7.1. These results showed that the synthesis of silica aerogel support resulted in reproducible data. The surface area of these materials was in the range of 720-840 m^2/g. The physical properties of pure silica aerogel support were in good agreement with the physical properties in the study conducted by Sivri et al. (2019). When the silica aerogel was compared with MCM-41 and SBA-15, its surface area is lower but its pore volume and pore size is higher than both MCM-41 and SBA-15 (Aydemir et al. (2016) and Obali et al. (2011)).

All the synthesized silica aerogel samples showed very low microporosity values. This is an attractive characteristic in the subsequent steps of metal impregnation and pyrolysis of polypropylene and polyethylene.

Table 7.1 The physical properties of the synthesized silica aerogel.

Sample ID	**BET Surface Area (m^2/g)**	**BJH Desorption average pore diameter (nm)**	**BJH Desorption cumulative volume of pores (cm^3/g)**	**Micro-porosity (%)**
SA1	795	11.1	3.63	3.7
SA2	839	10.7	3.76	4.2
SA3	723	10.6	3.21	4.3
SA4	730	11.8	3.53	4.7
Average	***772±55***	***11.1±0.5***	***3.53±0.23***	***4.2±0.4***

7.2.1.3. SEM Results

Figure 7.4 shows the SEM images of silica aerogel support at two different magnifications. Silica aerogel supports showed a spongy structure (Rida et al., 2014). The yellow circles on the SEM images show the different pore sizes. The aerogel support consists of different pore sizes which are in good agreement with the BET results that showed a large pore size distribution. This SEM image is similar to SEM image reported by Sivri et al. (2019).

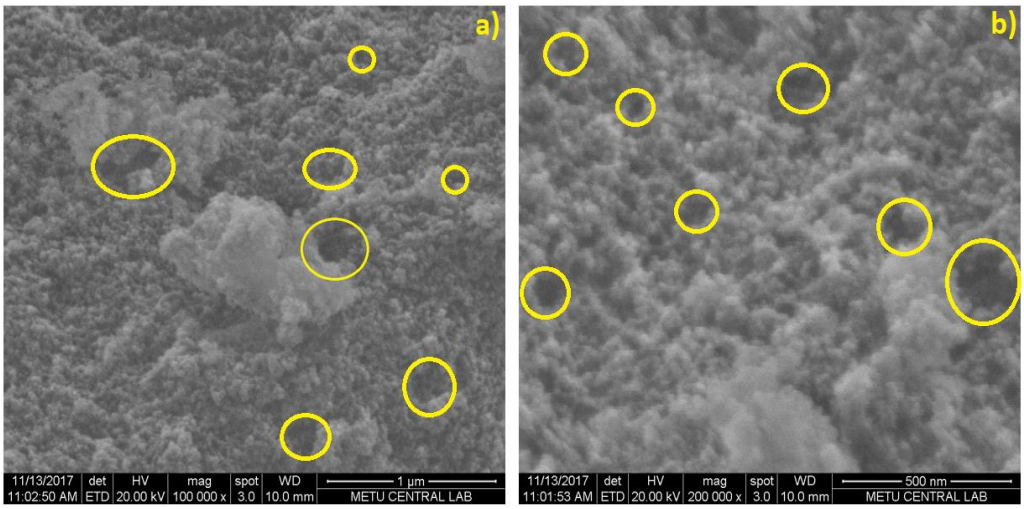

Figure 7.4 SEM images of silica aerogel support at (a) 100,000 and (b) 200,000 magnifications.

7.2.1.4. FTIR Results

The FTIR spectrum of silica aerogel support is shown in Figure 7.5. The strong band observed at 1078 cm^{-1} corresponds to the asymmetrical vibration of the Si-O-Si (siloxane) bond which forms the backbone of the silica matrix. The band at observed at 1078 cm^{-1} is characteristic of all silica products. This bond has a shoulder that appears at 1155 cm^{-1} which also corresponds to Si-O-Si bond. The peak observed at 758 and 809 cm^{-1} is due to the stretching vibration of Si-O-Si bond. The peaks observed at 548 and 958 cm^{-1} indicate the presence of stretching of the Si-O group (Sivri et al., 2019 and Rida et al., 2014).

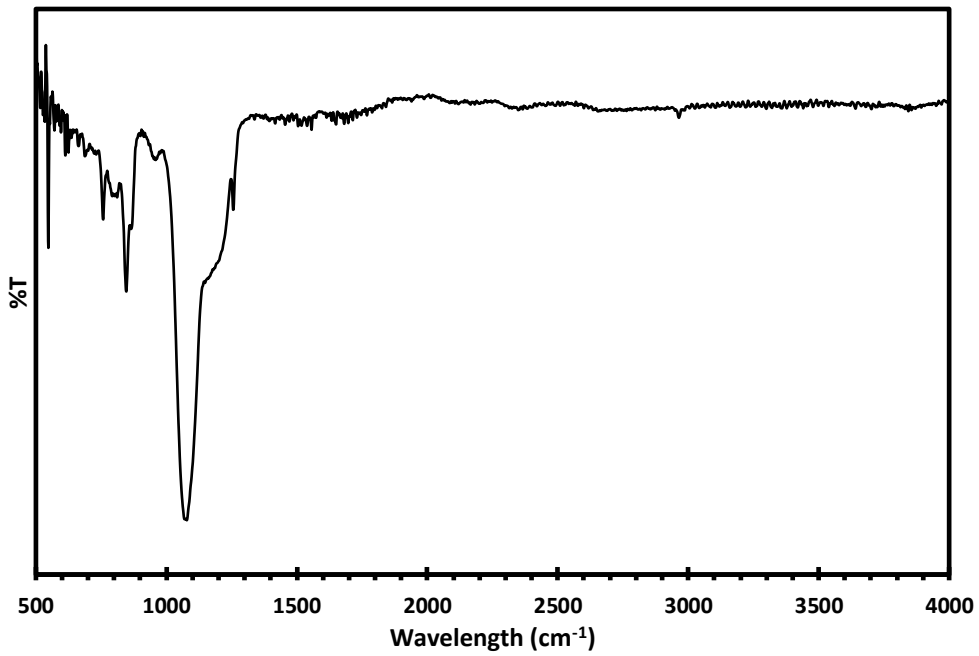

Figure 7.5 FTIR spectrum of pure silica aerogel.

The peaks observed at 1256 and 846 cm^{-1} correspond to Si-C bonds due to $-CH_3$ terminal groups which are introduced through surface modification by TMCS. This shows hydrophobic nature of the silica aerogel. The peak at 2963 cm^{-1} is the C-H stretching bond. (Shi et al., 2014). FTIR spectrum showed that the synthesized material is silica aerogel. This spectrum is in good agreement with the literature (Sivri et al., 2019, Rida et al., 2014 and Shi et al., 2014).

7.2.2. Characterization Results of Metal Loaded Mesoporous Silica Aerogel Catalysts

7.2.2.1. XRD Results

The XRD patterns of metal loaded catalysts are presented in Figure 7.6. For aluminium loaded catalysts, XRD patterns of silica aerogel support was preserved and aluminium ions were well dispersed in the silica aerogel structure. For TPA loaded catalysts, it is

not possible to say this. The catalysts loaded with high TPA percent except the SA-7Al-3W catalyst exhibited peaks at 2θ value of 26.9° and 36.8°. These peaks belong to the characteristic peaks of TPA. For TPA loaded catalysts, TPA was not well dispersed in the silica aerogel support except the SA-7Al-3W catalyst.

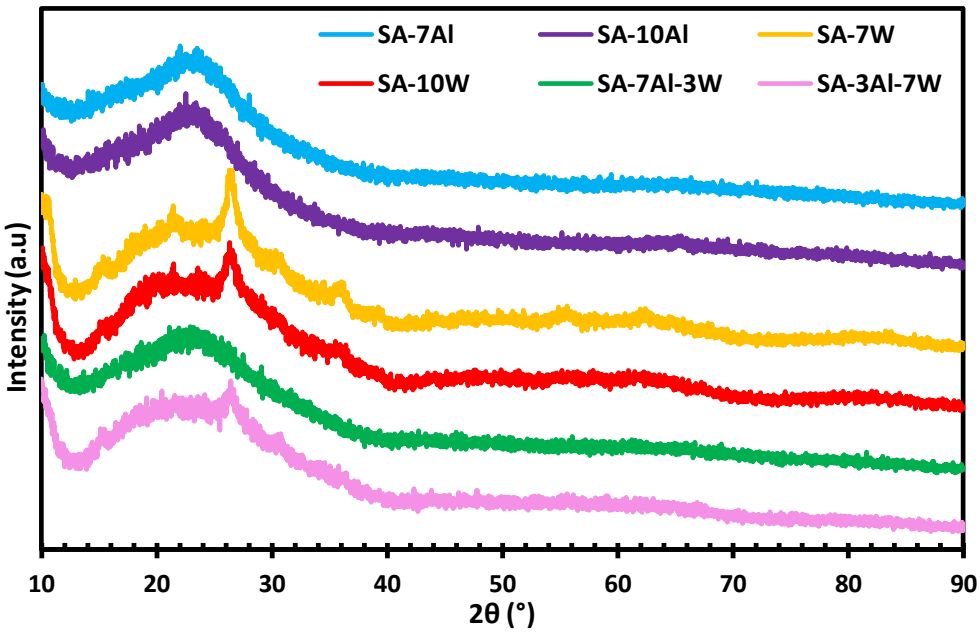

Figure 7.6 XRD patterns of metal loaded catalysts.

7.2.2.2. Nitrogen Physisorption Results

The nitrogen adsorption/desorption isotherms for aluminium loaded silica aerogel support are shown in Figure 7.7. The adsorbed N_2 volume decreased with addition of aluminium due to the blockage of pores with aluminium. Aluminium loaded silica aerogel catalysts exhibited Type IV with H3 hysteresis which indicates mesoporous structure and presence of slit shaped pores.

Figure 7.8 is the pore size distribution for aluminium loaded silica aerogel catalysts. It can be seen that the aluminium ions are located in both the mesopores and macropores within the support. BET analysis results revealed that the aluminium loaded silica aerogel catalysts were mesoporous materials.

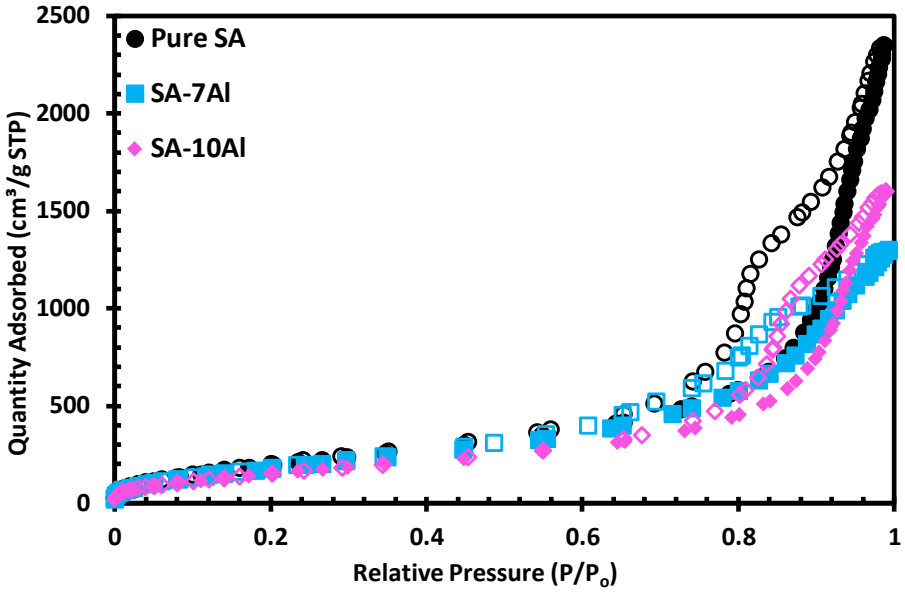

Figure 7.7 Nitrogen adsorption/desorption isotherms of aluminium loaded silica aerogel (filled dots: adsorption branches, empty dots: desorption branches).

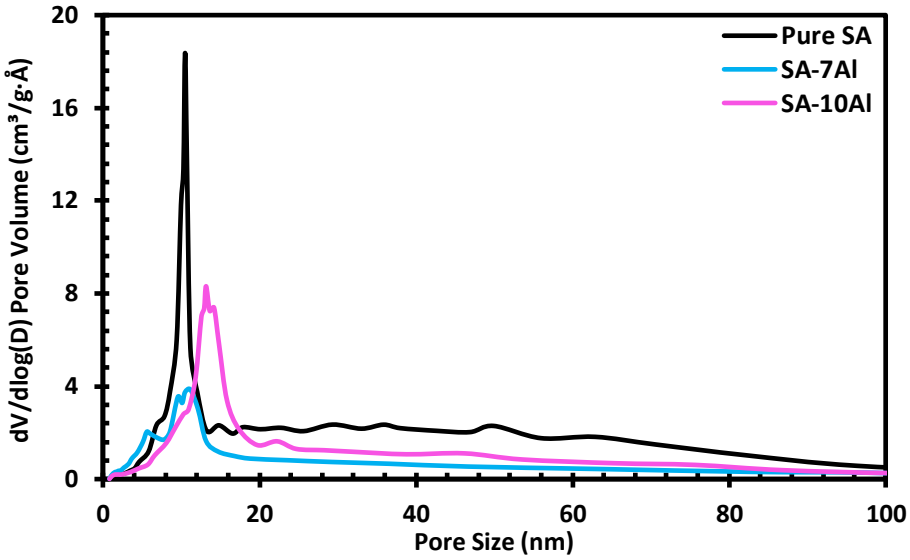

Figure 7.8 Pore size distributions of aluminium loaded silica aerogel.

N_2 physisorption isotherms of TPA loaded silica aerogel are presented in Figure 7.9. TPA loaded silica aerogels also exhibited Type IV isotherms with a H2 hysteresis loop. The adsorbed N_2 volume in the catalysts significantly decreased with an increase in TPA loading compared to aluminium loaded catalysts. This might be due to the blockage of pores with TPA.

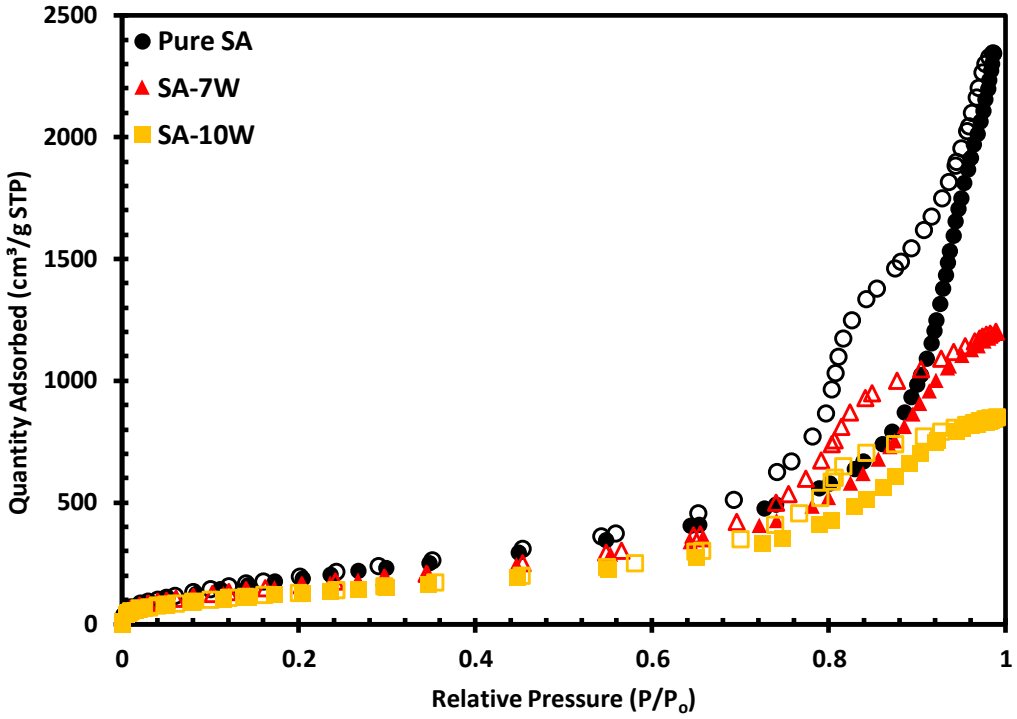

Figure 7.9 Nitrogen adsorption/desorption isotherms of TPA loaded silica aerogel (filled dots: adsorption branches, empty dots: desorption branches).

These TPA loaded catalysts mainly consist of mesopores as seen in Figure 7.10. With TPA loading, TPA was embedded in the macropores of the silica aerogel supports. Their average desorption pore diameter is in the range of 6.8-7.6 nm.

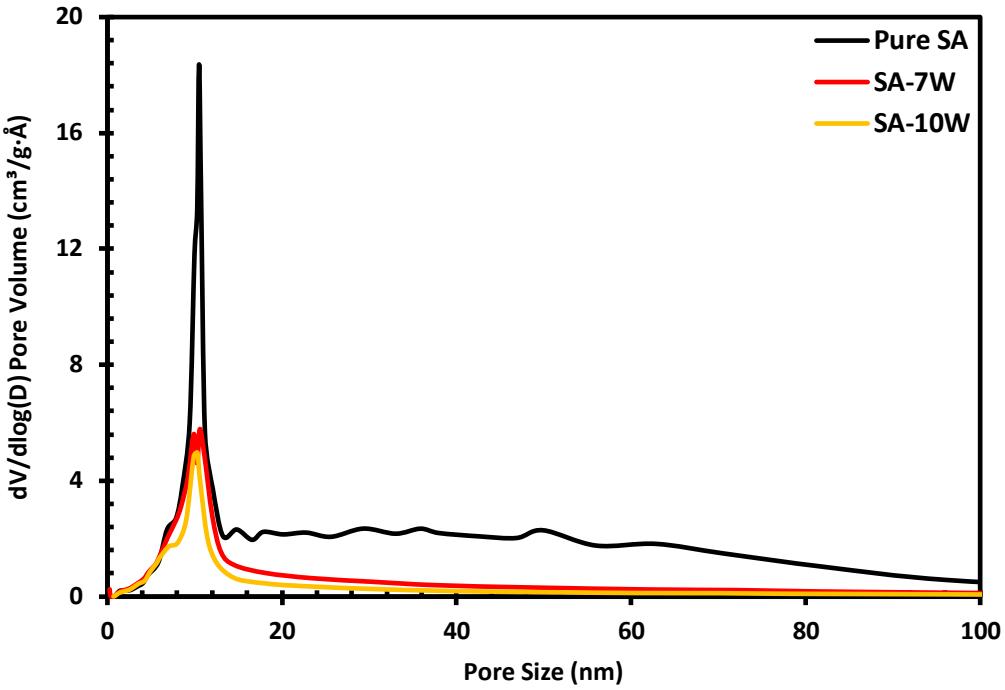

Figure 7.10 Pore size distributions of TPA loaded silica aerogel.

N_2 adsorption/desorption isotherm of double loaded metal catalyst is given in Figure 7.11. They exhibit Type IV isotherms but the hysteresis loops differ. The SA-7Al-3W catalyst has a H3 hysteresis loop indicating slit shaped pores while the SA-3Al-7W catalyst has a H2 hysteresis loop. A decrease in the adsorbed N_2 volume with metal loading into silica aerogel supports was observed due to blockage of silica aerogel pores with metal ions.

The pore size distribution of double metal loaded catalysts is presented in Figure 7.12. The average pore size of double metal loaded catalysts is in the range of 5.7-6.3 nm. TPA and aluminium ions were mainly embedded in the macropores of the support. BET results showed that all the metal loaded catalysts were mesoporous materials.

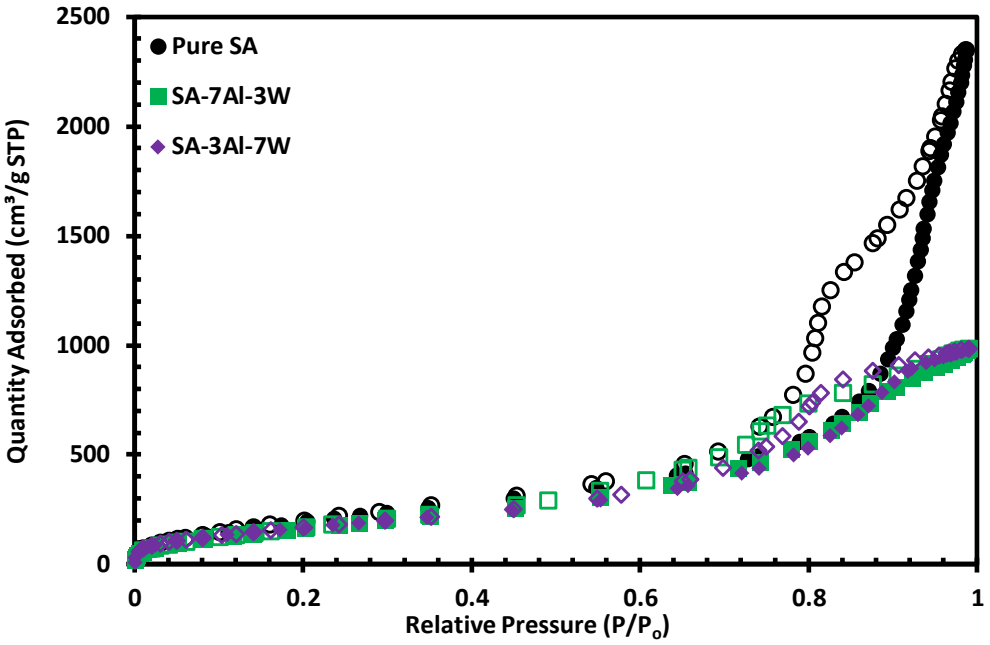

Figure 7.11 Nitrogen adsorption/desorption isotherms of double metal loaded silica aerogel (filled dots: adsorption branches, empty dots: desorption branches).

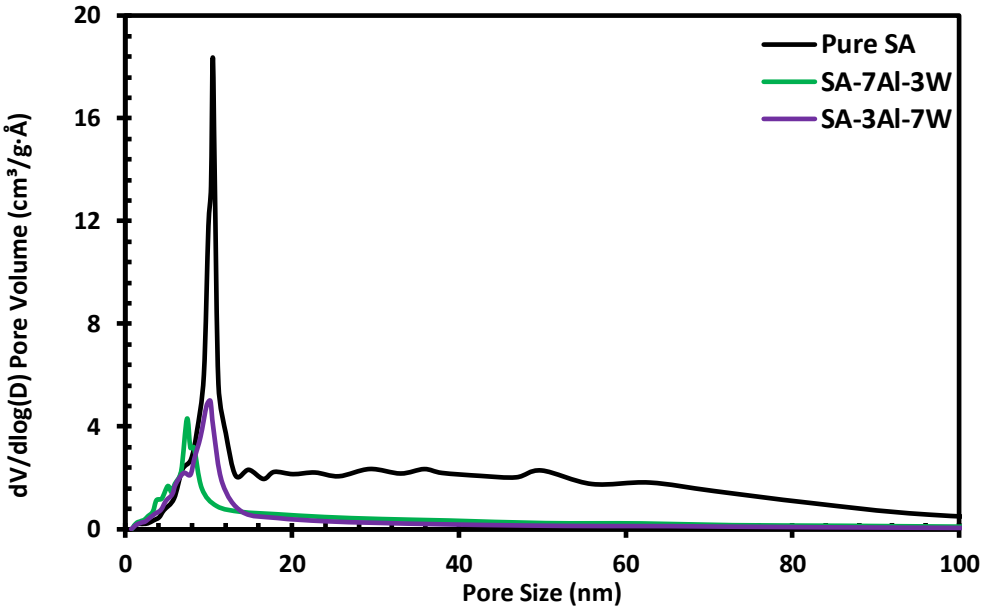

Figure 7.12 Pore size distributions of double metal loaded silica aerogel.

Table 7.2 lists the physical properties of the metal loaded silica aerogel catalysts. SA1 and SA2 indicate the silica aerogel support used for the metal loading.

Table 7.2 Physical Properties of metal loaded silica aerogel catalysts.

Sample ID	**BET Surface Area (m^2/g)**	**BJH Desorption average pore size (nm)**	**BJH Desorption cumulative volume of pores (cm^3/g)**	**Micro-porosity (%)**
SA1	795	11.1	3.63	3.7
SA1 + 7Al	730	6.9	2.01	6.4
SA1 + 10Al	603	10.6	2.48	4.8
SA1 + 7W	636	7.6	1.86	6.8
SA1 + 10W	508	6.8	1.32	7.5
SA2	839	10.7	3.76	4.2
SA2 + 7Al + 3W	671	5.7	1.52	7.3
SA2 + 3Al + 7W	639	6.3	1.52	8.2

It was observed that the surface area of the synthesized catalysts reduces with loading of both aluminium and tungsten. This can be attributed to the accumulation of the metal ions inside the pores of the silica aerogel structure resulting in a drop in the surface area and pore volume. Similarly, the pore size values of the catalysts lower with increasing metal loading. However, the pore diameter of 10% Al loaded is larger than that of 7% Al loaded and this is an unexpected result that may have arisen due to the uneven loading of the aluminium into the pores of the support and some of the aluminium in the 10% Al loaded support has mainly loaded into the macropores of the silica aerogel as can be seen its pore size distribution (Figure 7.8).

The physical property results of all synthesized catalysts are in accordance with the isotherm results. For the SA2-7Al-3W catalyst, the nitrogen adsorbed volumes were found to be 913.8 cm^3/g at P/P_0 value of 0.95 and 65.7 cm^3/g at P/P_0 value of 0.01. The N_2 adsorbed gas volumes at microporous region was 7.3%. The microporosity

values of the catalysts are given in Table 7.2. Their microporosity values are close to each other.

7.2.2.3. SEM and EDS Results

Figure 7.13a is the SEM image of the SA-7Al catalyst. The bright particles observed in the back scattered images (BSE) of the SA-7Al catalyst (Fig 7.13b) may represent aluminium particles in the silica aerogel support. For the SA-7Al catalyst, aluminium formed clusters within the support.

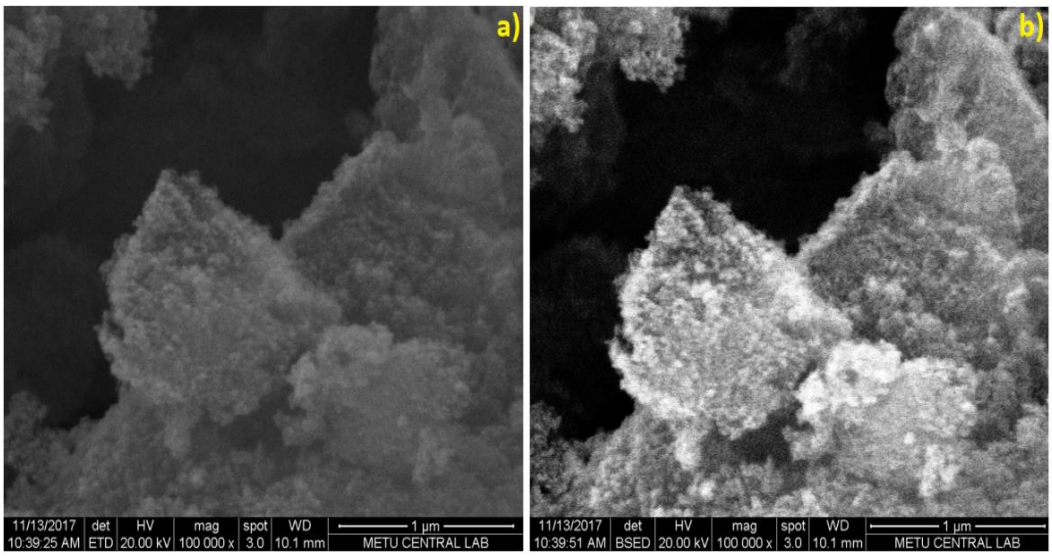

Figure 7.13 The SEM (a) and BSE (b) images of the SA-7Al catalyst at a magnification of 100,000X.

Figure 7.14 shows the SEM and BSE images of the SA-10Al catalyst. It can be observed that the aluminium ions formed small clusters in the silica aerogel support. These clusters appear less bright (Fig. 7.14b – yellow circles).

In addition to the SEM analysis, EDS analysis was also performed. The EDS spectra of the SA-7Al (Figure 7.15) and SA-10Al (Figure 7.16) catalysts showed presence of aluminium (Al), oxygen (O), Au, Pd and carbon (C) elements. Al was successfully

impregnated into the support. The carbon was due to the carbon tape used to hold the sample during analysis while Au and Pd were because of coating the samples.

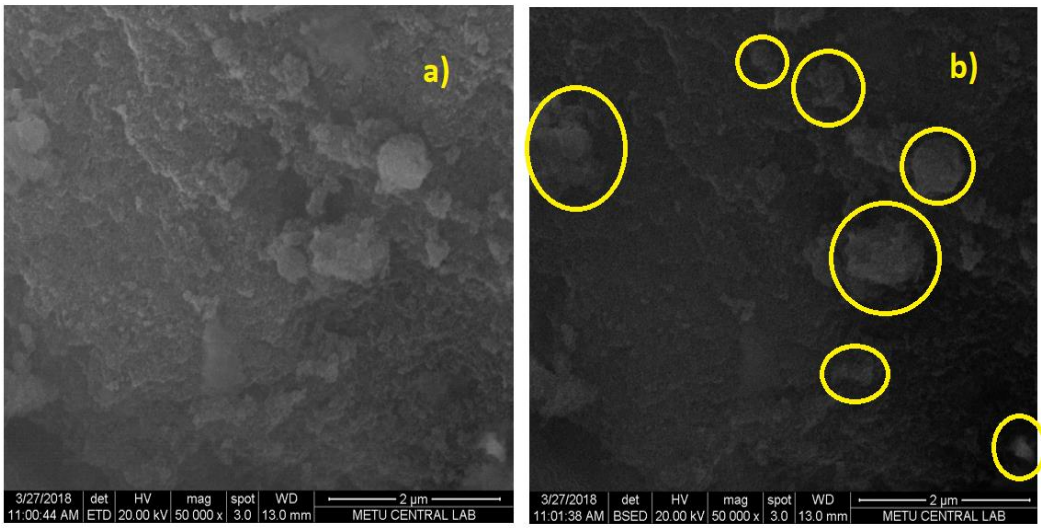

Figure 7.14 The SEM (a) and BSE (b) images of the SA-10Al catalyst at a magnification of 50,000X.

The EDS spectra for SA-7Al and SA-10Al in Figures 7.15 and 7.16 respectively, revealed that the particles in the silica aerogel support were aluminium.

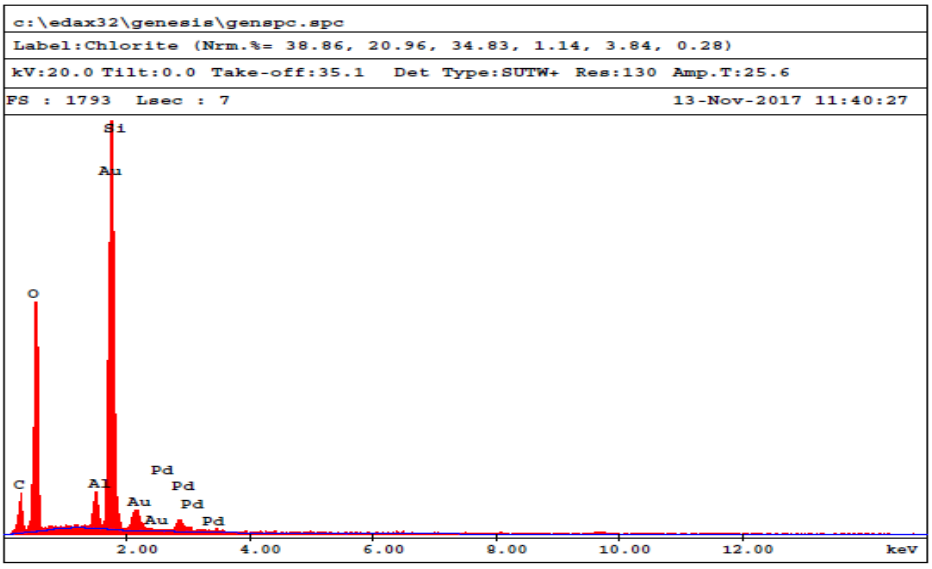

Figure 7.15 EDS spectrum of the SA-7Al catalyst.

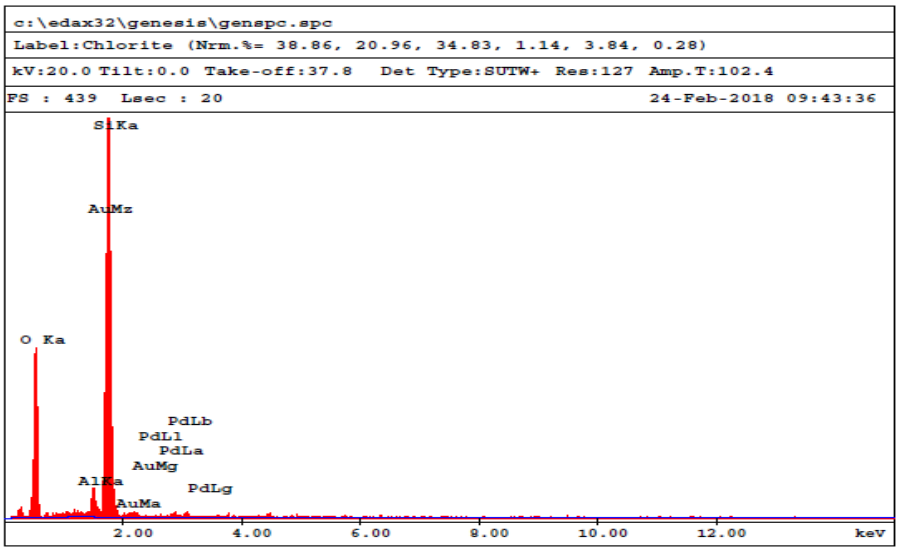

Figure 7.16 EDS spectrum of the SA-10Al catalyst.

Figure 7.17 shows the SEM image of the SA-7W catalyst. The spongy structure of silica aerogel support was preserved after loading of TPA and TPA clusters were observed. The brightness in the image indicates presence of W ions which is corroborated by the EDS spectrum in Figure 7.18.

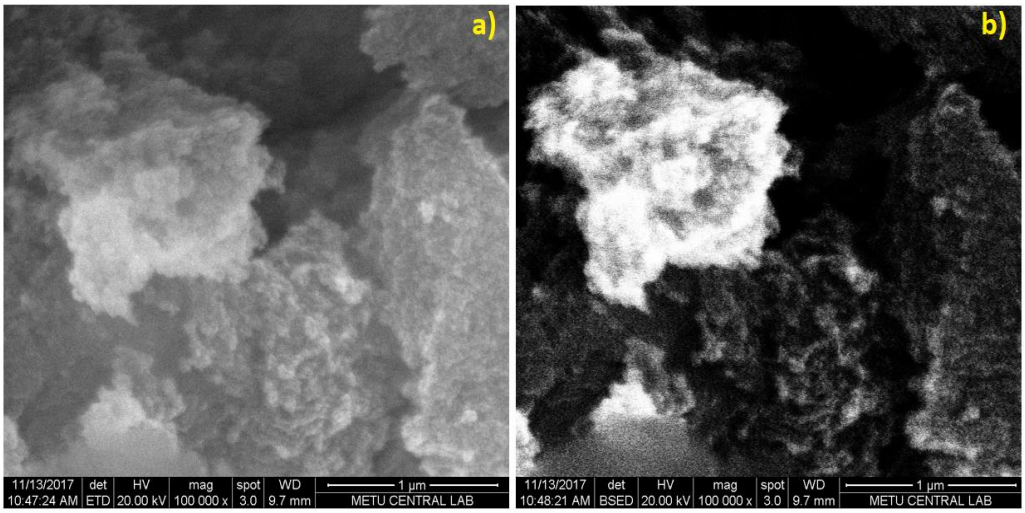

Figure 7.17 The SEM (a) and BSE (b) images of the SA-7W catalyst at a magnification of 100,000X.

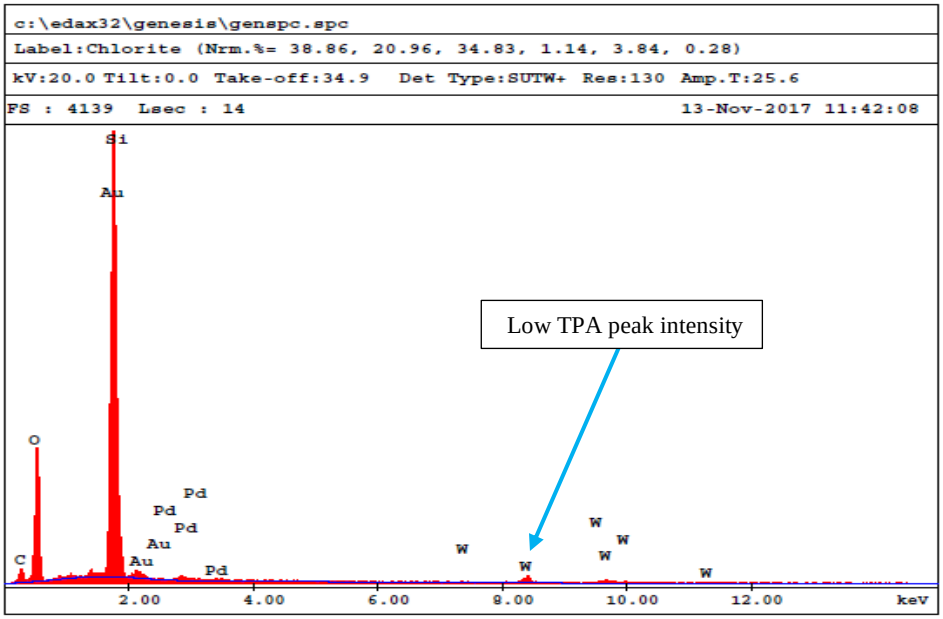

Figure 7.18 EDS spectrum of the SA-7W catalyst.

When the amount of tungsten was increased from 7 to 10 mole%, the SEM images also revealed that TPA was well dispersed but some clusters of W particles formed (shown in yellow circles) in the silica aerogel support as shown in Figure 7.19.

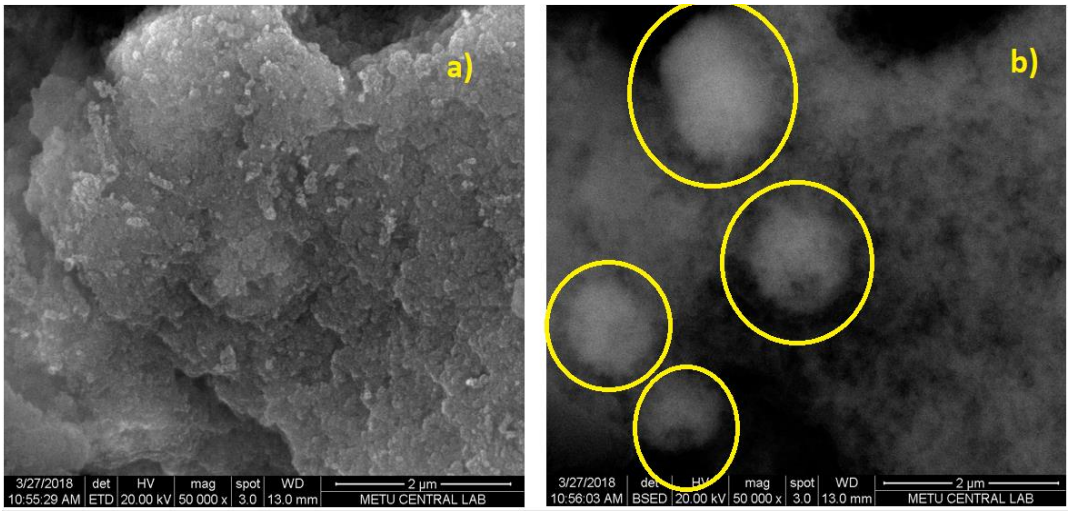

Figure 7.19 The SEM (a) and BSE (b) images of the SA-10W catalyst at a magnification of 50,000X.

The EDS spectra of the SA-10W catalyst showed that there was an increase in tungsten amount in the support as the TPA loading increased from 7 to 10 mole% (Fig. 7.20).

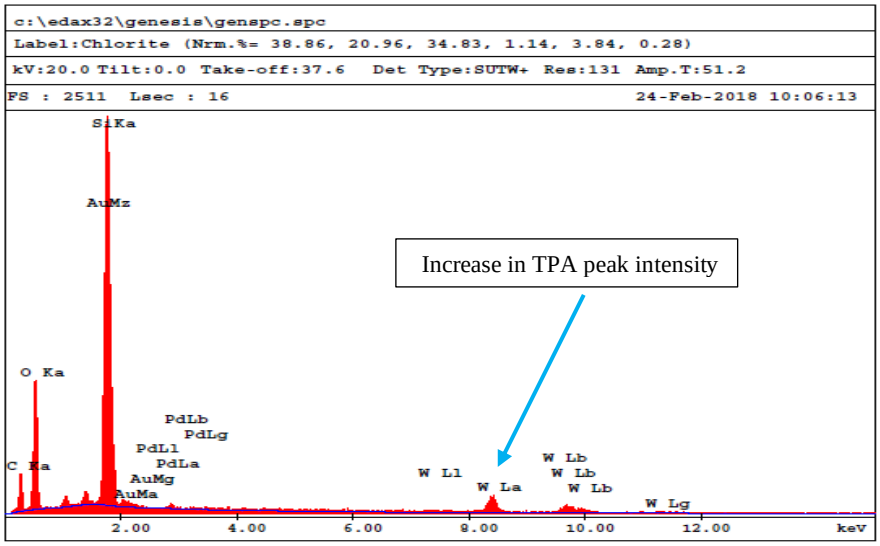

Figure 7.20 EDS spectrum of the SA-10W catalyst.

For the SA-7Al-3W catalyst, the SEM and BSE images are shown in Figure 7.21. Since there are two metals loaded on this catalyst, it may be hard to distinguish the metal particles in the images.

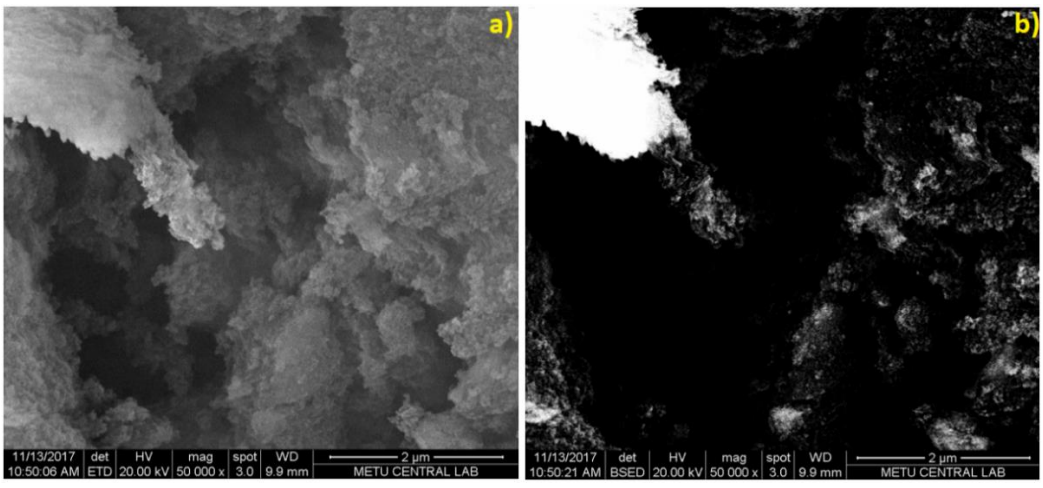

Figure 7.21 The SEM (a) and BSE (b) images of SA-7Al-3W catalyst at a magnification of 50,000X

Figure 7.22 shows the SEM images for the SA-3Al-7W catalyst. The SEM image showed a cluster of particles that was surrounded by smaller bright particles.

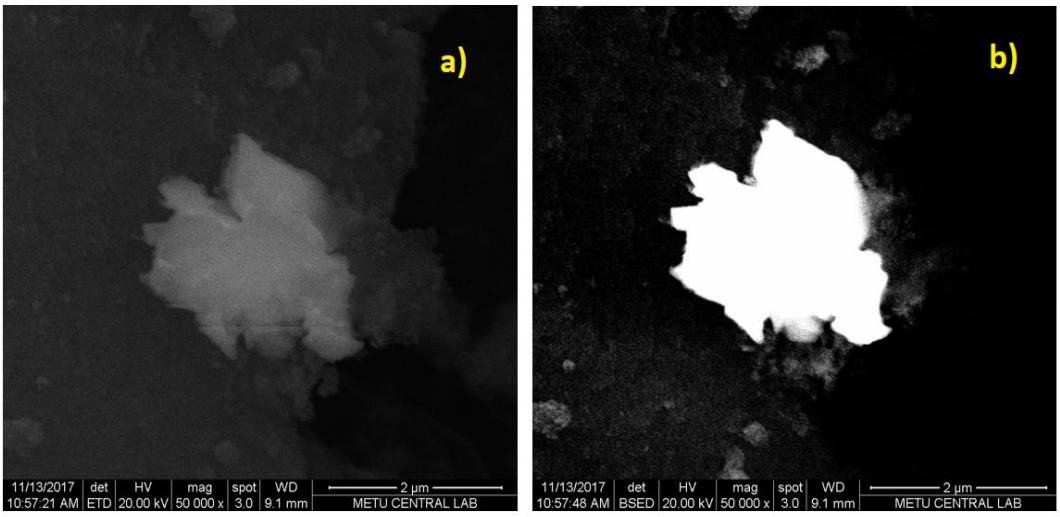

Figure 7.22 The SEM (a) and BSE (b) images of SA-3Al-7W catalyst at a magnification of 50,000X.

The EDS spectra of SA-7Al-3W and SA-3Al-7W catalysts presented in Figures 7.23 and 7.24 indicates that both Al and W are present in the silica aerogel support. With an increase in TPA amounts an increase in W peak intensity was observed for the SA-3Al-7W catalyst. However, with a decrease in aluminium amount, an increase in Al peak intensity was observed. This behavior shows that aluminium particles were not well dispersed in the support.

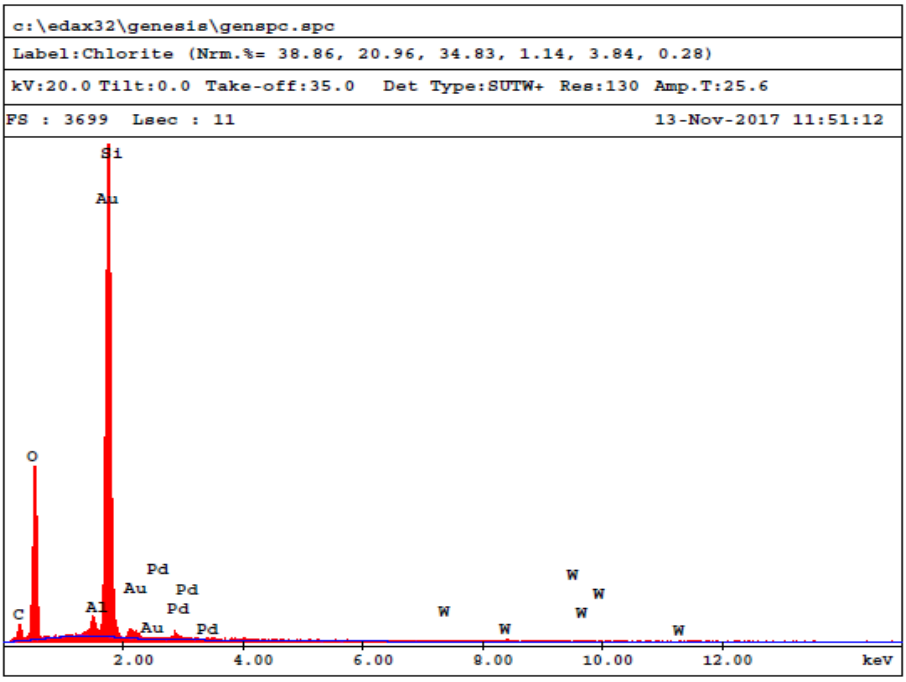

Figure 7.23 EDS spectrum of SA-7Al-3W catalyst.

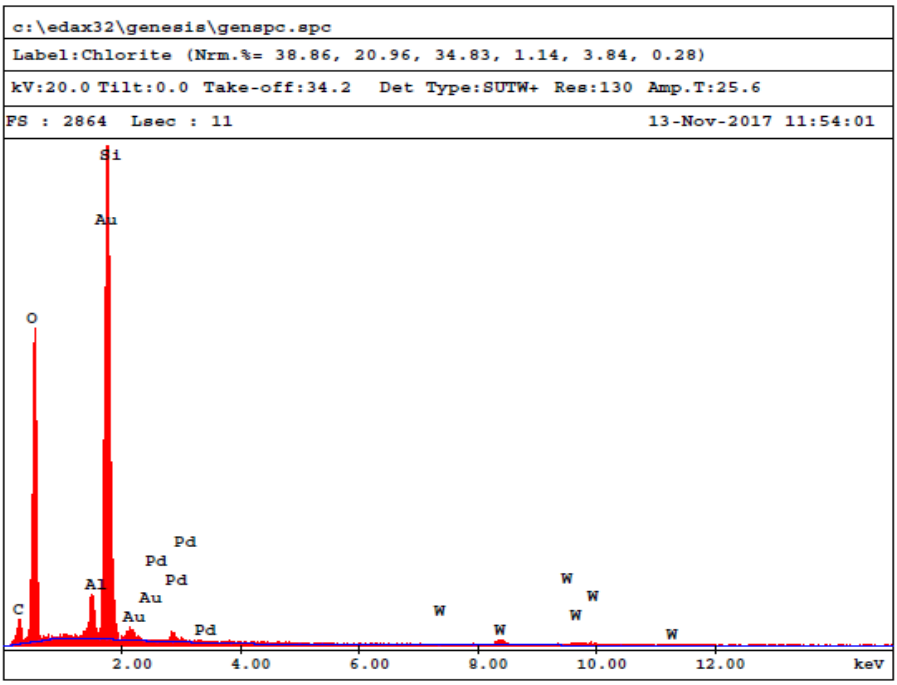

Figure 7.24 EDS spectrum of SA-3Al-7W catalyst.

The weight percent of metals in the support is given in Table 7.3. This table shows that metal ions were dispersed non-homogeneously on the support for the SA-7Al, SA-10W and SA-3Al-7W. This data is in agreement with SEM data. As can be seen in the SEM image of the SA-10W catalyst (Figure 7.19) the W is loaded in clusters. For the SA-3Al-7W catalyst it can be seen from its EDS spectra (Fig. 7.24) that more Al is dispersed in the support compared to W.

Table 7.3 Comparison of metal ions between real value and EDS by weight percent.

Catalyst ID	**Initial, wt%**		**EDS, wt%**	
	Al	**W**	**Al**	**W**
SA-7Al	2.70	-	3.81	-
SA-10Al	3.60	-	3.30	-
SA-7W	-	18.00	-	16.46
SA-10W	-	24.00	-	36.90
SA-7Al + 3W	2.50	7.40	1.71	3.85
SA-3Al + 7W	1.10	16.80	3.07	7.94

7.2.2.4. DRIFTS Results

In DRIFTS analysis pyridine was adsorbed on the synthesized catalysts in order to observe the existence of Lewis and Brønsted acid sites. The difference between the DRIFTS spectra of those samples adsorbed with pyridine and fresh samples results in a spectrum that has peaks at characteristic wavelength values which gives information about the Lewis and Brønsted acid sites. The DRIFTS spectra of synthesized catalysts are presented in Figure 7.25.

All synthesized catalysts had peaks corresponding to Lewis acid sites at a wavelength of 1447, 1575 and 1598 cm^{-1} and peaks at 1498 cm^{-1} corresponding to a combination of both Lewis and Brønsted acid sites. SA-7W, SA-10W and SA-3Al-7W exhibited Brønsted acid sites at a wavelength of 1540cm^{-1} while all synthesized catalysts exhibited Brønsted acid sites at a wavelength of 1640cm^{-1} (Aydemir, 2010).

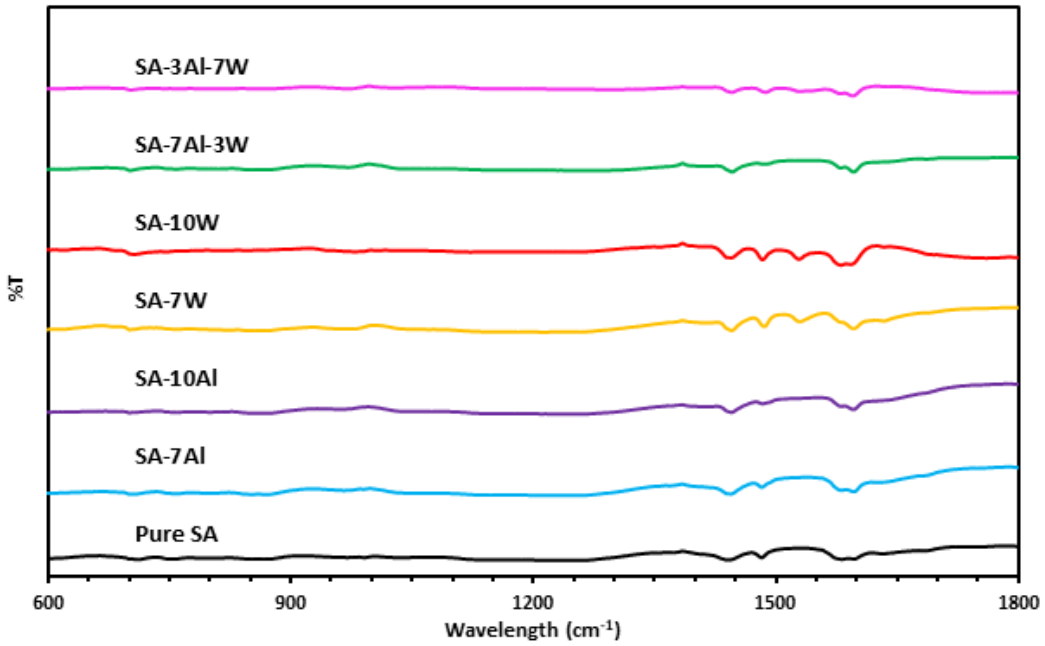

Figure 7.25 The DRIFTS spectra of synthesized materials.

For the SA-7W, SA-10W and SA-3Al-7W catalysts, the ratio of Brønsted acid sites at 1540 cm^{-1} to Lewis acid sites at 1447 cm^{-1} was 0.56, 1.00 and 0.67, respectively while the ratio of Brønsted acid sites at 1640 cm^{-1} to Lewis acid sites at 1447 cm^{-1} for the SA, SA-7Al, SA-10Al, SA-7W, SA-10W, SA-7Al-3W and SA-3Al-7W catalyst was 0.56, 0.67, 0.92, 0.67, 0.07, 0.50 and 0.17, respectively.

It can be concluded that the incorporation of TPA into silica aerogel introduced Brønsted acid sites at 1540 cm^{-1} except for the SA-7Al-3W catalyst and the incorporation of aluminium into silica aerogel enhanced the Brønsted acid sites at 1640 cm^{-1} except for the SA-3Al-7W catalyst.

7.2.2.5. ICP Results

Weight percent of Si, Al and W elements in the silica aerogel support is given in Table 7.4. In the SA-7Al, SA-10Al, SA-7Al-3W and SA-3Al-7W catalysts, the aluminium amounts are higher than the initial amounts. For example, the Al weight percent in the SA-7Al catalyst was found to be 3.6 wt% by ICP where its initial wt% was 2.70.

SA-7Al, SA-10Al, SA-7Al-3W and SA-3Al-7W catalysts had non-homogeneous metal dispersion. SA-7Al and SA-3Al-7W showed non-homogeneous dispersion in ICP and EDS analysis. These discrepancies in both EDS and ICP may be due to amount of sample analyzed for each analysis. Since in the ICP analysis higher amount of sample are used compared to EDS it gives a more accurate result.

Table 7.4 Amounts of aluminium and tungsten in the synthesized catalysts from ICP analysis.

Catalyst ID	**Element wt%**		
	Si	**Al**	**W**
SA-7Al	27.5±0.5	3.6±0.1	-
SA-10Al	27.1±0.4	5.0±0.1	-
SA-7W	26.6±0.6	-	14.3±0.1
SA-10W	24.6±0.1	-	19.3±0.2
SA-7Al + 3W	25.4±0.1	2.9±0.1	5.2±0.1
SA-3Al + 7W	23.9±0.3	1.22±0.01	13.3±0.1

The ICP results showed that Al and TPA were successfully loaded into the silica aerogel support.

7.2.2.6. TPD Results

The ammonia TPD spectra of the synthesized catalysts are given in Figure 7.26. For all the catalysts, the sharp peaks terminating at around 115°C are the ammonia physisorption peaks that indicate weak acidity.

The catalysts had major peaks as follows: SA-7Al at 464°C, SA-10Al at 466°C, SA-7W and SA-10W at 480°C, SA-7Al-3W at 300 and 475°C and SA-3Al-7W at 300 and 460°C. This means that all the synthesized catalysts had strong acidity. SA-10Al also had a moderate acidity peak at 395°C.

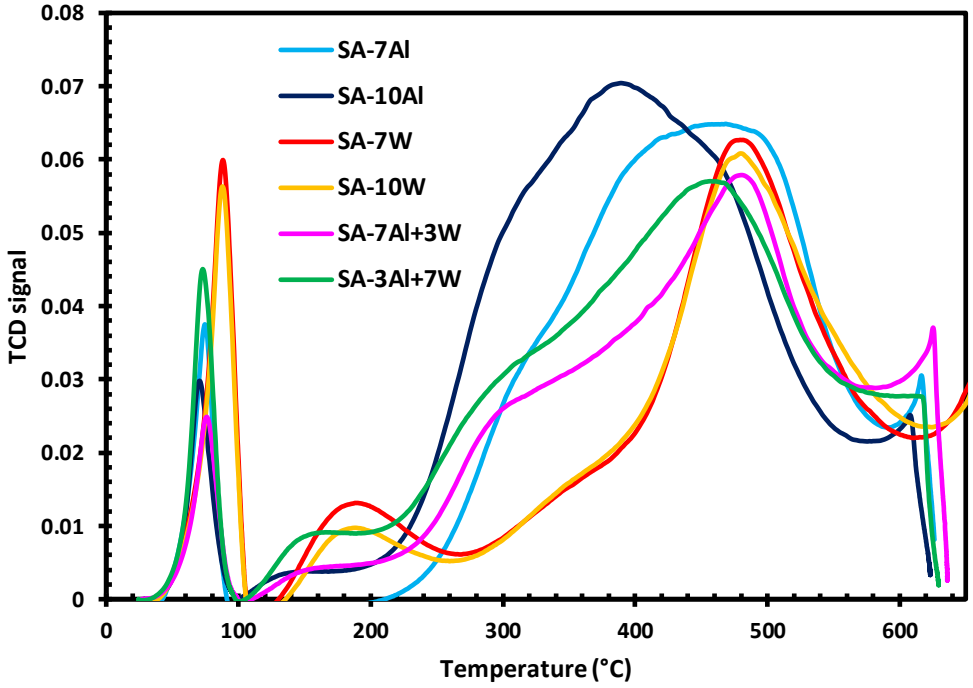

Figure 7.26 Ammonia TPD graphs for synthesized catalysts.

From Table 7.5, it can be seen that an increase in aluminium loading results in an increase in acidity of the catalyst. The loading of TPA results in close acid capacity.

Amongst all the synthesized, the highest and lowest acid capacities were found to be the SA-10Al and SA-7Al, respectively.

Table 7.5 Summary of acid capacity of the synthesized catalysts.

Catalyst	Total Acid Capacity (mmol/g catalyst)
SA-7Al	2.18
SA-10Al	2.70
SA-7W	2.40
SA-10W	2.30
SA-7Al-3W	2.40
SA-3Al-7W	2.56

7.2.3. TGA Results

Thermogravimetric experiments were performed to determine activation energies of both polypropylene and polyethylene cracking reactions in the presence of synthesized catalysts. These analyses were conducted in non-isothermal conditions and subjected to nitrogen atmosphere at a flow rate of 60 cc/min, a constant heating rate of 5°C/min and a catalyst to polymer weight ratio of 1/2.

7.2.3.1. TGA Results for Polypropylene Cracking Reactions

Figure 7.27 illustrates the TGA plots that resulted from the catalytic and non-catalytic pyrolysis of PP. Pure PP exhibits a steep weight loss in the temperature range of 350–480°C. The steep weight loss can be attributed to chain scission. This result is consistent with the result reported by Obali et al (2011). As shown in Figure 7.27, an increase in metal loading shifts the degradation curve for each pyrolysis to the left resulting in lower degradation temperatures. This is due to introduction of acid sites (Lewis and Brønsted) into the catalyst.

Furthermore, TGA data can be used to calculate the kinetic parameters for the PP degradation reactions. The calculation details are presented in Appendix B. The overall reaction order is found to be one for all the synthesized catalyst. This result is consistent with the literature (Obali et al (2011).

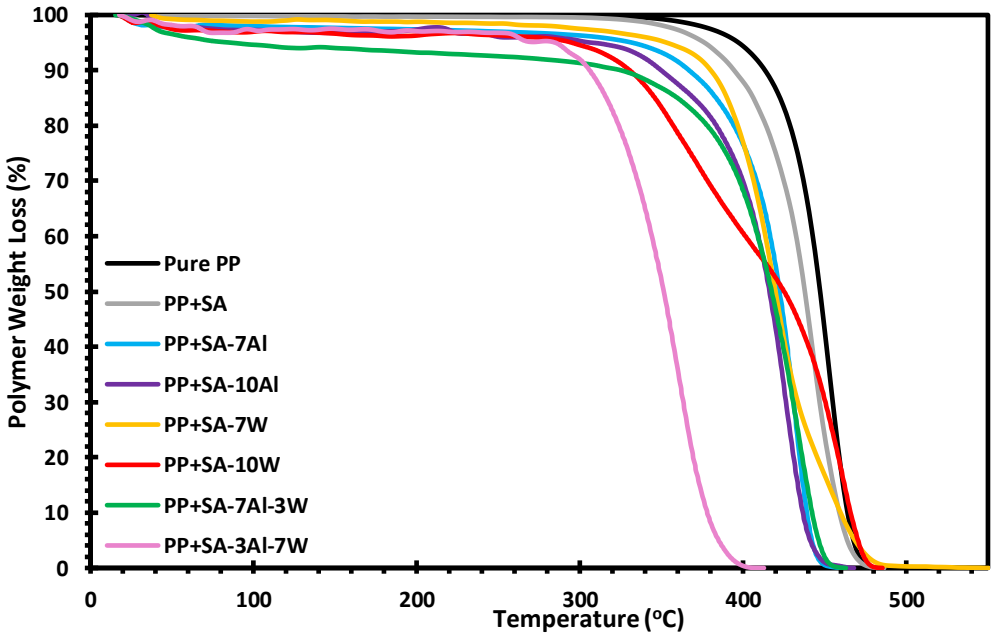

Figure 7.27 TGA plots describing the degradation of PP in catalytic and non-catalytic pyrolysis.

The activation energies for the degradation reaction of PP are presented in Table 7.6. As can be seen the activation energies of catalytic degradation of PP are lower than that of non-catalytic degradation reaction which is 174.4 kJ/mol. This value is close to that reported in the literature (Obali et al., 2011). Using pure silica aerogel as a catalyst lowers the activation energy of this reaction to 135.6 kJ/mol. This may be attributed to Lewis and Brønsted acid sites present in the support. Loading of aluminium and TPA into the support resulted in lower activation energies for the PP degradation reaction. Aluminium loaded catalyst had a little lower activation energy compared to TPA loaded which were in the ranges of 123.8-128.1 to 130.8-131.9 kJ/mol, respectively. Even though TPA loaded catalysts had Brønsted acid sites from

DRIFTS analysis, the surface areas and pore sizes of SA-7Al and SA-10Al are comparatively higher than those of SA-7W and SA-10W which may explain why aluminium loaded catalysts have lower activation energies. When both metals are loaded into the same catalyst the activation energy was lowered considerably compared to pure PP. Both double metal loaded catalysts exhibited high acidic capacity from ammonia TPD which may explain the lower activation energies. The SA-3Al-7W catalyst resulted in the lowest activation energy of the synthesized catalysts.

Table 7.6 Activation energy values for the PP degradation reaction in presence of metal loaded silica aerogel.

Sample ID	**Activation energy (E_A) values (kJ/mol)**
Pure PP	174.4
PP + SA	135.6
PP + SA-7W	131.9
PP + SA-10W	130.8
PP + SA-7Al	128.1
PP + SA-10Al	123.8
PP + SA-7Al-3W	121.4
PP + SA-3Al-7W	115.7

Obali et al., (2011) studied the effect of aluminium loaded SBA-15 on polypropylene degradation reaction. The use of pure SBA-15 lowered of the activation energy of the PP degradation reaction to a value close to that of pure silica aerogel reported in Table 7.6. SBA-15 loaded with 10 mole% aluminium resulted in a much higher drop in activation energy (56.1 kJ/mol) as compared to this study. This may be attributed to the presence of more Brønsted acid sites in the catalyst.

7.2.3.2. TGA Results for Polyethylene Cracking Reactions

Figure 7.28 shows the TGA plots of catalytic and non-catalytic pyrolysis of polyethylene (PE). As is the case with polypropylene, the addition of aluminium and tungsten in the support materials reduced the degradation temperature and activation

energies of the PE degradation reaction. Table 7.7 shows the activation energies of each synthesized catalyst in the pyrolysis of PE.

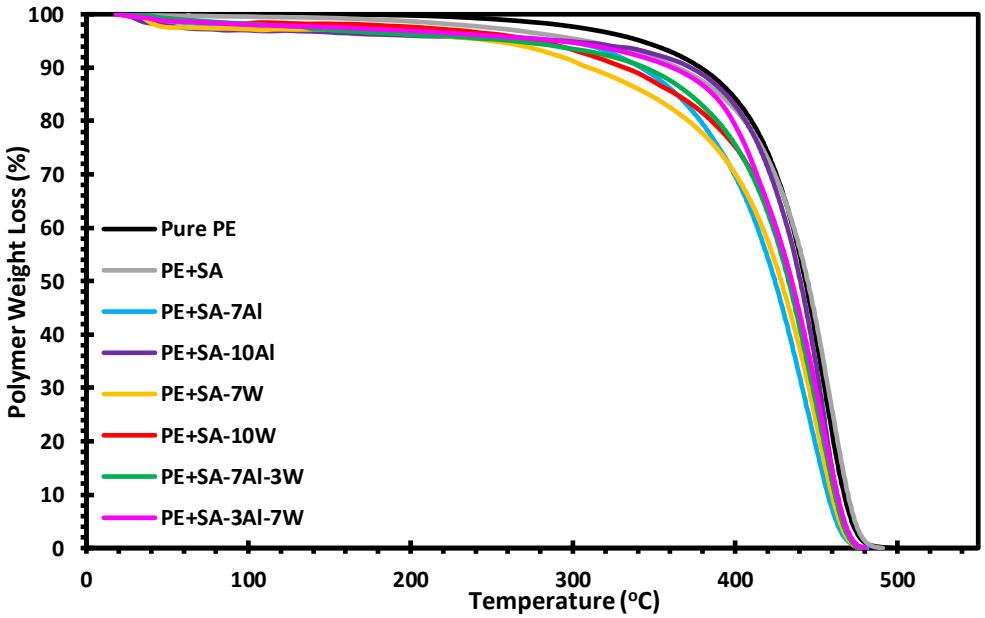

Figure 7.28 TGA plots describing the degradation of PE in catalytic and non-catalytic pyrolysis.

Table 7.7 Activation energy values for PE degradation reaction in presence of metal loaded silica aerogel.

Sample ID	**Activation energy (E_A) values (kJ/mol)**
Pure PE	134.0
PE + SA	129.8
PE + SA-7W	122.1
PE + SA-10W	129.1
PE + SA-7Al	120.1
PE + SA-10Al	122.1
PE + SA-7Al-3W	117.9
PE + SA-3Al-7W	123.0

From Table 7.7 it can be observed that the impregnation of both aluminium and tungsten metal ions resulted in a reduction in the activation energy. This can be

attributed to the formation of acid sites as seen from DRIFTS and TPD results. However, there is an increase in the activation energy when the amount of TPA is increased from 7 mole% to 10 mole%. This is unusual and can be attributed to the nonuniform distribution of TPA on the silica aerogel. As in the case for PP, when both metals were loaded onto the same catalyst the activation energy was lowered considerably. The SA-7Al-3W catalyst resulted in the lowest activation energy of the synthesized catalysts.

Aydemir et al., (2016) conducted the pyrolysis of PE using another mesoporous support, MCM-41. When pure MCM-41 was used, the activation energy was reported as 137 kJ/mol which is higher than that of silica aerogel in this study. This may be due to the presence of Brønsted acid sites in pure silica aerogel seen in DRIFTS analysis. Furthermore, Aydemir et al., (2016) loaded MCM-41 with aluminium which resulted in activation energies in the range of 106-128 kJ/mol which is comparable to the activation energy of aluminium loaded silica aerogel. When another mesoporous material, SBA-15 was loaded with 10 mole% TPA, it significantly lowered the activation energy for PE degradation reaction to 74 kJ/mol which may be due to higher surface area and more intense acid peaks from DRIFTS as compared to the SA-10W catalyst used in this study, however, pure SBA-15 had an activation energy of around 161 kJ/mol which is much higher than that of silica aerogel which is due to natural acid sites in silica aerogel (Aydemir et al, 2011).

7.3. Polymer Pyrolysis Reaction System

The catalytic and non-catalytic pyrolysis of PE and PP was carried out isothermally at different temperatures with a heating rate of 5°C/min under nitrogen flow of 60 cc/min and a catalyst to polymer weight ratio of 1:2 for catalytic pyrolysis. Three experimental runs were carried out for PP pyrolysis while two were done for PE pyrolysis to check the reproducibility of the data.

At the end of each catalytic and non-catalytic pyrolysis experiments the solid residue and liquid products were weighed. In the case of catalytic pyrolysis, the solid residue amount was obtained by subtracting the amount of catalyst from the solid collected after each run. The liquid product was collected and weighed. The amount of gas products was determined by subtracting solid residue and liquid products from the initial polymer amount. The product yield of polymer degradation for liquid and gaseous products were found. Yield calculation is given in Appendix C. Gas and liquid products were analyzed using GC. The mole fraction and selectivity of each gas product and liquid product were calculated using calibration factors. The calibration factors for gas and liquid products are given in Appendix D.

The sample calculations for selectivity and mole fraction of each gas product is given in Appendix C. The raw data for mole fraction and selectivity of gas and liquid products are given in Appendix E for PP and Appendix F for PE degradation experiments.

7.3.1. Polypropylene Pyrolysis Results

7.3.1.1. Results of the Analysis of Gas Products obtained from Non-catalytic PP pyrolysis

The non-catalytic PP degradation reaction was performed at two temperatures, 400 and 425°C for 30 min and the product yield is presented in Figure 7.29. From the results presented in Figure 7.29, it can be seen that an increase in reaction temperature results in an increased liquid and gaseous product yield. On the other hand, amount of solid residue significantly decreased. This may be attributed to the cracking of higher hydrocarbon chains to form smaller hydrocarbon chains as the temperature increases. This product yield is in close agreement to that reported in the literature (Obali et al., 2012).

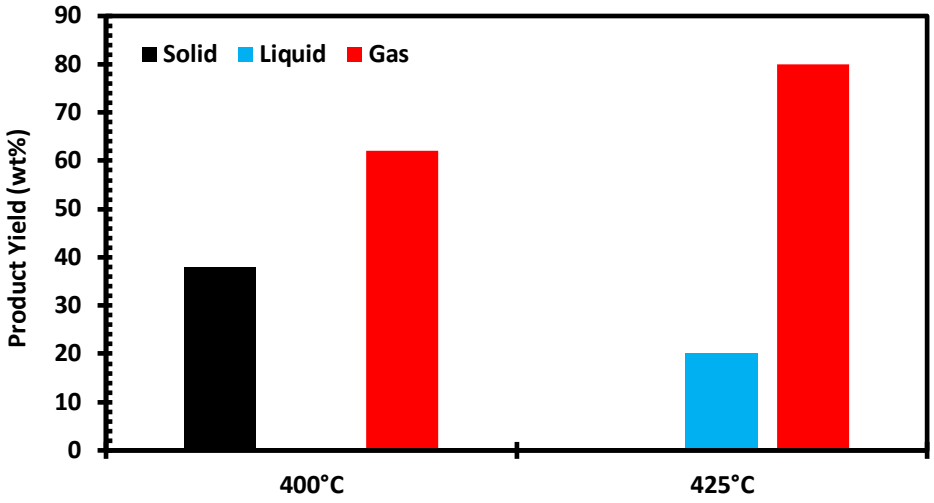

Figure 7.29 Product yield from the non-catalytic pyrolysis of PP at different reaction temperatures for 30 minutes.

GC results showed that at 400°C ethane, ethylene, propylene and isobutane gases formed. When the temperature increased to 425°C, methane formed in addition to these gases.

Figure 7.30 shows the mole fractions of non-catalytic degradation of PP at 400 to 425°C. For both temperatures more than 50% of the gaseous product was composed of propylene. The composition of ethane and ethylene is almost the same at both temperatures while isobutane reduced by almost half. There was a small amount of methane at 425°C.

The effect of temperature on the mole fraction and selectivity of gaseous products obtained from the non-catalytic thermal degradation of PP is shown in Figures 7.30 and 7.31 respectively. It can be seen that as temperature increased from 400 to 425°C, the selectivities of ethane and ethylene remained almost the same while the selectivity of propylene increased from 0.18 to 0.21. The selectivity of isobutane reduced from 0.06 to 0.04. Methane was observed at 425°C with a selectivity of 0.01. This may be due to the increase in temperature promoting more cracking of longer hydrocarbon chains forming smaller hydrocarbon chain molecules.

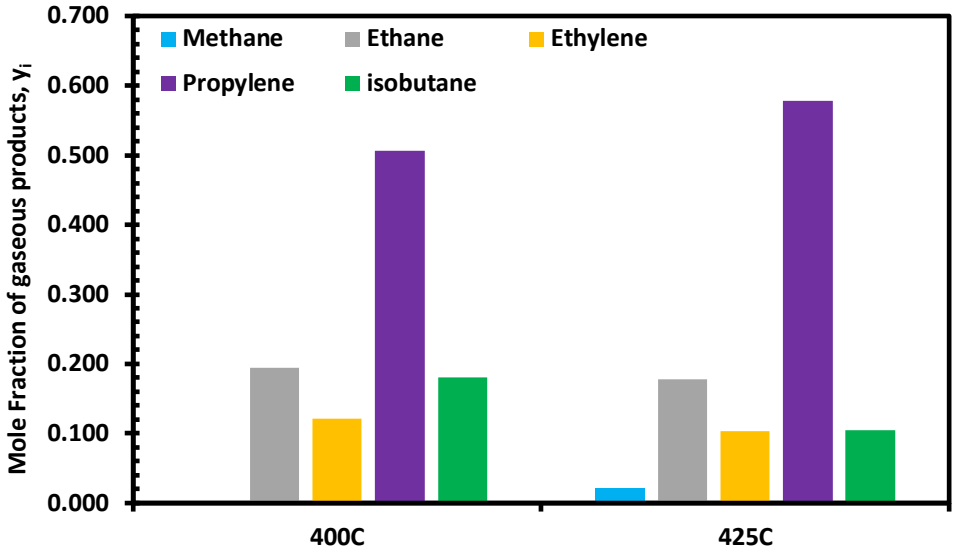

Figure 7.30 The effect of temperature on mole fraction of gaseous products obtained from the non-catalytic thermal degradation of PP.

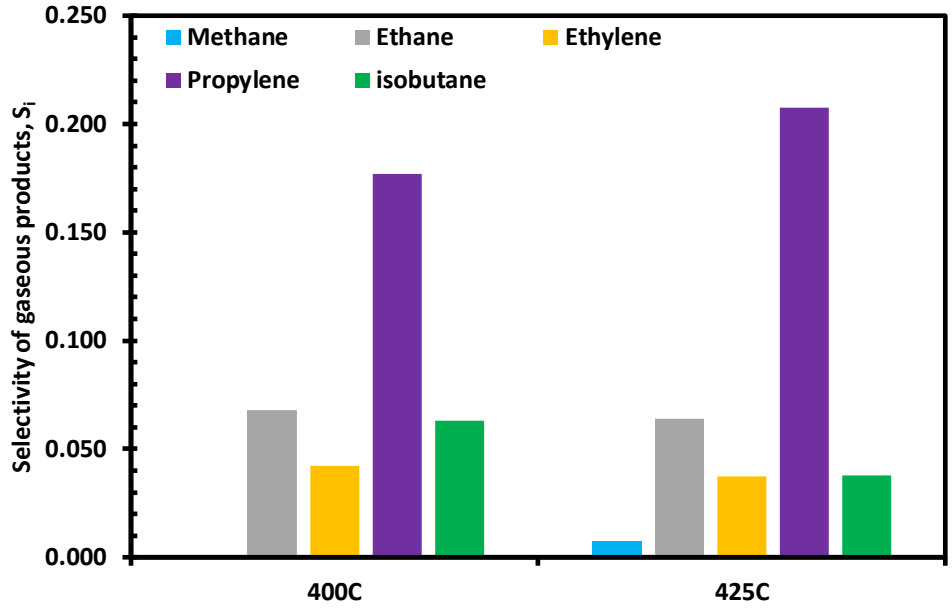

Figure 7.31 The effect of temperature on selectivity of gaseous products obtained from the non-catalytic thermal degradation of PP.

7.3.1.2. Results of the Analysis of Liquid Products obtained from the Non-catalytic PP pyrolysis

The mole fraction results of liquid products obtained from the non-catalytic pyrolysis of PP at 400 and 425°C for 30 min are presented in Figure 7.32. C5, C6, C8 and C9 were not formed at 400°C. As the temperature was increased more products of smaller hydrocarbon number were produced as the amount of C5-C6 increased significantly. C7 and C10 did not form at 425°C but around 4.8 and 0.8 mole percent of C8 and C9, respectively were produced at this temperature. Furthermore, an increase in temperature also resulted in a significant increase in the amount of C11, C12 and C14 while there was a significant drop in the amount of C13, C16 and especially C18. This may indicate that an increase in temperature promotes the breaking of larger hydrocarbon chains to form smaller hydrocarbon chains. Since most of the products formed at 400°C start increasing after C16, it can be assumed that most of the products obtained at this temperature have carbon numbers higher than 18 (i.e carbon number>C18).

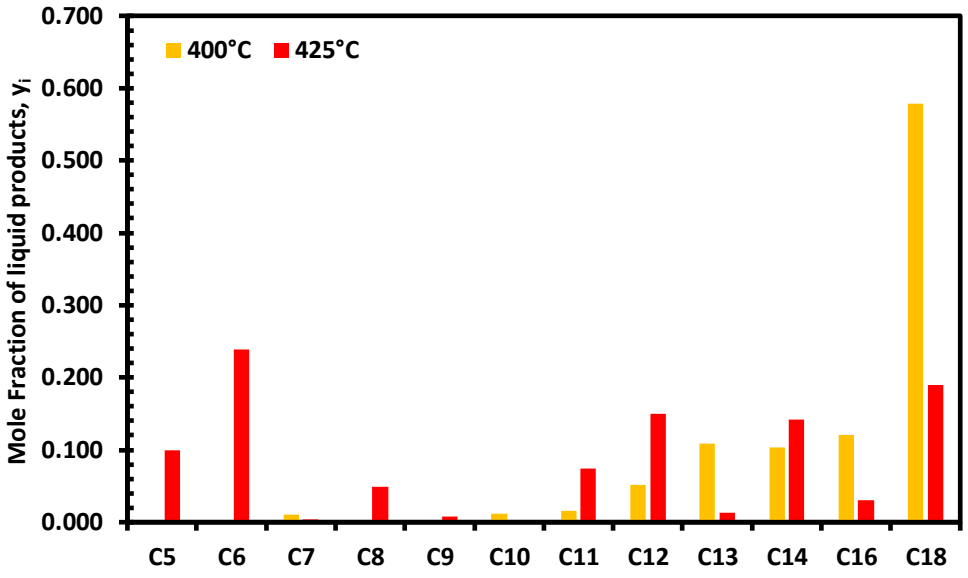

Figure 7.32 The effect of temperature on the mole fraction of liquid products obtained from the non-catalytic thermal degradation of PP.

The effect of increasing temperature on the selectivity of liquid products obtained from the non-catalytic pyrolysis of PP from 400 to 425°C for 30 min are presented in Figure 7.33. It can be observed that an increase in temperature results in an increase in the selectivities of C5-C12 and C14. The selectivities of C13, C16 and C18 were also significantly decreased with an increase in temperature. For example, the selectivity of C18 dropped from 0.572 at 400°C to 0.273 at 425°C. The full mole fraction and selectivity values of liquid products obtained from non-catalytic pyrolysis of PP are presented in Appendix E.

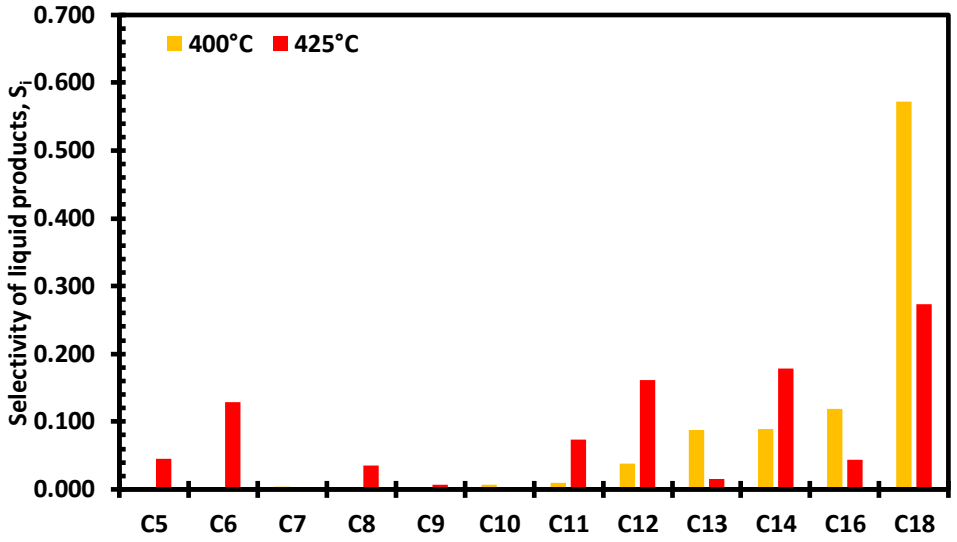

Figure 7.33 The effect of temperature on the selectivity of liquid products obtained from the non-catalytic thermal degradation of PP.

These results are in close agreement with those presented in the literature (Obali, 2010).

7.3.1.3. Results of the Analysis of Gas Products obtained from the Catalytic PP Pyrolysis

Catalytic pyrolysis of PP was carried out at 400°C for 30 minutes. The product and solid residue yield for different synthesized catalysts is given in Figure 7.34 comparing

with the result of pure PP pyrolysis at 400°C. The product yield obtained in weight percent for the three experiments done per catalyst was reproducible.

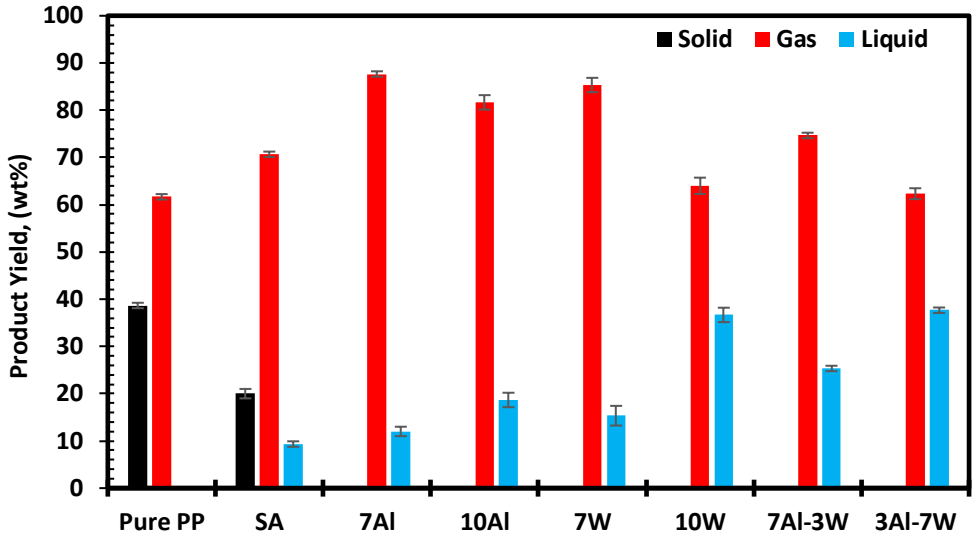

Figure 7.34 Product yield of catalytic pyrolysis of PP at 400°C for 30 min.

As can be observed from Figure 7.34, the use of catalyst resulted in no solid residue except for the silica aerogel support. In the presence of silica aerogel support solid residue yield decreased from 38 to 20 wt%. Catalysts also favored the formation of more gaseous and liquid products. The increase in metal loading resulted in an increase in liquid products, but a significant increase was with an increase in TPA loading. However, this behavior was not observed with an increase in aluminium loading. The liquid product was light yellow in color and flowed easily which indicates presence of lower molecular weight hydrocarbons in the liquid mixture.

In the presence of all catalysts, acetylene, ethylene, propylene, isobutane and n-butane formed. Only methane in the presence of silica aerogel support and ethane in the presence of SA-10W were not observed. Methane, acetylene and n-butane gases did not form in the non-catalytic pyrolysis of PP.

The mole fractions for each gas component produced through the catalytic and non-catalytic thermal degradation of PP at 400°C are presented in Figure 7.35. The percent of propylene in the gas product for catalytic pyrolysis of PP reduced significantly from the non-catalytic PP pyrolysis. Methane, acetylene and n-butane composition increased significantly when catalysts are used.

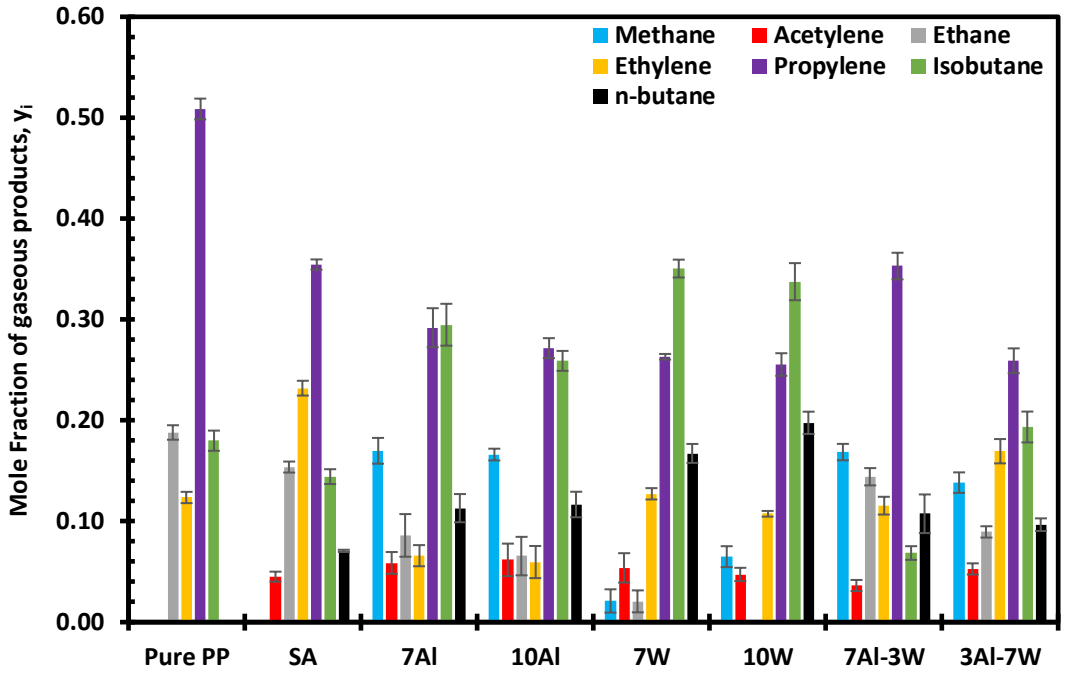

Figure 7.35 Mole fraction comparison of gaseous products obtained from the catalytic and non-catalytic thermal degradation of PP at 400°C for 30 min.

This study improves on the mole fraction results of methane, acetylene, ethane and ethylene when compared to the use of a zeolite (ZSM-5) catalyst in the thermal degradation of PP reported in the literature (Achilias et al., 2007). The use of ZSM-5 resulted in the formation of 0.02, 0.00, 0.02 and 0.03 mole percent of methane, acetylene, ethane and ethylene, respectively. These values are comparable to the lowest values of each component in this study.

The selectivity values of the gaseous products in the presence of catalysts are given in Figure 7.36.

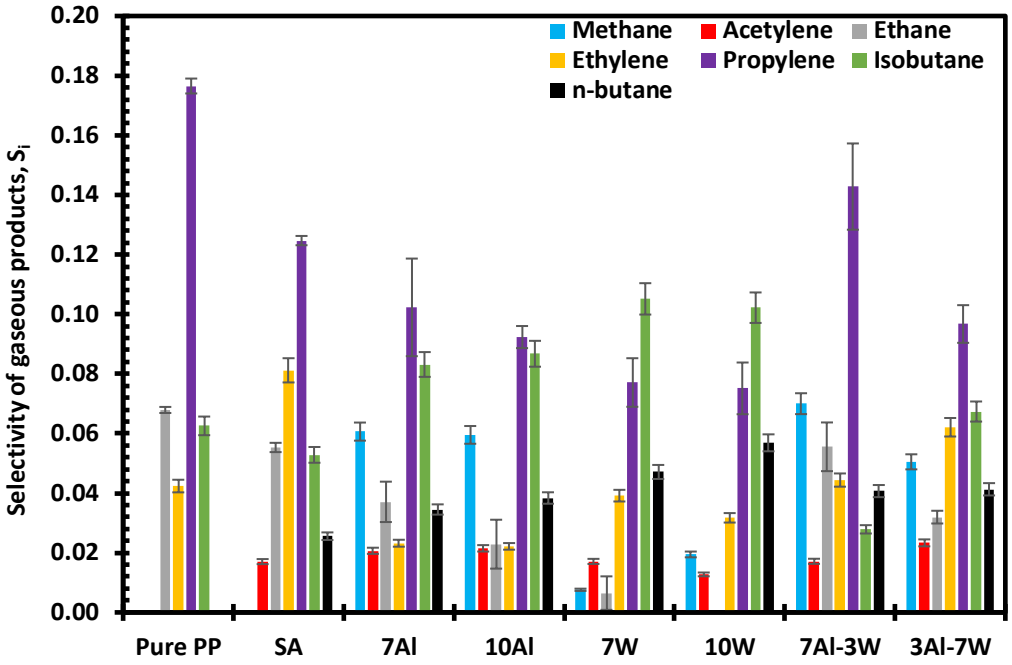

Figure 7.36 Selectivity comparison of gaseous products obtained from the catalytic and non-catalytic thermal degradation of PP at 400°C for 30 min.

It can be seen from Figure 7.36, use of aluminium loaded catalysts resulted in higher selectivity values of methane, acetylene, ethane and propylene compared to use of TPA loaded silica aerogel. For silica aerogel loaded with only aluminium, there is almost no change in methane, ethane, ethylene, propylene and isobutane selectivities with an increase in aluminium loading. The aluminium catalysts resulted in nearly the same selectivity values for the gaseous products which may be attributed to the close weight percent values revealed from ICP analysis. For TPA loaded catalysts, selectivities of methane, acetylene, ethane and propylene are significantly lower than aluminum catalysts. However, ethylene, isobutane and n-butane selectivities are higher than aluminium catalysts. Ethane was not observed in SA-10W.

For double metal loaded catalysts methane selectivity is significantly larger than for TPA catalysts but comparable to aluminium catalysts. Ethane and ethylene selectivities are higher than SA-7Al, SA-10Al, SA-7W and SA-10W catalysts. The

SA-7Al-3W catalyst had the highest propylene selectivity of any of the catalysts and the lowest isobutane selectivity of any of the catalysts. Apart from the propylene selectivity data for the SA-7Al and SA-7Al-3W catalysts, the gaseous product data from catalytic and non-catalytic pyrolysis were reproducible. Silica aerogel support, the SA-7Al, SA-10Al, SA-7Al-3W and SA-3Al-7W catalysts are propylene selective while the SA-7W and SA-10W catalysts are isobutane selective. These results showed that reaction mechanisms were different for aluminium and TPA loaded silica aerogel catalysts

7.3.1.4. Results of the Analysis of Liquid Products obtained from the Catalytic PP Pyrolysis

Figure 7.37 shows the effect of catalysts on the liquid products obtained from the catalytic thermal degradation of PP at 400°C and a residence time of 30 min. In the presence of all the catalysts, a significant decrease in the mole fraction of C18 was observed and the highest C18 mole fraction was 0.02. C18 did not form when the SA-3Al-7W catalyst was used. The mole fraction of C16 hydrocarbons also decreased significantly with the use of catalyst. C5, C6, C8 and C9 hydrocarbons did not form in the non-catalytic pyrolysis of PP. The use of silica aerogel as a catalyst resulted in the highest amount for C13, C16 and C18 being produced. The increase of aluminium loading resulted in a slight increase in the amount of C5 but a significant increase in C6, C8, C9 and C10 was observed. The amount of C7, C11, C12, C13, C14, C16 and C18 decreased as the aluminium amount was increased in the catalyst. The increase in amount of TPA resulted in a significant increase in C5, C6, C8 and C16 while the amount of C7, C10, C11, C12, C13 and C14 hydrocarbons decreased with an increase in TPA loading. However, the increase in TPA loading had a small effect on the production of C9. The double metal loaded catalysts resulted in formation of the smaller hydrocarbon products and significantly reduced the amount of hydrocarbons in the range of C14-C18. The double metal loaded catalysts resulted in the two highest amounts of C5, C8 and C10 hydrocarbons.

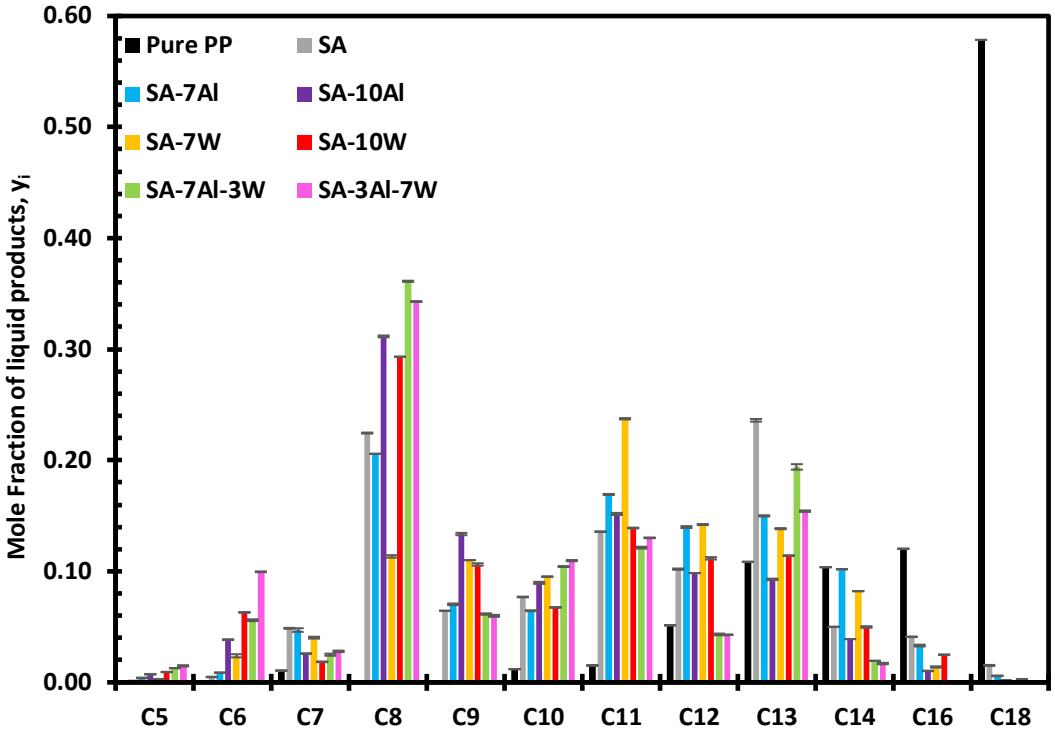

Figure 7.37 Mole fraction comparison of liquid products obtained from the catalytic and non-catalytic thermal degradation of PP at 400°C.

All the synthesized catalysts resulted in the formation of lower carbon number range. Heavier hydrocarbons like C14-C18 were significantly reduced by using these catalysts.

The selectivity comparisons for the catalytic and non-catalytic thermal degradation of PP at 400°C are presented in Figure 7.38. All the synthesized catalysts reduced the selectivity of C16 and C18 considerably. The synthesized catalysts also increased the selectivity of C8-C13 when compared to the non-catalytic pyrolysis of PP. There was an increased selectivity of smaller hydrocarbons in the range of C6-C7. C5 selectivity was increased in a small amount by all the synthesized catalysts except the SA catalyst. The synthesized catalysts increased the selectivity of the products within the gasoline range of C5-C12. All the synthesized catalysts were C8 selective except the SA, SA-7Al and SA-7W catalysts which were C13, C13 and C11 selective, respectively. The

mole fraction and selectivity values of liquid products obtained from the catalytic pyrolysis of PP are presented in Appendix E.

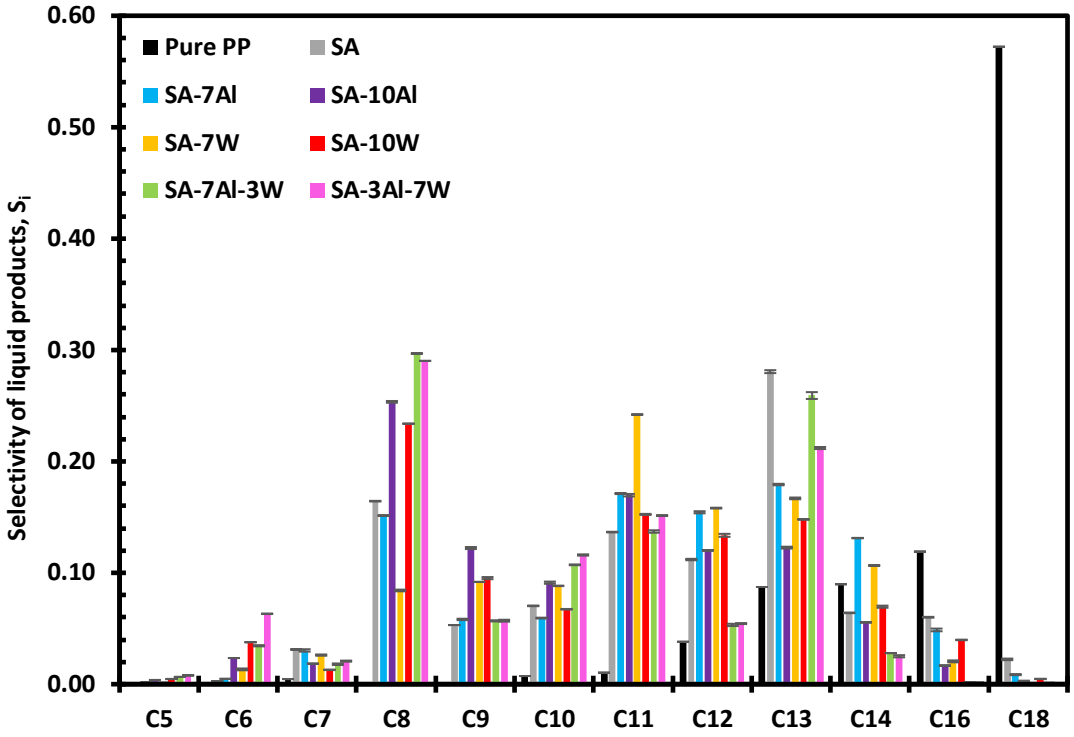

Figure 7.38 Selectivity comparison of liquid products obtained from the catalytic and non-catalytic thermal degradation of PP at 400°C.

The SA-3Al-7W catalyst had the best liquid product results as it did not produce the heavier C16 and C18 products and also increased the amount of lighter hydrocarbons like C5-C13. It enhanced the formation of the products within the gasoline range of C5-C12.

The results obtained in this study greatly improved on the results reported in the literature by Achilias et al., (2007) which found that PP pyrolysis catalyzed by ZSM-5 produced around 40 mole% of hydrocarbons in the range higher than C15, while no C5-C7 range hydrocarbons were formed.

By considering the TGA results, gas and liquid product analysis, it can be concluded that for the catalytic thermal degradation of PP the best catalyst was the SA-3Al-7W catalyst. Its only drawback was the high amount of coke formation. This may be overcome by regenerating the catalyst at certain intervals.

7.3.1.5. Coke Formation Results for PP Pyrolysis Reactions

TGA analyses of used catalysts were performed. The amount of coke deposition in the synthesized catalyst was tabulated in Table 7.8.

Table 7.8 Amount of coke deposition in the synthesized catalysts during PP degradation reactions.

Catalyst ID	Coke deposition (wt%)
Pure SA	15
SA-7Al	17
SA-10Al	11
SA-7W	18
SA-10W	21
SA-7Al-3W	48
SA-3Al-7W	48

For all the catalysts, the coke formed was amorphous. All the synthesized catalysts were active during the reaction but coke formation may cause deactivation of the catalyst at a longer reaction time. In PP degradation reaction, an increase in aluminium loading resulted in a drop in coke formation. The double metal loaded catalysts resulted in the highest coke formation. This may be attributed to the pore sizes of the SA-7Al-3W and SA-3Al-7W catalysts which were smaller than the other catalysts. The small pore sizes may have led to the higher coke formation in these two catalysts.

7.3.2. Polyethylene Pyrolysis Results

7.3.2.1. Results of Analysis of Gas Products obtained from Non-catalytic PE pyrolysis

The non-catalytic thermal degradation experiments were performed at 430 and 450°C for 15 min. The product yield of the non-catalytic pyrolysis of PE at different temperatures is presented in Figure 7.39.

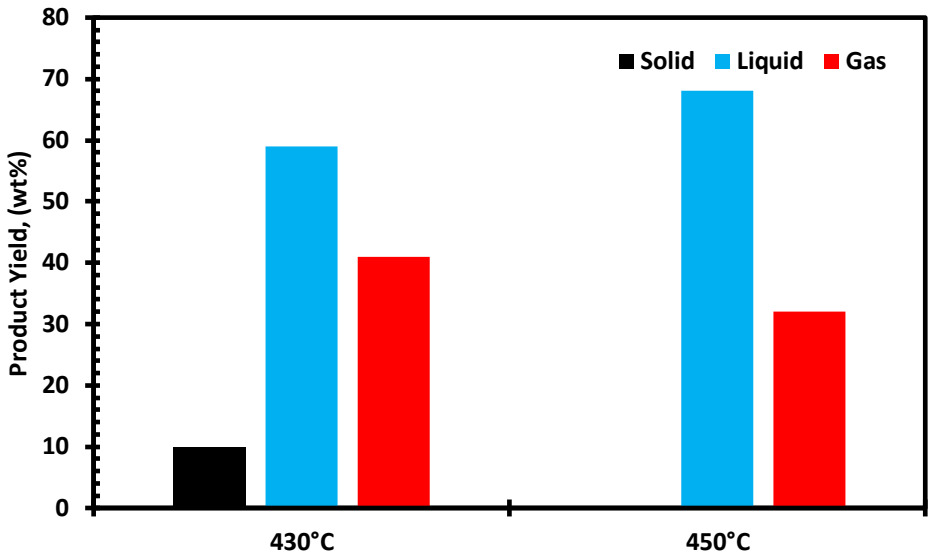

Figure 7.39 Product yield from the non-catalytic pyrolysis of PE at different reaction temperatures for 15 min.

An increase in temperature from 430 to 450°C resulted in a decrease in gaseous product while liquid products increased in the same temperature range. No solid residue was observed at 450°C. The liquid product had an orangish color which may indicate presence of heavier hydrocarbons. These results are in good agreement with the literature (Aydemir et al., 2013).

At 430°C methane, acetylene, ethane, ethylene, propylene, propane and isobutane formed. There was not a big difference in terms of gaseous products when the temperature was increased from 430 to 450°C. Isobutane was not formed at 450°C.

This may be due to a narrowing of the product distribution as an increase in temperature resulted in cracking of heavier hydrocarbon to lighter hydrocarbons.

The mole fractions for the gaseous products of the non-catalytic thermal degradation of PE at 430 and 450°C are presented in Figure 7.40. At 430°C the main component of the gas product is ethane at around 25 mole%. The amount of acetylene, ethylene and propylene is almost the same at 15 mole% while methane and isobutane are around 11 mole%. Propane has the lowest mole fraction. When temperature is increased to 450°C, methane and propane mole fractions significantly increase while acetylene and ethane have significant decreases in their mole fractions. These results are in good agreement with the literature (Aydemir et al., 2013).

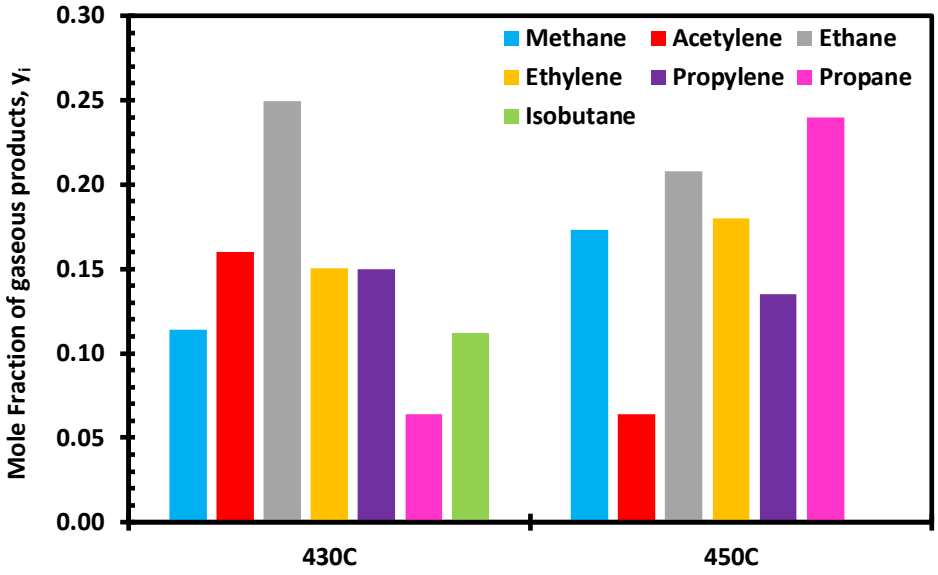

Figure 7.40 Mole fraction comparison of gaseous products obtained from the non-catalytic thermal degradation of PE at 430 and 450°C.

The selectivity of PE pyrolysis gas products is presented in Figure 7.41. An increase in temperature resulted in a small increase in methane (0.05 to 0.08) and ethylene (0.07 to 0.08) selectivities and a significant increase in propane (0.03 to 0.11) selectivity. On the other hand, there was a decrease in the selectivities of acetylene (0.07 to 0.03), ethane (0.11 to 0.09) and isobutane (0.05 to 0). The selectivity of polypropylene was

almost unaffected by the increase in temperature from 430 to 450°C. The increase in methane and ethylene selectivity coupled with a decrease in isobutane selectivity gives more evidence that a rise in temperature resulted in degradation of PE to lighter hydrocarbons.

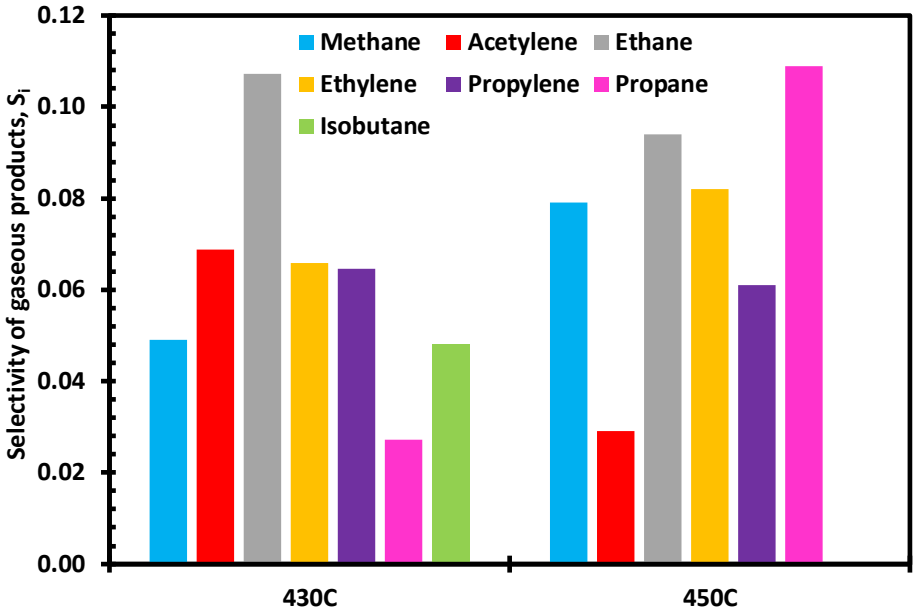

Figure 7.41 Selectivity comparison of gaseous products obtained from the non-catalytic thermal degradation of PE at 430 and 450°C.

7.3.2.2. Results of the Analysis of Liquid Products obtained from Non-catalytic PE pyrolysis

Figure 7.42 shows the liquid products obtained from the non-catalytic thermal degradation of PE at two different temperatures (430 and 450°C). C5 and C8-C18 hydrocarbons formed at both temperatures while C6 and C7 did not form at both temperatures. An increase in temperature resulted in a decrease in C5, C8, C10, C16 and C18. The decrease in the heavier C16 and C18 may be attributed to the increase in temperature enhancing the breaking of the hydrocarbon chains. However, the increase in temperature increased the amount of hydrocarbons in the range of C11-

C14. The increase in temperature narrowed the molecular weight distribution of the products.

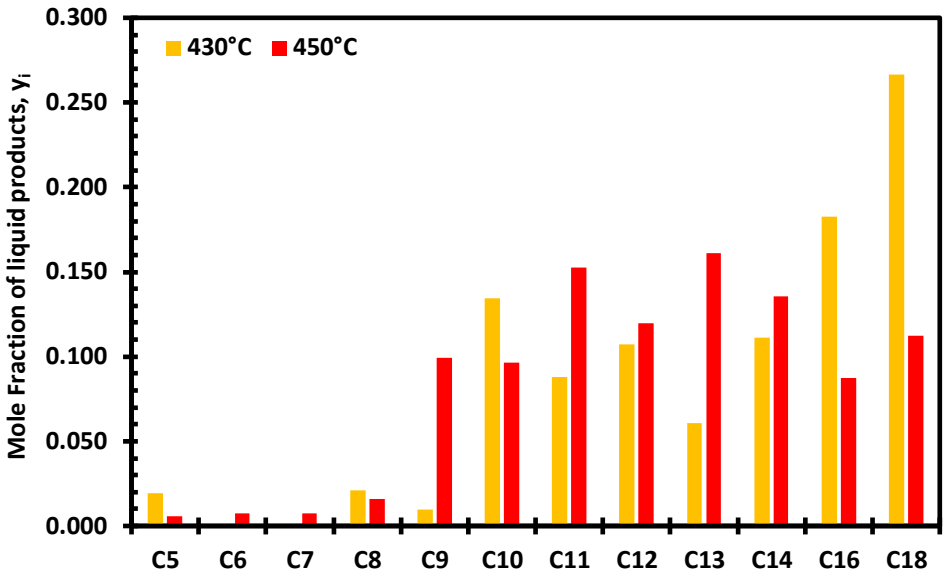

Figure 7.42 The effect of temperature on the mole fraction of liquid products obtained from the non-catalytic thermal degradation of PE.

Figure 7.43 illustrates the effect of temperature on the selectivity of products obtained from the non-catalytic thermal degradation of PE. At both temperatures, the selectivity of products in the range of C5-C8 was very low. An increase in temperature to 450°C increased the selectivity of C9, C11, C13 and C14 considerably. The selectivity of heavier hydrocarbons like C16 and C18 reduced significantly, for example the selectivity of C18 dropped from 0.30 at 450°C to 0.14 at 450°C. The full mole fraction and selectivity values of liquid products obtained from PE non-catalytic pyrolysis are presented in Appendix F.

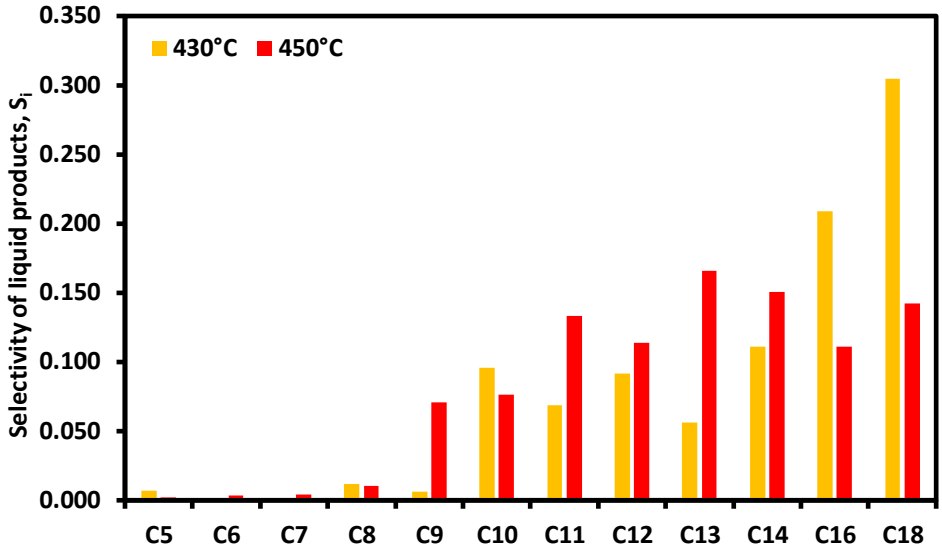

Figure 7.43 The effect of temperature on the selectivity of liquid products obtained from the non-catalytic thermal degradation of PE.

The results obtained from the non-catalytic thermal degradation of PE at 430 and 450°C are in close agreement with the results obtained in the literature (Aydemir., 2010).

7.3.2.3. Results of the Analysis of Gas Products obtained from Catalytic PE pyrolysis

Figure 7.44 shows the product yield of catalytic pyrolysis of PE. In both catalytic and non-catalytic pyrolysis of PE at 430°C no solid residue was obtained. The use of catalysts resulted in an increase in formation of gaseous products. TPA loaded catalysts resulted in higher liquid product compared to aluminium catalysts which may be attributed to stronger Brønsted acid sites in TPA loaded catalysts. Aluminium catalysts favored more gaseous production as compared to TPA loaded catalysts. The liquid product was light yellow in color and easily flowed indicating the presence of lighter hydrocarbons. An increase in metal loading increased the liquid product yield which may be due to increased acidity with metal loading. The product yield of PE catalytic and non-catalytic thermal degradation reactions was reproducible.

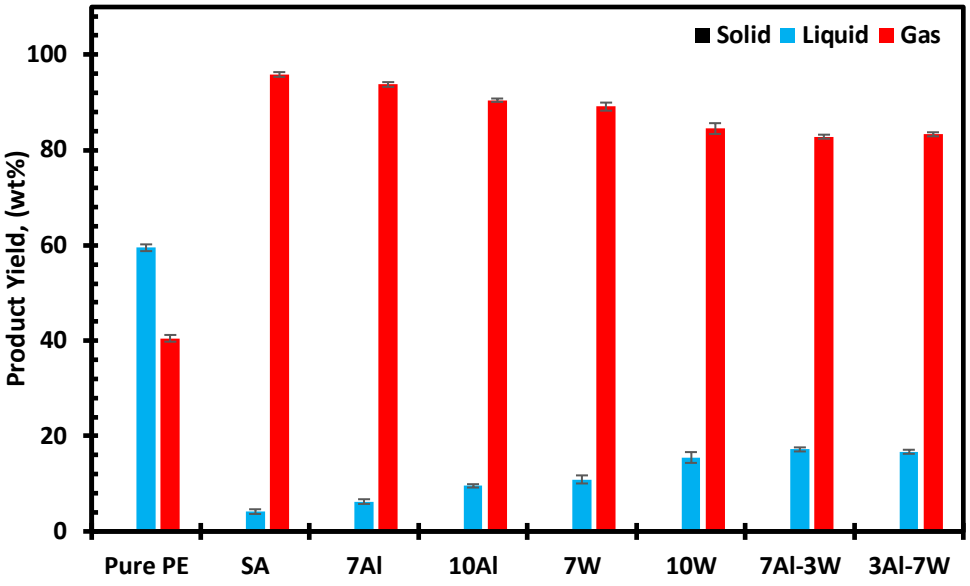

Figure 7.44 Product yield of catalytic pyrolysis of PE at 430°C for 15 min.

The liquid product yield of the PE degradation reaction with the synthesized catalysts are less than that reported in the literature for the degradation of PE using aluminium loaded MCM-41 and TPA loaded SBA-15 (Aydemir et al., 2013).

Figure 7.45 shows the mole fraction of the gaseous products for the catalytic pyrolysis of PE compared with the non-catalytic pyrolysis of PE. It can be seen that methane in the gas product of catalytic pyrolysis of PE is very high around 40 mole% for all metal loaded catalysts except the SA-7Al-3W catalyst where methane had 50 mole%. Heavier components like isobutane were in small amounts (between 3 mole% to 16 mole%) indicating cracking of heavier hydrocarbon into lighter hydrocarbons by using catalysts. These results are different from those in the literature (Aydemir et al., 2013). This study used aluminium loaded MCM-41 and TPA loaded SBA-15 and the catalysts were mainly n-butane and isobutane selective. No methane was formed in any of the experiments while propane was only formed in TPA loaded SBA-15.

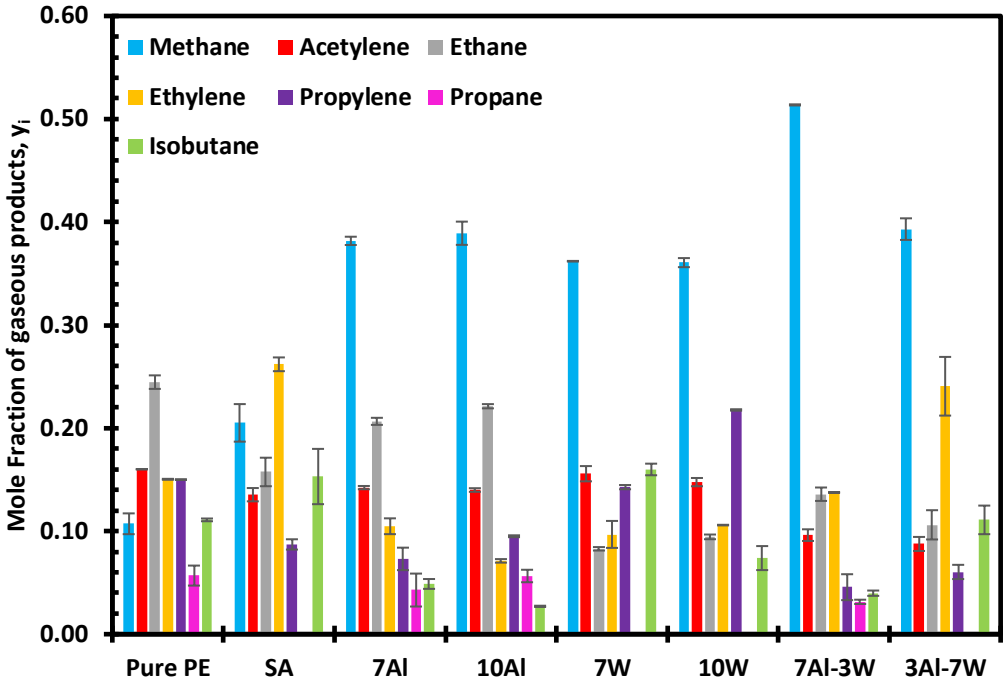

Figure 7.45 Mole fraction comparison of gaseous products obtained from the catalytic and non-catalytic thermal degradation of PE at 430°C.

The selectivity values of each gas component from the catalytic thermal degradation of PE are presented in Figure 7.46. Methane, acetylene, ethane, ethylene, propylene and isobutane formed when the synthesized catalysts were used. Propane however, formed only when the SA-7Al, SA-10Al and SA-7Al-3W catalysts were used. Methane, ethane and propane selectivities were higher in aluminium loaded catalysts compared to TPA loaded catalysts. The SA-7Al-3W catalyst resulted in the highest methane selectivity. Acetylene selectivity remained almost the same even when aluminium and TPA loading increased. However, for the double metal loaded catalysts, acetylene selectivity decreased. Ethylene selectivity increased when silica aerogel support and double metal loaded catalysts were used when compared to single loading of aluminium and TPA. Propane was formed only when aluminium catalysts were used. Some propane was formed when the SA-7Al-3W catalyst was used but this can be attributed to the higher aluminium loading percent compared to TPA.

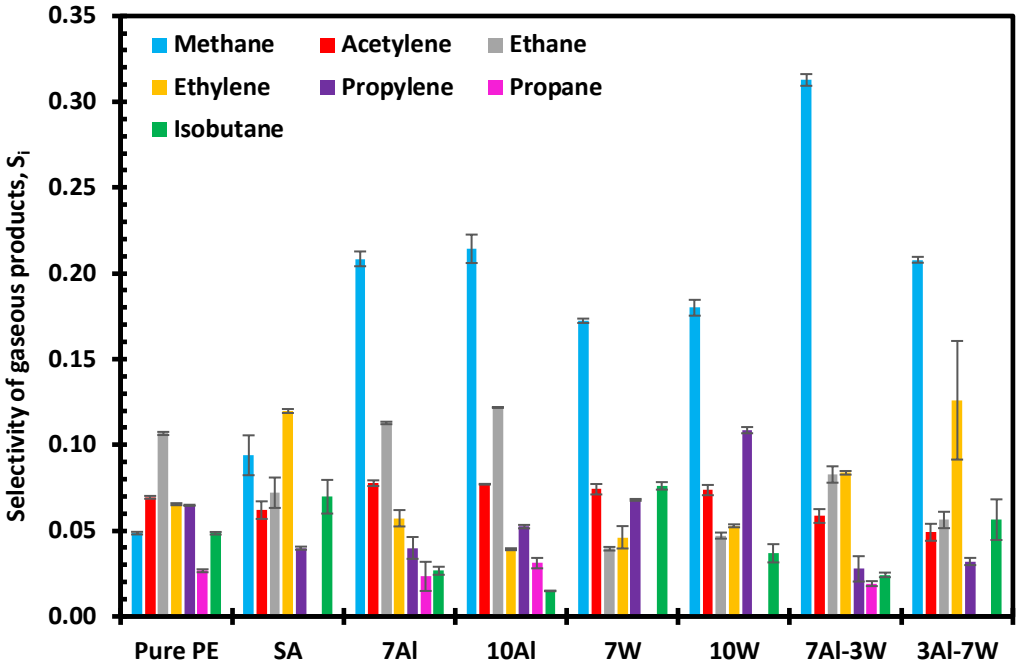

Figure 7.46 Selectivity comparison of gaseous products obtained from the catalytic and non-catalytic thermal degradation of PE at 430°C.

TPA loaded catalysts had higher propylene selectivity compared to silica aerogel support, aluminium and double loaded catalysts. Isobutane selectivity was high when silica aerogel support, the SA-7W and SA-3Al-7W catalysts were used. There was no formation of n-butane for all the PE pyrolysis experiments. Ethylene selectivity in the SA-3Al-7W catalyst had the highest standard deviation of any of the gas products obtained. The results of the two experiments per catalyst were reproducible. All the synthesized catalysts except silica aerogel support were methane selective. Silica aerogel support was ethylene selective.

7.3.2.4. Results of the Analysis of Liquid Products obtained from Catalytic PE pyrolysis

The mole fractions of liquid products obtained from the catalytic thermal degradation of PE at 430°C and a residence time of 15 min are presented in Figure 7.47.

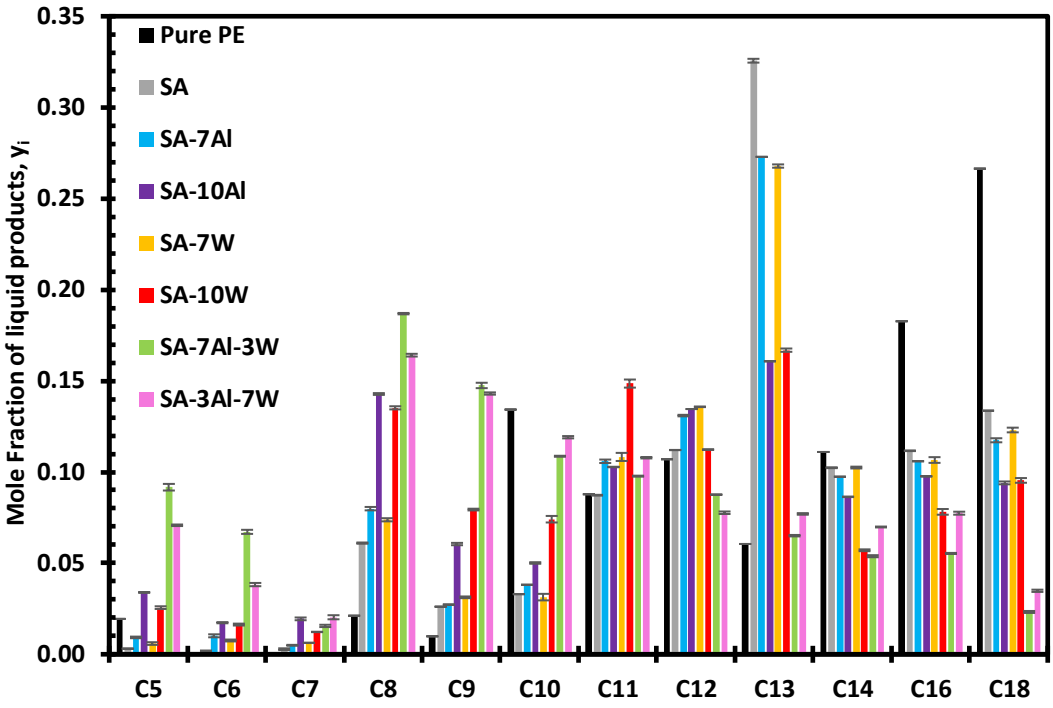

Figure 7.47 Mole fraction comparison of liquid products obtained from the catalytic and non-catalytic thermal degradation of PE at 430°C.

All the synthesized catalysts except the SA catalyst resulted in more C5-C8 hydrocarbon range. When all the synthesized catalysts except the double metal loaded catalysts were used, the amount of C13 formed increased significantly when compared to the non-catalytic PE pyrolysis. However, the amount of C5 hydrocarbon increased considerably in the presence of double metal loaded catalysts compared to the non-catalytic one.

With an increase in metal loading amount an increase in the amount of hydrocarbons in the carbon number range of 5-10 was observed. The SA-7Al-3W and SA-3Al-7W catalysts significantly reduced the formation of C14-C18 while significantly increasing the formation of products in the range of C5-C9. The combination of the aluminum and TPA metal ions worked better than the individual ions in forming products in the gasoline range of C5-C12.

The synthesized catalysts resulted in formation of products predominantly in the C8-C18 range even though the synthesized catalysts significantly reduced the amount of C16 and C18 which were produced in high amounts in the non-catalytic pyrolysis of PE. The catalysts also significantly increased the amount of C5-C9 range hydrocarbons. This means that the catalysts narrowed the molecular weight distributions of the products and enhanced formation of products within the gasoline range, C5-C12.

The selectivity of liquid products obtained from the catalytic thermal degradation of PE at 430°C and a residence time of 15 min is shown in Figure 7.48.

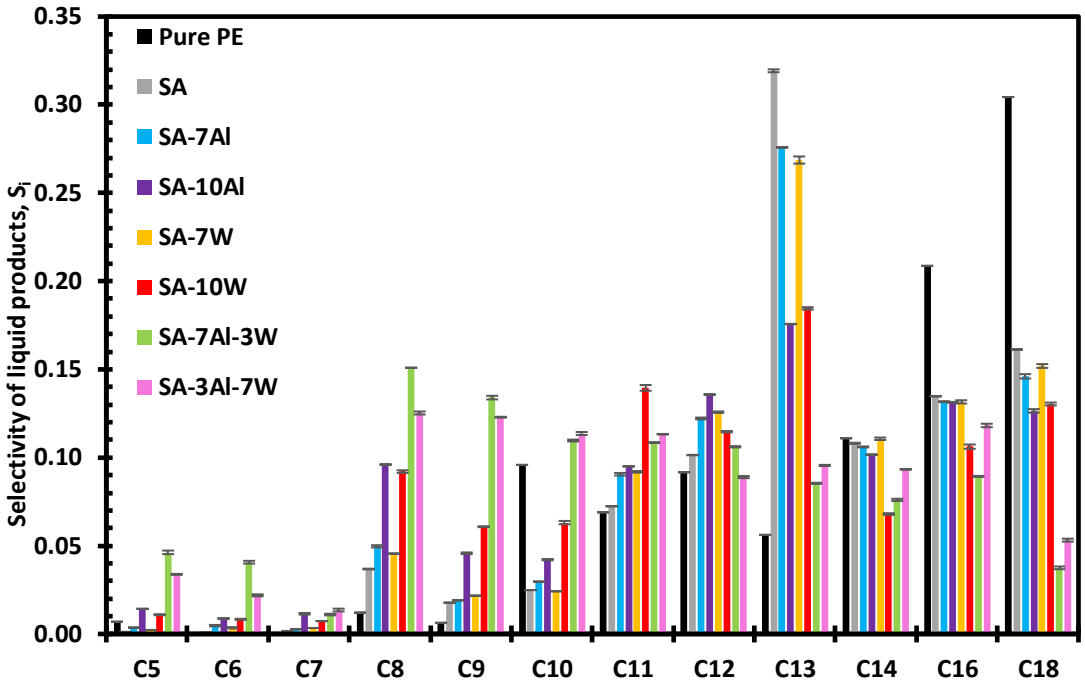

Figure 7.48 Selectivity comparison of liquid products obtained from the catalytic and non-catalytic thermal degradation of PE at 430°C.

The selectivity of C16 and C18 significantly reduced with the use of the synthesized catalysts while the selectivity of C5-C9 range hydrocarbons increased when compared to the non-catalytic pyrolysis of PE. The aluminium loaded catalysts were more selective of products in the C5-C8 hydrocarbon range as compared to the TPA loaded

catalysts. An increase in aluminium loading resulted in reduced selectivity of C13 hydrocarbon. With an increase in TPA loading there was a decrease in selectivity of C13-C18 range products. An increase in aluminium and TPA loading separately resulted in significant increase in the selectivities of products in the C5-C11 range. This means that addition of metal ions resulted in lower hydrocarbons forming resulting in narrow molecular weight distribution and products in the gasoline range.

The SA-7Al-3W and SA-3Al-7W catalysts significantly reduced selectivity of C16 and C18 while increasing the selectivity of C5-C10 range hydrocarbons. The combination of the two metal ions performed better than the individually loaded catalysts. They formed more products in the gasoline range than the SA, SA-7Al, SA-10Al, SA-7W and SA-10W catalysts.

The SA, SA-7Al, SA-10Al, SA-7W and SA-10W catalysts were C13 selective while the SA-7Al-3W and SA-3Al-7W catalysts were C8 selective. The mole fraction and selectivity data for catalytic pyrolysis of PE are presented in Appendix F.

The results obtained are similar to those reported in the literature (Aydemir et al., 2013). The study in the literature used SBA-15 loaded 10, 25 and 40 mole%. The silica aerogel results were close to those obtained in the literature when SBA-15 with 25 mole% was used in the catalytic pyrolysis of PE. This means that silica aerogel loaded with more than 25 mole% TPA may result in better quality liquid products.

The SA-7Al-3W catalyst gave the best results in the catalytic pyrolysis of PE. It's the catalyst with the highest selectivity of liquid products in the range of C5-C9. It is also significantly reduced the selectivity of C14-C18 range hydrocarbons. Thus, it enhanced the formation of products within the gasoline range more than the other synthesized catalysts. Furthermore, the catalyst gave the best results in the gaseous products analysis and had the lowest activation energy of any one the synthesized catalysts used in the pyrolysis of PE. Another advantage of this catalyst was its low coke formation. It can be used for a longer period of time before decoking is done.

7.3.2.5. Coke Formation Results for PE Pyrolysis Reactions

TGA analyses of used catalysts were performed. The amount of coke deposition in the synthesized catalyst was tabulated in Table 7.9.

Table 7.9 Amount of coke deposition in the synthesized catalysts during PE degradation reactions.

Catalyst ID	Coke deposition (wt%)
Pure SA	15
SA-7Al	27
SA-10Al	4
SA-7W	17
SA-10W	9
SA-7Al-3W	9
SA-3Al-7W	36

For all the catalysts, the coke formed was amorphous. All the synthesized catalysts were active during the reaction but coke formation may increase with a longer reaction time and it may cause deactivation of the catalyst.

For PE degradation reactions, the increase in both aluminium and TPA metal loading resulted in a significant drop in coke formation. Despite both the SA-7Al-3W and SA-3Al-7W catalysts having small pore sizes, the SA-7Al-3W catalyst has a lower activation energy compared to the SA-3Al-7W catalyst which may explain the difference in the amount of coke formed.

CHAPTER 8

CONCLUSIONS AND RECOMMENDATIONS

In this study, the catalytic activity of metal loaded silica aerogel support in the pyrolysis of polyethylene and polypropylene was investigated. The metal loaded silica aerogel catalysts were synthesized and characterized as described in the experimental section of this thesis.

A thermogravimetric analyzer was used to determine the activation energy values of the PE and PP degradation reactions. Following this, the catalytic activity of these catalysts was investigated in the PP and PE degradation reactions and the products were analyzed using the gas chromatograph. For comparison, the non-catalytic degradation of PP and PE reactions were carried out.

The major conclusions reached as a result of this study are:

- Silica aerogel support was synthesized successfully and reproducibly. The XRD pattern showed that pure silica aerogel support had an amorphous structure. The silica aerogel support exhibited a Type IV isotherm with a H3 hysteresis loop which indicates a mesoporous material.
- In all cases metal loading resulted in a decrease in silica aerogel surface area and pore sizes due to blockage of pores with metals. The TPA, aluminium and double metal loaded catalysts exhibited isotherms which were Type IV, with H3 hysteresis loops for aluminium loaded and SA-7Al-3W catalysts while TPA loaded catalysts and SA-3Al-7W catalysts had H2 hysteresis loop. All the metal loaded catalysts were mesoporous materials.

- DRIFTS analysis of synthesized metal loaded silica aerogel support revealed formation of Lewis and Bronsted acid sites due to metal loading into the support. TPA loading resulted in stronger Brønsted acid sites.
- The total acid capacity of each catalyst from ammonia TPD in ranked from the highest to the lowest as SA-10Al>SA-3Al-7W>SA-7Al-3W≥SA-7W>SA-10W>SA-7Al.
- SEM image of silica aerogel support revealed a spongy surface with numerous pores of different sizes. SEM of metal loaded silica aerogel revealed that the metal ions were incorporated into the support but EDS and ICP results revealed that the incorporation was not homogenous.
- For PP degradation reaction, metal loading decreased the activation energy from 174.4 kJ/mol to a range of 115.7-131.9 kJ/mol. For PE degradation reactions, metal loading decreased the activation energy from 134.0 kJ/mol to a range of 117.9-131.9 kJ/mol. Among the synthesized catalysts the lowest activation energy for PP and PE degradation reactions were obtained in the presence of the SA-3Al-7W and SA-7Al-3W catalysts respectively.
- Catalytic pyrolysis of PP at 400°C showed that selectivity of methane and acetylene increased with metal loading. Aluminium loaded silica aerogel support showed higher selectivity for methane, acetylene, and ethane compared to TPA loading. Double metal loading increased selectivities of these lower carbon chain hydrocarbons and reduced the selectivites of larger hydrocarbons like isobutane and n-butane. This shows that for the gaseous products catalysts narrowed the molecular weight distribution. Aluminium and double loaded catalysts were propylene selective while TPA loaded catalysts were isobutane selective.
- Catalytic pyrolysis of PE at 430°C showed that aluminium loaded silica aerogel support significantly increased the selectivities of methane, ethane and propane when compared to TPA loaded catalysts. While TPA loading favoured selectivities of ethylene, propylene and isobutane. Double metal

loading resulted in higher methane selectivity and significantly lower selectivities for propylene and isobutane. These catalysts narrowed the molecular weight distribution of the products. Metal loaded silica aerogel support catalysts were methane selective.

- The liquid products obtained in the catalytic pyrolysis of PP revealed that there was an increase in products in the C5-C12 hydrocarbon range indicating formation of more gasoline range products. All the synthesized catalysts were C8 selective except the SA, SA-7Al and SA-7W catalysts which were C13, C13 and C11 selective respectively.
- The liquid products obtained in the catalytic pyrolysis of PE also revealed more products in the C5-C12 hydrocarbon range. The SA, SA-7Al, SA-10Al, SA-7W and SA-10W catalysts were C13 selective while the SA-7Al-3W and SA-3Al-7W catalysts were C8 selective.
- The SA-3Al-7W catalyst resulted in the highest coke formation for both PE and PP degradation reactions.
- By considering the TGA results, gas and liquid product analysis, it can be concluded that for the catalytic thermal degradation of PP the best catalyst was the SA-3Al-7W catalyst. The SA-7Al-3W catalyst gave the best results in the catalytic pyrolysis of PE.

Recommendations for future work are:

- Perform pyrolysis experiments on a combination of PE & PP. This is due to the fact that most waste is not homogeneously composed of only one polymer.
- Perform pyrolysis experiments for longer reaction times to see catalyst activity and life span.
- Perform pyrolysis experiments using used catalysts. The used catalyst can be re-activated using dry air and can then be used in pyrolysis reactions. This can help study the life span of the catalysts.

REFERENCES

Achilias, D. Roupakias, C., Megalokonomos, P., Lappas, A.A., & Antonakou, V. (2007). Chemical recycling of plastic wastes made from polyethylene (LDPE and HDPE) and polypropylene (PP). *Journal of Hazardous Materials*, *149*(3), p.536–542.

Aegerter, M., Leventis, N., & Koebel, M. (2011). *Aerogels handbook (Advances in Sol-Gel Derived Materials and Technologies)*. *Springer*.

Ahmad, I., Ismail Khan, M., Khan, H., Ishaq, M., Tariq, R., Gul, K., & Ahmad, W. (2015). Pyrolysis study of polypropylene and polyethylene into premium oil products. *International Journal of Green Energy*, *12*(7), p.663–671.

Almeida, D., & Marque, M. de F. (2015). Thermal and Catalytic Pyrolysis of Polyethylene Plastic Waste in Semi. *Polimeros*, *26*(1), 1–8.

Almustapha, M. N., & Andrésen, J. M. (2013). Recovery of Valuable Chemicals from High Density Polyethylene (HDPE) Polymer: a Catalytic Approachfor Plastic Waste Recycling. *International Journal of Environmental Science and Development*, *3*(3), 263–267.

Aydemir, B. (2010). Synthesis of Mesoporous Catalysts and their Performance in Pyrolysis of Polyethylene. M.Sc. thesis, Middle East Technical University (METU).

Aydemir, B, & Sezgi, N. A. (2016). Pyrolysis of Polyethylene over Aluminum-Incorporated MCM-41 Catalyst. *Chemical Engineering Communications*, *203*(5), 635–641.

Aydemir, B, & Sezgi, N. A. (2013). Alumina and tungstophosphoric acid (TPA) loaded mesoporous catalysts for the polyethylene degradation reaction. *Industrial and Engineering Chemistry Research*, *52*(44), 15366–15371.

Aydemir, B., Sezgi, N.A., and Doğu, T. (2011). Synthesis of TPA Impregnated SBA-15 Catalysts and Their Performance in Polyethylene Degradation Reaction. *American Institute of Chemical Engineers*, *58*(504), 2466–2472.

Balani, K., Verma, V., Agarwal, A., & Narayan, R. (2015). Physical, Thermal, and Mechanical Properties of Polymers. *Biosurfaces A Materials Science and Engineering Perspective*, First Edition, p.329–344.

Degirmenci, L., Oktar, N., & Dogu, G. (2010). ETBE synthesis over silicotungstic acid and tungstophosphoric acid catalysts calcined at different temperatures. *Fuel Processing Technology*, *91*(7), 737–742.

Dorcheh, S. A., & Abbasi, M. H. (2008). Silica aerogel; synthesis, properties and characterization. *Journal of Materials Processing Technology*, *199*(1), 10–26.

Grosman, A., & Ortega, C. (2008). Capillary Condensation in Porous Materials . Hysteresis and Interaction without Pore Blocking / Percolation Process To cite this version : Capillary Condensation in Porous Materials . Hysteresis and. *Langmuir*, *24*(8), 3977–3987.

Gurav, J. L., Jung, I. K., Park, H. H., Kang, E. S., & Nadargi, D. Y. (2010). Silica aerogel: Synthesis and applications. *Journal of Nanomaterials*. Volume 2010, Issue 1, p. 1-11

Jeremic, D. (2014). Polyethylene. *Ulmann's Encyclopedia of Industrial Chemistry*. 7th Edition p. 1-42, Wiley-VCH, Weinheim.

Kasapoğlu, C. (2013). Synthesis and Characterization of TPA Loaded Mesoporous Catalysts and their Performance in Pyrolysis of Polypropylene. M.Sc. thesis, Middle East Technical University.

Kong, Y., & Hay, J. N. (2002). The measurement of the crystallinity of polymers by DSC. *Polymer*, *43*(14), 3873–3878.

Li, M., Jiang, H., Xu, D., Hai, O., & Zheng, W. (2016). Low density and hydrophobic silica aerogels dried under ambient pressure using a new co-precursor method. *Journal of Non-Crystalline Solids*, *452*, 187–193.

Liu, P. S., & Chen, G. F. (2014). General Introduction to Porous Materials. *Porous Materials*, First Edition, p. 1–20.

Lowell S., Shields J.E., Thomas M.A., Thommes M. (2004) Adsorption Isotherms. In: Characterization of Porous Solids and Powders: Surface Area, Pore Size and Density. Particle Technology Series, vol 16. Springer, Dordrecht.

Maddah, H. A. (2016). Polypropylene as a Promising Plastic: A review. *American Journal of Polymer Science*, *6*(1), p. 1–11.

Mahadik, D. B., Rao, A. V., Rao, A. P., Wagh, P. B., Ingale, S. V., & Gupta, S. C. (2011). Effect of concentration of trimethylchlorosilane (TMCS) and hexamethyldisilazane (HMDZ) silylating agents on surface free energy of silica aerogels. *Journal of Colloid and Interface Science*, *356*(1), 298–302.

Maleki, H. (2016). Recent advances in aerogels for environmental remediation applications: A review. *Chemical Engineering Journal*, *300*, 98–118.

Miandad, R., Barakat, M. A., Aburiazaiza, A. S., Rehan, M., & Nizami, A. S. (2016). Catalytic pyrolysis of plastic waste: A review. *Process Safety and Environmental Protection*, *102*, 822–838.

Obali, Z., Sezgi, N. A., & Doğu, T. (2011). The synthesis and characterization of aluminum loaded SBA-type materials as catalyst for polypropylene degradation reaction. *Chemical Engineering Journal*, *176–177*, 202–210.

Obali, Z., Sezgi, N. A., & Doğu, T. (2012). Catalytic degradation of polypropylene over alumina loaded mesoporous catalysts. *Chemical Engineering Journal*, *207–208*, 421–425.

Obali, Z., Sezgi, N. A., & Doğu, T. (2009). Performance of acidic MCM-Like aluminosilicate catalysts in pyrolysis of polypropylene. *Chemical Engineering Communications*, *196*(1–2), 116–130.

Pajonk, G. M. (2003). Some applications of silica aerogels. *Colloid and Polymer Science*, *281*(7), 637–651.

Peacock, A. J. (2000). *Handbook of Polyethylene: Structures, Properties and Applications*. *Marcel Dekker, Inc.* Retrieved from http:/ /www.dekker.com

Rao, A. P., Rao, A. V., & Pajonk, G. M. (2005). Effect of preparation conditions on the physical and hydrophobic properties of two step processed ambient pressure dried silica aerogels. *Journal of Materials Science*, *36*(3), 3841–3489.

Ratnasari, D. K., Nahil, M. A., & Williams, P. T. (2017). Catalytic pyrolysis of waste plastics using staged catalysis for production of gasoline range hydrocarbon oils. *Journal of Analytical and Applied Pyrolysis*, *124*, 631–637.

Rida, M. A., & Harb, F. (2014). Synthesis and Characterization of Amorphous Silica Nanoparitcles from Aqueous Silicates Uisng Cationic Surfactants, *24*(1), 37–42.

S.A, S., Patil, R., & Ekbote, T. (2016). Investigation of Mechanical and Thermal Behaviour of Aluminium Hydroxide/Epoxy composite filled with Silica Aerogel Material. *International Journal of Mechanical Engineering*, *2*(11), 1–5.

Schüth, Ferdi & Schmidt, W. (2002). Microporous and Mesoporous Materials. *Advanced Engineering Materials*, 4, No.5, 269–279.

Shi, F., Wang, L., & Liu, J. (2006). Synthesis and characterization of silica aerogels by a novel fast ambient pressure drying process. *Materials Letters*, *60*(29–30), 3718–3722.

Shi, H., Cui, J., Shen, H., & Wu, H. (2014). Preparation of Silica Aerogel and Its Adsorption Performance to Organic Molecule. *Advances in Materials Science and Engineering*, Volume 2014, 1–8.

Singh, N., Hui, D., Singh, R., Ahuja, I. P. S., Feo, L., & Fraternali, F. (2017). Recycling of plastic solid waste: A state of art review and future applications. *Composites Part B: Engineering*, *115*, 409–422.

Sivri, S., Dilek, C., & Sezgi, N. A. (2019). Synthesis and Characterization of Aluminum Containing Silica Aerogel Catalysts for Degradation of PLA. *International Journal of Chemical Reactor Engineering*, 20180163, 1–10.

Tamon, H., Kitamura, T., & Okazaki, M. (1998). Preparation of Silica Aerogel from TEOS, *Journal of Colloid and Interference Science*. *359*(197), 353–359.

Wang, L. J., Zhao, S. Y., & Yang, M. (2008). Structural characteristics and thermal conductivity of ambient pressure dried silica aerogels with one-step solvent exchange/surface modification. *Materials Chemistry and Physics*, *113*(1), 485–490.

APPENDICES

A. CALCULATION OF ALUMINUM AND TUNGSTOPHOSPHORIC ACID AMOUNTS TO BE IMPREGNATED INTO SYNTHESIZED SILICA AEROGEL

A.1. Calculation of Aluminium Amount to be Impregnated into Silica Aerogel Support

All calculations were carried out on the assumption that silica aerogel was purely composed of SiO_2. Aluminium tri-isopropylate was used as the aluminium source and the amount used for impregnation was calculated as follows:

Approximately 1.0 g of silica aerogel is weighed for use in impregnation and using the molecular weight of SiO_2 (60 g/mol), mole number of SiO_2 was found using equation A.1:

$$n_{SiO2} = \frac{m_{SiO2}}{MW_{SiO2}} \qquad (A.1)$$

For a desired ratio of Al/Si, mole number of aluminium was calculated from equation A.2:

$$\frac{n_{Al}}{n_{SiO2}} = \frac{n_{Al}}{n_{Si}} = R \qquad (A.2)$$

where R is the desired molar ratio of Al/Si to be used in the synthesis of the catalysts and n_{Al} is the mole number of aluminium triisopropylate.

When the number of moles of aluminium isopropylate was calculated, it is known that there is 1 mole of aluminum in every 1 mole of aluminium triisopropylate ($C_9H_{21}AlO_3$); therefore, number of moles of aluminium was equal to number of moles of aluminium triisopropylate. Consequently, the amount of aluminium triisopropylate to be used was found from equation A.3;

$$m_{Al} = n_{Al} * MW_{Al} \qquad (A.3)$$

where m_{Al} is mass of aluminium trisipropylate ($C_9H_{21}AlO_3$) and MW_{Al} is the molecular weight of aluminium triisopropylate which is 204.25 g/mol.

A.2. Calculation of Tungstophosphoric Acid Amount to be Impregnated into Silica Aerogel Support

The following calculations were made with the assumption that silica aerogel was purely composed of SiO_2. Tungstophosphoric acid (TPA) was used as the source of tungsten and the amount of TPA used in the impregnation process was calculated as follows:

For impregnation approximately 1.0 g of silica aerogel was weighed and using the molecular weight of SiO_2 (60 g/mol), mole number of SiO_2 was obtained from equation A.4;

$$n_{SiO2} = \frac{m_{SiO2}}{MW_{SiO2}} \qquad (A.4)$$

where m_{SiO2} and n_{SiO2} are the mass of silica aerogel material support used in the catalyst synthesis and mole number of SiO_2, respectively. For a desired molar ratio of W/Si, mole number of tungsten was calculated using the following;

$$\frac{n_W}{n_{Si}} = R \qquad (A.5)$$

where n_w is the mole number of W and R is the desired ratio of W/Si.

When calculating the mole number of tungsten, for every 1 mole of TPA ($H_3PW_{12}O_{40}$), there are 12 moles of tungsten i.e. number of moles of TPA is 1/12 of $n_{W.}$ Therefore, the amount of TPA to be used was as follows;

$$m_{TPA} = \left(\frac{n_W}{12}\right) * MW_{TPA} \qquad (A.6)$$

where m_{TPA} is the mass of TPA and MW_{TPA} is the molecular weight of TPA which is 2880 g/mol.

B. DETERMINATION OF KINETIC PARAMETERS

The procedure to determine the kinetic parameters using TGA data for the catalytic and non-catalytic degradation of polyethylene and polypropylene follows the method presented by Obali et al. (2011). The following reaction takes place during cracking of polymer, P.

$$pP_{(S)} \rightarrow aA_{(s)} + bB_{(g)}$$

The rate of disappearance of P is expressed in equation B.1.

$$\frac{\mathrm{d}\alpha}{\mathrm{dt}} = k_{avg}(1-\alpha)^n \qquad (\mathrm{B}.1)$$

In equation B.1, k is the rate constant, n is the overall reaction order and α is the fraction of P decomposed at time t and is defined as follows:

$$\alpha = \frac{\mathrm{w_0} - \mathrm{w_t}}{\mathrm{w_0} - \mathrm{w_\infty}} \qquad (\mathrm{B}.2)$$

where, w_o is the initial sample weight, w_t is the sample weight at time t, and w_∞ is the sample weight at infinity. The rate constant k_{avg} is the Arrhenius temperature dependency shown in B.3. A and E are the pre-exponential factor and activation energy of the reaction, respectively.

$$k_{avg} = \mathrm{A}\mathrm{e}^{\frac{-\mathrm{E}}{\mathrm{RT}}} \qquad (B.3)$$

The temperature at any given time is calculated using equation B.4 where q represents the heating rate, t is the time and T_0 is the initial temperature.

$$T = T_0 + qt \qquad (B.4)$$

Inserting equations B.3 and B.4 into B.1, the rearranged decomposition rate expression is obtained as:

$$\frac{d\alpha}{(1-\alpha)^n} = \frac{A}{q}\exp\left(\frac{-E}{RT}\right)dT \qquad (B.5)$$

Using integration by substitution method with the boundary conditions of α=0 when T=T_0 and α=α when T=T. Equation B.6 is obtained for n≠1.

$$\frac{1-(1-\alpha)^{(1-n)}}{(1-n)T^2} = \frac{AR}{qE}\left(1-\frac{2RT}{E}\right)\exp\left(-\frac{E}{RT}\right) \qquad (B.6)$$

Assuming 2RT/E <<1 and taking the natural logarithm of both sides, equation B.7 is obtained for n≠1.

$$\ln\left(\frac{1-(1-\alpha)^{(1-n)}}{(1-n)T^2}\right) = \ln\left(\frac{AR}{qE}\right) - \frac{E}{RT} \qquad (B.7)$$

Equation (B.8) can be applied for a first-order reaction (n=1):

$$\ln\left(\frac{-\ln(1-\alpha)}{T^2}\right) = \ln\left(\frac{AR}{qE}\right) - \frac{E}{RT} \qquad (B.8)$$

By using the α values, a graph of the left-hand side of equations B.7 and B.8 versus 1/T results in straight lines for a value of n. The activation energy is obtained from the slope of this line while the pre-exponential factor is obtained from the intercept.

For first and second order PE pyrolysis reactions, the plots are presented in Figures B.1 and B.2, respectively. It can be seen that the R^2 value for n=1 (Fig. B.1) is higher. Thus, it can be concluded that the PE degradation reactions is first order. Figures B.3 and B.4 are the first and second order PP pyrolysis reactions and since the R^2 value for n=1 is larger than the R^2 value for n=2, PP degradation reactions are first order.

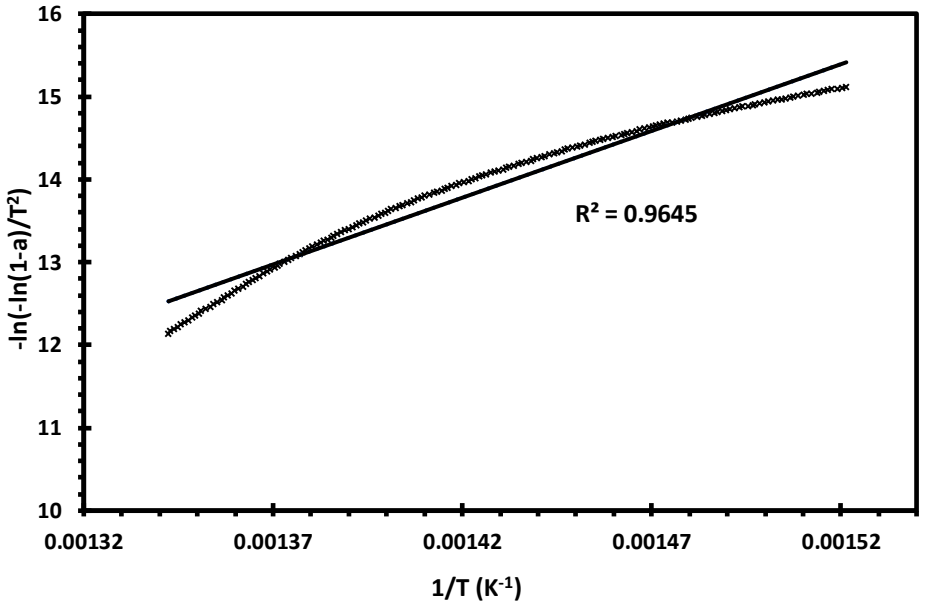

Figure B.1 First order reaction for the thermal degradation of PE.

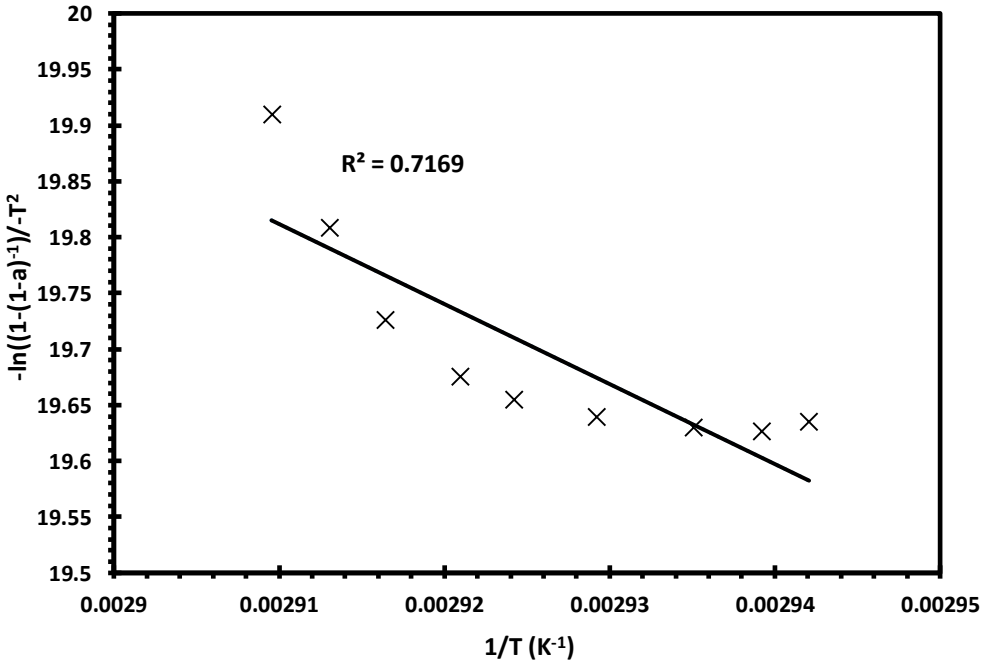

Figure B.2 Second order reaction for the thermal degradation of PE.

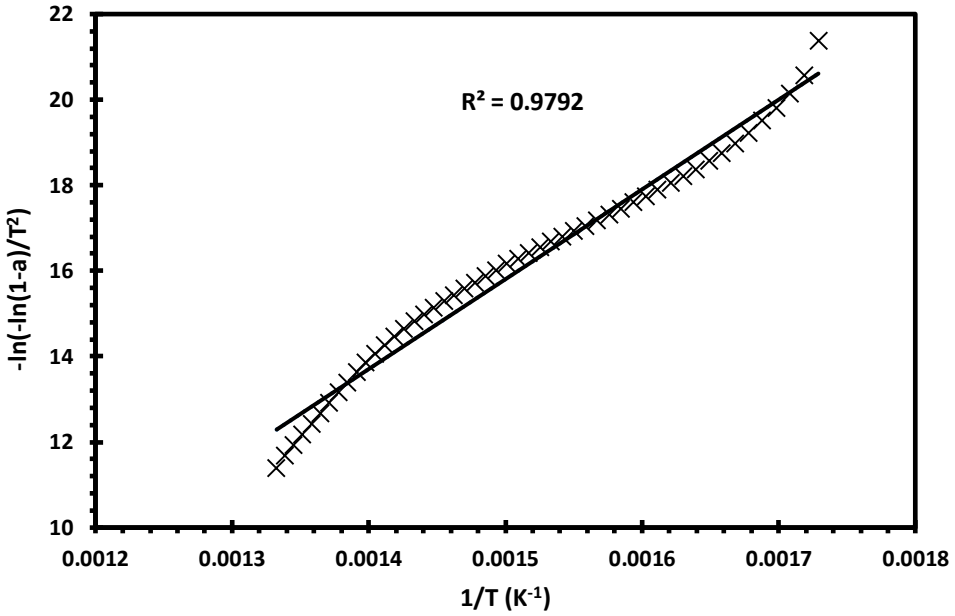

Figure B.3 First order reaction for the thermal degradation of PP.

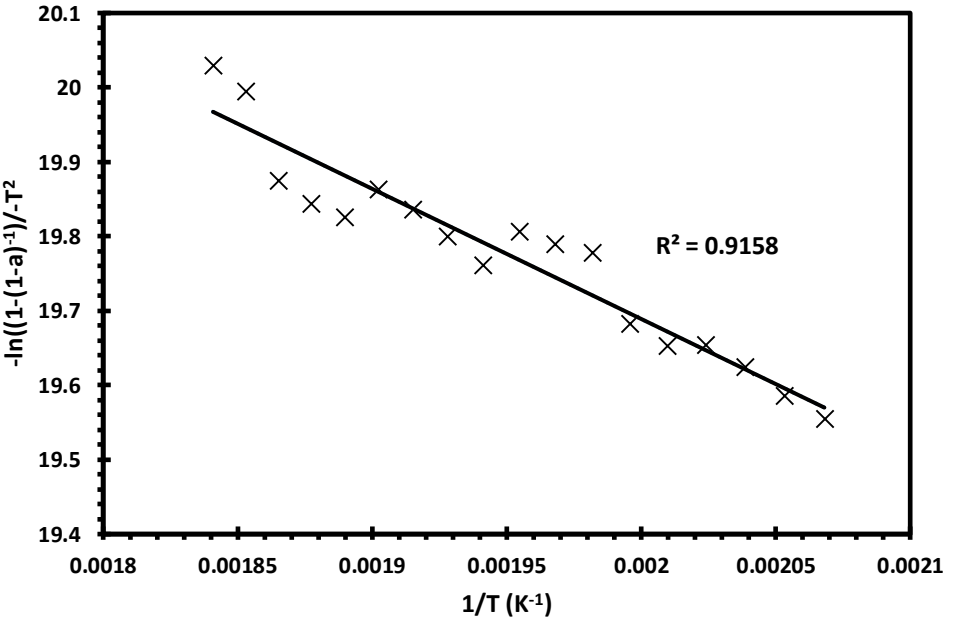

Figure B.4 Second order reaction for thermal degradation of PP.

C. CALCULATION OF GAS CHROMATOGRAPHY CALIBRATION FACTORS FOR PYROLYSIS PRODUCTS

C.1. Calibration Factors for Gas Products

Calibration experiments using GC were carried out in order to identify gas products, determine the composition of gas products obtained from the catalytic and non-catalytic thermal degradation of PE and PP, their retention times and their calibration factors. In the calibration gas, mole fraction of each component was 1% and the rest was N_2. For gaseous products, the calibration factors obtained are listed in Table C.1:

Table C.1 Retention times, average areas and calibration factors of gas products obtained through the degradation of polyethylene and polypropylene.

Gas ID	Retention time (minutes)	$A_{average}$ (mVolt.sec)	Calibration Factor, β
CH_4 (A)	0.56	13.2	1
C_2H_2 (B)	1.51	29.8	0.44
C_2H_6 (C)	1.92	19.2	0.69
C_2H_4 (D)	3.21	31.7	0.42
C_3H_6 (E)	6.42	24.7	0.54
C_3H_8 (F)	7.13	23.7	0.56
i-C_4H_{10} (G)	25.01	22.6	0.59
n-C_4H_{10} (F)	29.78	22.6	0.59

The calibration factor of CH_4 was taken as 1. The β factors of gas component B was calculated using equation C.2 which was obtained from equation C.1:

$$\frac{\mathbf{n_B}}{\mathbf{n_A}} = \frac{\mathbf{A_B} * \boldsymbol{\beta_B}}{\mathbf{A_A} * \boldsymbol{\beta_A}} \qquad (\boldsymbol{C.1})$$

$$\boldsymbol{\beta_B} = \frac{\mathbf{A_A} * \boldsymbol{\beta_A}}{\mathbf{A_B}} * \frac{\mathbf{n_B}}{\mathbf{n_A}} \qquad (\boldsymbol{C.2})$$

Sample calculation for C_2H_2 (B) component is as follows where $\mathbf{n_A = n_B = 1}$, **and** $\boldsymbol{\beta_A = 1}$:

$$\boldsymbol{\beta_B = \frac{A_A}{A_B} = \frac{13.2}{29.8} = 0.44}$$

C.2. Calibration Factors for Liquid Products

Calibration experiments using GC were carried out in order to identify the liquid products, determine the composition of the liquid products obtained from the catalytic and non-catalytic thermal degradation of PE and PP, their retention times and their calibration factors. For the identification of liquid products, three paraffin mixtures were used and presented in Table C.2 and several equal volume mixtures with n-hexane as the common compound are prepared and presented in Table C.3.

Table C.2 Standard paraffin mixtures used in liquid calibration (C9-C18).

Mixture 1		**Mixture 2**		**Mixture 3**	
Liquid ID	**wt %**	**Liquid ID**	**wt %**	**Liquid ID**	**wt %**
n-C_9H_{20}	25	n-$C_{11}H_{24}$	25	n-$C_{12}H_{26}$	25
n-$C_{10}H_{22}$	25	n-$C_{12}H_{26}$	25	n-$C_{14}H_{30}$	25
n-$C_{11}H_{24}$	25	n-$C_{13}H_{28}$	25	n-$C_{16}H_{34}$	25
n-$C_{12}H_{26}$	25	n-$C_{14}H_{30}$	25	n-$C_{18}H_{38}$	25

Table C.3 Calibration mixtures prepared using equal volumes.

Mixture	**Compounds**	**Volume (%)**
1	n-hexane + n-pentane	50-50
2	n-hexane + isooctane	50-50
3	n-hexane + cyclohexane	50-50
4	n-hexane + benzene	50-50
5	n-hexane + xylene	50-50
6	n-hexane + toluene	50-50
7	n-hexane + n-heptane	50-50
8	n-hexane + n-octane	50-50
9	n-hexane + n-decane	50-50

In the calculation of calibration factors (β), n-hexane was chosen to have a β value of 1.0. Thus, it becomes possible to calculate the β values of all components in Table C.3 using the equation C.2.

$$z_A = x_A \frac{MW_A}{\rho_A} \qquad (C.2)$$

The total amount of moles for the paraffin mixture 1 where C9: A, C10: B, C11: C and C12: D can be calculated using equation C.3. The mole fractions of each liquid component were calculated using equation C.4. For two components where β value is known for one component, the other component's β value is calculated using equation C.5, where the mole fraction was obtained from equation C.2.

$$n_{total} = A_A\beta_A + A_B\beta_B + A_C\beta_C + A_D\beta_D \qquad (C.3)$$

$$x_A = \frac{n_A}{n_{total}} = \frac{A_A\beta_A}{A_A\beta_A + A_B\beta_B + A_C\beta_C + A_D\beta_D} \qquad (C.4)$$

$$\frac{x_A}{x_i} = \frac{n_A}{n_i} = \frac{A_A\beta_A}{A_i\beta_i} \qquad (C.5)$$

The calibration factors of the other compounds were calculated using the same procedure. The retention times and calibration factors for the liquid hydrocarbons are given in Table C.4.

Table C.4 Retention times and calibration factors of liquid hydrocarbons.

Liquid Compound	**Formula**	**Retention Time (min)**	**Calibration factor, β**
n-Pentane	n-C_5H_{12}	2.81	1.20
n-Hexane	n-C_6H_{14}	3.30	1.00
Cyclohexane	C_6H_{12}	4.02	0.83
Benzene	C_6H_6	4.10	0.92
n-Heptane	n-C_7H_{16}	4.67	0.59
Iso-octane	i-C_8H_{18}	4.84	0.80
Toluene	C_7H_8	6.79	0.76
n-Octane	n-C_8H_{18}	7.79	0.65
m,p-xylene	$C_6H_4(CH_3)_2$	12.7	0.69
n-Nonane	n-C_9H_{20}	14.9	0.95
n-Decane	n-$C_{10}H_{22}$	19.0	0.61
n-Undecane	n-$C_{11}H_{24}$	23.1	0.60
n-Dodecane	n-$C_{12}H_{26}$	26.6	0.47
n-Tridecane	n-$C_{13}H_{28}$	29.7	0.41
n-Tetradecane	n-$C_{14}H_{30}$	32.6	0.38
n-Hexadecane	n-$C_{16}H_{34}$	40.7	0.34
n-Octadecane	n-$C_{18}H_{38}$	56.4	0.30

D. CALCULATION OF PRODUCT YIELD, MOLE FRACTIONS AND SELECTIVITY OF PRODUCT

D.1. Calculation of product yield

Product yield, Y_i were calculated as follows:

$$Y_{liquid} = \frac{L(g) * 100}{Polymer\ feed\ (g)} = \frac{0.88 * 100}{1.001} = 87.9 = \mathbf{88}\%$$

$$Y_{gas} = \frac{G(g) * 100}{Polymer\ feed\ (g)} = \frac{0.12 * 100}{1.001} = 11.98 = \mathbf{12}\%$$

$$Y_{solid} = \frac{S(g) * 100}{Polymer\ feed\ (g)} = \frac{0.00 * 100}{1.001} = 0.0 = \mathbf{0}\%$$

Where S, L and G are amounts of solid residue, liquid and gaseous products in grams respectively.

D.2. Calculation of mole fraction and selectivity of product

The following is a sample calculation to determine the molar fractions and selectivities of one of the experiments carried out in this study.

Reaction conditions: Polymer: Polypropylene, Catalysts: SA-7Al, T_{rxn} = 400°C and t_{rxn} = 30 min.

Components:

A: CH_4 B: C_2H_4 C: C_2H_6, D: C_2H_4, E: C_3H_6, F: i-C_4H_{10} G: n-C_4H_{10}

Mole fraction of component i,

$$y_i = \frac{n_1}{n_{total}} = \frac{A_1\beta_1}{A_A\beta_A + A_B\beta_B + A_C\beta_C + A_D\beta_D + A_E\beta_E + A_F\beta_F + A_G\beta_G}$$

Selectivity calculations were done using carbon balance.

Methane selectivity:

$$S_A = \frac{n_A}{n_A + 2n_B + 2n_C + 2n_D + 3n_E + 4n_F + 4n_G}$$

Using the calibration factors, the number of moles of each component is obtained as presented in Table D.1.

Table D.1 Areas of peak, calibration factors and number of moles of gaseous products from the non-catalytic pyrolysis of PP at 400°C for 30min.

Gas ID	**$A_{average}$ (mVolt.sec)**	**Calibration Factor, β**	**n_i**
C_2H_6 (C)	6.05	0.69	4.17
C_2H_4 (D)	6.18	0.42	2.60
C_3H_6 (E)	20.2	0.54	10.9
i-C_4H_{10} (F)	6.55	0.59	3.86

The mole fraction and selectivity of ethane were calculated as follows:

$$y_C = \frac{n_C}{n_{total}} = \frac{4.17}{4.17 + 2.60 + 10.88 + 3.86} = \mathbf{0.19}$$

$$S_C = \frac{4.17}{(2 \times 4.17) + (2 \times 2.60) + (3 \times 10.88) + (4 * 3.86)} = \mathbf{0.07}$$

The same procedure was used to calculate the mole fractions and selectivities for all the catalytic and non-catalytic thermal degradation of PP and PE at the selected reaction temperatures and times.

E. SELECTIVITY AND MOLE FRACTION VALUES OF PRODUCTS FOR THE POLYPROPYLENE DEGRADATION EXPERIMENTS

The area of each component peak was used in calculating mole fraction and selectivity of each compound present in the reactor effluent stream for the non-catalytic and catalytic pyrolysis of PP and presented in Tables E.1 and E.2.

Table E.1 Peak areas of components in the reactor effluent stream of pure PP pyrolysis at different temperatures.

Gas Products	$A_{average}$ (mVolt.sec)	
	400°C	425°C
Methane	0.00	2.01
Ethane	6.05	3.39
Ethylene	6.18	3.65
Propylene	20.2	15.5
Isobutane	6.55	1.78

Table E.2 Peak areas of components in reactor effluent stream for the catalytic pyrolysis of PP.

Gas Products	$A_{average}$ (mVolt.sec)						
	Pure SA	SA-7Al	SA-10Al	SA-7W	SA-10W	SA-7Al-3W	SA-3Al-7W
Methane	0.00	5.98	6.67	1.28	1.14	2.04	1.19
Acetylene	1.23	4.38	5.38	1.42	1.90	1.06	1.07
Ethane	2.62	2.58	2.42	1.31	0.00	2.50	3.66
Ethylene	6.42	5.59	4.03	5.00	4.69	3.32	4.13
Propylene	7.81	18.6	22.8	12.1	8.77	7.62	2.82
Isobutane	3.09	17.3	23.6	20.7	10.5	1.36	2.82
n-butane	1.46	7.20	7.54	7.27	6.20	2.12	1.48

The mole fractions and selectivity of gaseous products obtained from the non-catalytic thermal degradation reaction of PP at 400 and 425°C for 30 min are tabulated in Table E.3. The catalytic thermal degradation reaction of PP was done at 400°C for 30 min. These mole fraction and selectivity values are listed in Tables E.4 and E.5.

Table E.3 Mole fractions and selectivities of gas products obtained from the non-catalytic thermal degradation of PP at 400 and 425°C for 30 min.

Gas Products	Selectivity		Mole Fraction	
	400°C	425°C	400°C	425°C
Methane	0.00	0.01	0.00	0.02
Ethane	0.07	0.06	0.19	0.18
Ethylene	0.04	0.04	0.12	0.10
Propylene	0.18	0.21	0.51	0.58
Isobutane	0.06	0.04	0.18	0.11

Table E.4 Mole fraction values of gaseous products obtained from the catalytic degradation of PP at 400°C (t=30 min).

Gas Products	Mole fractions						
	Pure SA	SA-7Al	SA-10Al	SA-7W	SA-10W	SA-7Al-3W	SA-3Al-7W
Methane	0.00	0.17	0.17	0.02	0.06	0.17	0.14
Acetylene	0.05	0.06	0.06	0.05	0.05	0.04	0.05
Ethane	0.15	0.07	0.05	0.02	0.00	0.15	0.09
Ethylene	0.23	0.07	0.06	0.13	0.11	0.12	0.17
Propylene	0.35	0.29	0.27	0.27	0.25	0.35	0.26
Isobutane	0.15	0.24	0.26	0.36	0.34	0.07	0.19
n-butane	0.07	0.10	0.12	0.17	0.20	0.11	0.10

Table E.5 Selectivity values of gaseous products obtained from the catalytic degradation of PP at 400°C (t=30 min).

Gas Products	Selectivity						
	Pure SA	SA-7Al	SA-10Al	SA-7W	SA-10W	SA-7Al-3W	SA-3Al-7W
Methane	0.00	0.06	0.06	0.01	0.02	0.07	0.05
Acetylene	0.02	0.02	0.02	0.02	0.01	0.02	0.02
Ethane	0.05	0.03	0.02	0.01	0.00	0.06	0.03
Ethylene	0.08	0.03	0.02	0.04	0.03	0.05	0.06
Propylene	0.13	0.10	0.10	0.08	0.08	0.14	0.10
Isobutane	0.05	0.09	0.09	0.11	0.10	0.03	0.07
n-butane	0.03	0.04	0.04	0.05	0.06	0.04	0.04

The mole fractions and selectivities of the components analyzed in the liquid products obtained from the non-catalytic pyrolysis of PP at 400 and 425°C are presented in Tables E.6 while the mole fractions and selectivities of liquid components obtained from the catalytic pyrolysis of PP at 400°C are presented in Table E.7 and E.8.

Table E.6 Mole fractions and selectivities of liquid products obtained from the non-catalytic thermal degradation of PP at 400 and 425°C for 30 min.

Carbon No.	Mole Fraction		Selectivity	
	400°C	425°C	400°C	425°C
C5	0.000	0.100	0.000	0.045
C6	0.000	0.239	0.000	0.129
C7	0.011	0.003	0.005	0.002
C8	0.000	0.048	0.000	0.035
C9	0.000	0.008	0.000	0.006
C10	0.012	0.003	0.007	0.003
C11	0.015	0.074	0.010	0.073
C12	0.051	0.150	0.038	0.162
C13	0.109	0.013	0.087	0.015
C14	0.104	0.142	0.090	0.179
C16	0.120	0.031	0.119	0.044
C18	0.579	0.190	0.572	0.273

Table E.7 Mole fraction values of liquid products obtained from the catalytic degradation of PP at 400°C (t=30 min).

Carbon No.	Mole fraction						
	SA	SA-7Al	SA-10Al	SA-7W	SA-10W	SA-7Al-3W	SA-3Al-7W
C5	0.001	0.004	0.007	0.003	0.009	0.013	0.015
C6	0.005	0.009	0.038	0.024	0.063	0.056	0.100
C7	0.049	0.047	0.026	0.040	0.018	0.025	0.028
C8	0.224	0.206	0.312	0.113	0.293	0.361	0.343
C9	0.064	0.070	0.134	0.110	0.106	0.062	0.060
C10	0.077	0.065	0.090	0.095	0.067	0.104	0.110
C11	0.136	0.169	0.152	0.237	0.139	0.121	0.130
C12	0.102	0.140	0.098	0.142	0.112	0.043	0.043
C13	0.236	0.150	0.093	0.138	0.114	0.194	0.154
C14	0.050	0.102	0.039	0.082	0.050	0.019	0.017
C16	0.041	0.033	0.010	0.014	0.025	0.001	0.001
C18	0.015	0.006	0.002	0.001	0.003	0.001	0.000

Table E.8 Selectivity values of liquid products obtained from the catalytic degradation of PP at 400℃ (t=30 min).

Carbon No.	Selectivity						
	SA	SA-7Al	SA-10Al	SA-7W	SA-10W	SA-7Al-3W	SA-3Al-7W
C5	0.000	0.002	0.004	0.001	0.005	0.007	0.008
C6	0.003	0.005	0.023	0.013	0.038	0.034	0.063
C7	0.031	0.030	0.018	0.026	0.013	0.018	0.021
C8	0.164	0.151	0.253	0.084	0.234	0.297	0.290
C9	0.053	0.058	0.122	0.092	0.095	0.057	0.057
C10	0.070	0.059	0.091	0.088	0.067	0.107	0.116
C11	0.137	0.171	0.170	0.242	0.152	0.137	0.151
C12	0.112	0.154	0.120	0.158	0.134	0.053	0.054
C13	0.281	0.179	0.123	0.167	0.148	0.259	0.212
C14	0.064	0.131	0.055	0.107	0.070	0.028	0.025
C16	0.060	0.049	0.017	0.021	0.040	0.002	0.001
C18	0.022	0.009	0.003	0.001	0.005	0.001	0.001

F. SELECTIVITY AND MOLE FRACTION VALUES OF PRODUCTS FOR THE POLYETHYLENE DEGRADATION EXPERIMENTS

The area of each component peak was used in calculating mole fraction and selectivity of each compound present in the reactor effluent stream for the non-catalytic and catalytic pyrolysis of PE and presented in Tables F.1 and F.2.

Table F.1 Peak areas of components in the reactor effluent stream of pure PE pyrolysis at different temperatures.

Gas Products	$A_{average}$ (mVolt.sec)	
	430°C	450°C
Methane	2.26	2.72
Acetylene	7.09	2.29
Ethane	6.95	4.74
Ethylene	5.68	6.74
Propylene	5.41	3.93
Propane	2.48	6.99
Isobutane	3.84	0.00

Table F.2 Peak areas of components in the reactor effluent stream for the catalytic pyrolysis of PE.

Gas Products	$A_{average}$ (mVolt.sec)						
	Pure SA	SA-7Al	SA-10Al	SA-7W	SA-10W	SA-7Al-3W	SA-3Al-7W
Methane	1.58	10.8	11.5	3.48	5.04	13.7	5.69
Acetylene	2.37	9.12	9.42	3.40	4.69	5.82	3.07
Ethane	1.76	8.45	9.50	1.16	1.92	5.24	2.24
Ethylene	4.81	7.04	5.02	2.22	3.53	8.71	8.17
Propylene	1.25	3.82	5.22	2.54	5.64	2.24	1.63
Isobutane	0.00	2.24	3.10	0.00	0.00	1.55	0.00
n-butane	2.01	2.33	1.36	2.61	1.70	1.79	2.70

The selectivity and mole fractions of gaseous products obtained from the non-catalytic thermal degradation reactions of PE at 430 and 450°C for 15 min are tabulated as follows in Table F.3.

Table F.3 Mole fractions and selectivities of gas products obtained from the non-catalytic thermal degradation of PE at 430 and 450℃ for 15 min.

Gas Products	Selectivity		Mole Fraction	
	430°C	450°C	430°C	450°C
Methane	0.05	0.08	0.11	0.17
Acetylene	0.07	0.03	0.16	0.06
Ethane	0.11	0.09	0.25	0.21
Ethylene	0.07	0.08	0.15	0.18
Propylene	0.07	0.06	0.15	0.14
Propane	0.03	0.11	0.06	0.24
Isobutane	0.05	0.00	0.11	0.00

The catalytic thermal degradation reaction of PE was done at 400°C for 30 min. These mole fraction and selectivity values are listed in Tables F.4. and F.5.

Table F.4 Mole Fraction values of gaseous products obtained from the catalytic degradation of PE at 430℃ (t=15 min).

Gas Products	Mole Fractions						
	Pure SA	SA-7Al	SA-10Al	SA-7W	SA-10W	SA-7Al-3W	SA-3Al-7W
Methane	0.205	0.382	0.389	0.362	0.361	0.514	0.392
Acetylene	0.135	0.142	0.140	0.156	0.148	0.096	0.093
Ethane	0.157	0.207	0.221	0.083	0.094	0.136	0.106
Ethylene	0.262	0.105	0.071	0.097	0.106	0.138	0.242
Propylene	0.087	0.073	0.095	0.143	0.218	0.046	0.060
Propane	0.000	0.043	0.056	0.000	0.000	0.031	0.000
Isobutane	0.153	0.049	0.027	0.160	0.074	0.040	0.107

Table F.5 Selectivity values of gaseous products obtained from the catalytic degradation of PE at 430°C (t=15 min).

Gas Products	Selectivity						
	Pure SA	SA-7Al	SA-10Al	SA-7W	SA-10W	SA-7Al-3W	SA-3Al-7W
Methane	0.09	0.21	0.21	0.17	0.18	0.3	0.21
Acetylene	0.06	0.08	0.08	0.07	0.07	0.06	0.05
Ethane	0.07	0.11	0.12	0.04	0.05	0.08	0.06
Ethylene	0.12	0.06	0.04	0.05	0.05	0.08	0.13
Propylene	0.04	0.04	0.05	0.07	0.11	0.03	0.03
Propane	0.00	0.02	0.03	0.00	0.00	0.02	0.00
Isobutane	0.07	0.03	0.02	0.08	0.04	0.02	0.06

The mole fractions and selectivities of the components analyzed in the liquid products obtained from the non-catalytic pyrolysis of PE at 430 and 450°C are presented in Tables F.6 while the mole fractions and selectivities of liquid components obtained from the catalytic pyrolysis of PE at 430°C are presented in Table F.7 and F.8.

Table F.6 Mole fractions and selectivities of liquid products obtained from the non-catalytic thermal degradation of PE at 430 and 450°C for 15 min.

Carbon No.	Mole Fraction		Selectivity	
	430°C	450°C	430°C	450°C
C5	0.019	0.006	0.007	0.002
C6	0.000	0.007	0.000	0.003
C7	0.000	0.008	0.000	0.004
C8	0.021	0.016	0.012	0.010
C9	0.010	0.099	0.006	0.071
C10	0.134	0.096	0.096	0.076
C11	0.088	0.153	0.069	0.133
C12	0.107	0.119	0.092	0.113
C13	0.061	0.161	0.056	0.166
C14	0.111	0.136	0.111	0.150
C16	0.183	0.088	0.209	0.111
C18	0.266	0.112	0.304	0.142

Table F.7 Mole Fraction values of liquid products obtained from the catalytic degradation of PE at 430℃ (t=15 min).

Carbon No.	Mole fraction						
	SA	SA-7Al	SA-10Al	SA-7W	SA-10W	SA-7Al-3W	SA-3Al-7W
C5	0.003	0.009	0.034	0.006	0.026	0.092	0.071
C6	0.002	0.010	0.017	0.008	0.016	0.067	0.038
C7	0.003	0.005	0.019	0.006	0.012	0.016	0.020
C8	0.061	0.080	0.143	0.074	0.135	0.187	0.164
C9	0.026	0.027	0.060	0.031	0.079	0.147	0.143
C10	0.033	0.038	0.050	0.031	0.074	0.109	0.119
C11	0.087	0.106	0.103	0.108	0.149	0.098	0.108
C12	0.112	0.131	0.135	0.136	0.112	0.088	0.078
C13	0.326	0.273	0.161	0.268	0.167	0.065	0.077
C14	0.102	0.097	0.086	0.102	0.057	0.054	0.070
C16	0.112	0.106	0.098	0.107	0.078	0.055	0.077
C18	0.134	0.117	0.094	0.123	0.095	0.023	0.035

Table F.8 Selectivity values of liquid products obtained from the catalytic degradation of PE at 430℃ (t=15 min).

Carbon No.	Selectivity						
	SA	SA-7Al	SA-10Al	SA-7W	SA-10W	SA-7Al-3W	SA-3Al-7W
C5	0.001	0.004	0.014	0.002	0.011	0.046	0.034
C6	0.001	0.005	0.009	0.004	0.008	0.041	0.022
C7	0.001	0.003	0.011	0.003	0.007	0.011	0.014
C8	0.037	0.050	0.096	0.046	0.092	0.151	0.125
C9	0.018	0.019	0.046	0.022	0.061	0.134	0.123
C10	0.025	0.030	0.042	0.024	0.063	0.110	0.114
C11	0.072	0.091	0.095	0.092	0.140	0.109	0.113
C12	0.101	0.122	0.136	0.126	0.115	0.106	0.089
C13	0.319	0.276	0.176	0.269	0.185	0.085	0.096
C14	0.108	0.106	0.102	0.111	0.068	0.076	0.093
C16	0.135	0.132	0.131	0.132	0.106	0.089	0.118
C18	0.161	0.146	0.126	0.152	0.130	0.037	0.053